



## Mechanically invisible encapsulations

**Mazurek, Piotr Stanislaw; Skov, Anne Ladegaard; Hvilsted, Søren**

*Publication date:*  
2015

*Document Version*  
Publisher's PDF, also known as Version of record

[Link back to DTU Orbit](#)

*Citation (APA):*  
Mazurek, P. S., Skov, A. L., & Hvilsted, S. (2015). Mechanically invisible encapsulations. Kgs. Lyngby: Technical University of Denmark (DTU).

## DTU Library

Technical Information Center of Denmark

---

### General rights

Copyright and moral rights for the publications made accessible in the public portal are retained by the authors and/or other copyright owners and it is a condition of accessing publications that users recognise and abide by the legal requirements associated with these rights.

- Users may download and print one copy of any publication from the public portal for the purpose of private study or research.
- You may not further distribute the material or use it for any profit-making activity or commercial gain
- You may freely distribute the URL identifying the publication in the public portal

If you believe that this document breaches copyright please contact us providing details, and we will remove access to the work immediately and investigate your claim.



# **Mechanically invisible encapsulations**

Ph.D. Thesis

**Piotr Mazurek**

December 2015

Supervised by Assoc. Prof. Anne Ladegaard Skov  
Co-supervised by Prof. Søren Hvilsted

**DTU Chemical Engineering**  
Department of Chemical and Biochemical Engineering

---



## Preface

The work presented in this Ph.D. dissertation was carried out at the Danish Polymer Centre, Department of Chemical and Biochemical Engineering, Technical University of Denmark, between 1<sup>st</sup> January 2013 and 31<sup>st</sup> December 2015. The financial support of DTU Proof of Concept as well as the Danish Advanced Technology Foundation is highly acknowledged.

I owe my deepest gratitude to Assoc. Prof. Anne Ladegaard Skov, who supervised me throughout the three years of the project. I cannot express how fortunate I was to have the opportunity to work in your group. I highly appreciate your guidance, patience and motivation, all of which created the best possible working environment. I will never forget the friendly and inspiring atmosphere during our meetings and in everyday conversations.

I am also highly grateful to my co-supervisor Prof. Søren Hvilsted for many irreplaceable contributions to the development of my scientific skills as well for the input into the progress of my work. I furthermore acknowledge constructive and encouraging conversations held with Assoc. Prof. Anders Egede Daugaard. I am indebted to Kim Chi Szabo for her assistance with multiple laboratory issues.

I am very thankful to my big DPC family. All of you contributed to creating a wonderful atmosphere in laboratories, offices, meetings... Your positive attitudes made these three years very special to me – I will never forget the moments shared with you!

I am grateful to my family and friends for the unlimited support and for always being there for me when I needed it. Foremost, I would like to thank my beloved fiancée – Gosia – whose patience, understanding and kindness make it possible to reach any goal.

Piotr Mazurek

December 2015  
Kgs. Lyngby

## Abstract

Research into dielectric elastomers has intensified within the last two decades, due to the realisation that these materials undergo significant deformations when subjected to high electric fields. High efficiency, lightweight, low-cost and simple working principles are the main advantages of this technology. A major part of the research on dielectric transducers is dedicated to the development of elastomeric membranes that create a basis for each potential application. It has been recognised that higher energy density and more durable materials need to be created in order to enable the commercialisation of such devices. Therefore, this project was dedicated to exploring the possibility of using polar liquids as high dielectric constant fillers for dielectric PDMS-based elastomers. Incorporating polar liquids in the form of discrete droplets into nonpolar membranes was expected to produce a two-fold improvement with respect to a reference material. Firstly, dielectric constant enhancement and, secondly, a Young's modulus decrease were anticipated.

In the first approach a flow-focusing microfluidic technique was employed, in order to encapsulate polar liquids within a soft elastomeric shell. The produced core-shell microspheres served as a carrier for liquids, enabling the uniform dispersion of the filler droplets within PDMS prepolymer. The dielectric constant of the prepared water-PDMS composite was proven to be enhanced by 30% following the incorporation of 4.5 wt.% of water. Due to the favourable structure of the capsules, mechanical properties remained unaffected. Importantly, the approach substantiated the high potential of liquid-PDMS composites for dielectric transducers.

In the second part of the study a new method for producing liquid-PDMS composites was developed and thoroughly investigated. Applying very high shear forces to mixtures of PDMS pre-elastomers and polar liquids facilitated the preparation of stable and uniform emulsions. Upon crosslinking the PDMS (which formed the continuous phase of the emulsions), stable hybrid elastomers were obtained. The method allowed for incorporating up to 50% by volume of various liquids, which resulted in significant improvements to the dielectric constant of the composites. An incorporation of 120 wt.% of glycerol increased the dielectric constant of a commercial PDMS composition by 380%. Additionally a three-fold decrease in the elastic modulus was observed. Although the dielectric properties of the composites were very promising, the materials exhibited leakage current at high electric fields. Therefore, further study on improving high-voltage performance was conducted, exhibiting the high potential of the material.

The second approach brought a breakthrough in the research on liquid-PDMS composites. The developed technique proved to be very versatile, thereby allowing for the preparation of multiple hybrid materials with very distinct properties – an attractive proposition from the point of view of multiple scientific fields.

## Resumé

Forskningen vedrørende dielektriske elastomerer er intensificeret gennem de sidste to dekader efter det blev klart, at disse materialer undergår betydelige deformationer under elektriske felter. Den høje effektivitet, den lave vægt, lave pris og simple operationsmekanisme er hovedfordelene ved denne transducer-teknologi. En stor del af forskningen indenfor dielektriske elastomer transducerer vedrører optimeringen af den dielektriske elastomermembran, som er basis for alle potentielle applikationer. For at opnå udbredt kommerciel udsprelse er det nødvendigt at udvikle elastomerer med højere energitæthed samt levetid. Derfor dedikeres dette projekt til udforskningen af polære væsker i form af diskrete dråber som høj-permittivitets-fyldstoffer i dielektriske PDMS-baserede elastomerer. Inklusionen af de polære væsker på dråbeform i den upolære PDMS forventedes at bringe en kombineret forbedring i form af en forøget dielektrisk permittivitet samt et reduceret Young's modul.

I den første del af projektet blev der udviklet et flow-fokuserende mikrofluidisk system til at indkapsle de polære væsker i en blød elastomer-skal. De producerede kapsler blev dernæst reageret ind i PDMS elastomeren, hvormed en effektiv dispergering opnåedes. Denne inkorporation forøgede den dielektriske permittivitet med 30% ved 4.5 vægtprocent vand, og de favorable mekaniske egenskaber var bevaret. Metoden beviste dermed sit værd som metode for forbedrede dielektriske elastomerer.

I den anden del af projektet var fokus på en ny metode til at producere væske-PDMS kompositter på en simplere måde end i første del. Ved at tilføje store forskydningskræfter til elastomer-reaktionsblandingen med iblandet polær væske blev der opnået stabile og homogene emulsioner. PDMS (den kontinuerte fase) i denne emulsion kunne dernæst krydsbindes, og stabile hybrid-elastomerer blev opnået. Metoden tillod for op til 50 volumen% af forskellige polære væsker, hvilket bevirkede meget høje dielektriske konstanter af hybrid-elastomererne (op til 380%). Der ud over blev Young's modulet reduceret med op til en faktor 3 uden at påvirke det viskoelastiske tab. Selvom disse resultater var meget lovende for dielektriske elastomerer, blev det dog vist, at lækstrømme ved højspænding gav problemer, og derfor blev der foretaget et større studium for at klarlægge disse fænomener.

Den anden teknik bragte et gennembrud med hensyn til at inkorporere polære substanser i upolære PDMS elastomerer, og mulighederne for hybrid-elastomerne er ikke kun begrænset til dielektriske elastomerer.



## Contents

Abbreviations and symbols.....	1
Outline.....	3
<b>1 Introduction .....</b>	<b>4</b>
1.1 Electroactive polymers .....	4
1.2 Ionic electroactive actuators .....	4
1.3 Dielectric electroactive actuators .....	5
1.3.1 Overview on dielectric polymers for DEAs .....	7
1.3.2 Improving DEA performance.....	8
1.4 Research motivation .....	13
<b>2 Two-step preparation of water-containing PDMS composites .....</b>	<b>14</b>
<b>2.1 Preparing mono-dispersed liquid core PDMS microcapsules from thiol-ene-epoxy-tailored flow-focusing microfluidic device.....</b>	<b>15</b>
2.1.1 Introduction .....	15
2.1.2 Results and discussion.....	16
2.1.3 Conclusions .....	29
<b>2.2 Novel encapsulation technique for incorporation of high-permittivity filler into silicone elastomers .....</b>	<b>30</b>
2.2.1 Introduction .....	30
2.2.2 Results and discussion.....	30
2.2.3 Conclusions .....	35
<b>3 One-step preparation of liquid-containing PDMS composites.....</b>	<b>36</b>
<b>3.1 Green silicone elastomer obtained from a counterintuitively stable mixture of glycerol and PDMS.....</b>	<b>37</b>
3.1.1 Introduction .....	37
3.1.2 Sample preparation.....	38
3.1.3 Results and discussion.....	39
3.1.4 Conclusions .....	49
<b>3.2 Glycerol-PDMS composites as very high-dielectric constant DE candidates .....</b>	<b>50</b>
3.2.1 Introduction .....	50
3.2.2 Results and discussion.....	50
3.2.3 Conclusions .....	59



<b>3.3</b>	<b>Overview of PDMS compositions containing various polar liquids .....</b>	<b>61</b>
3.3.1	Introduction .....	61
3.3.2	Results and discussion.....	61
3.3.3	Conclusions .....	70
<b>4</b>	<b>Conclusions and future work .....</b>	<b>71</b>
<b>5</b>	<b>Experimental methods .....</b>	<b>73</b>
	Bibliography.....	75

## Abbreviations and symbols

A	surface area
AMA	allylmalonic acid
APFB	allylpentafluorobenzene
ATFA	allyl trifluoroacetate
ATR FTIR	attenuated total reflectance Fourier transform infrared spectroscopy
BADGE	bisphenol A diglycidyl ether
C	capacitance
CV	coefficient of variation
$\Delta T$	temperature increase
$\delta$	solubility parameter
d	thickness
DBN	1,5-diazabicyclo-[4,3,0]-non-5-ene
DE	dielectric elastomer
DFHA	2,2,3,3,4,4,5,5,6,6,7,7-dodecafluoroheptyl acrylate
DMPA	2,2-dimethoxy-2-phenylacetophenone
DSC	differential scanning calorimetry
$\epsilon$	relative dielectric constant
$\epsilon_0$	vacuum permittivity
$\epsilon_c$	dielectric constant of a composite
$\epsilon_{c,\min}$ & $\epsilon_{c,\max}$	lower limit and upper limit for dielectric constant of a binary composite
$\epsilon_f$	dielectric constant of a filler
$\epsilon_m$	dielectric constant of a matrix
E	electrical field
EAP	electroactive polymer
IL	ionic liquid
IPN	interpenetrating polymer network
IR	infrared light
J&M	model by Jayasundere and Smith
M&G	model by Maxwell and Garnett
$\overline{M}_n$	average number molecular weight
$v_f$	volume fraction of a filler in a composite
$v_m$	volume fraction of a polymeric matrix in a composite
OS-20	commercial methylsiloxane fluid
OSTE	off-stoichiometry thiol-ene mixture
OSTE+	off-stoichiometry thiol-ene-epoxy mixture
p	Maxwell pressure
P7684	Elastosil P 7684/60 A/B silicone
PANI	polyaniline
PC	propylene carbonate

---

PDMS	polydimethylsiloxane
PEG	poly(ethylene glycol)
PETMP	pentaerythritol tetrakis(3-mercaptopropionate)
PFD	1H,1H,2H-perfluoro-1-decene
phr	per hundred rubber
PI	photoinitiator
PMMA	poly(methyl methacrylate)
PMN-PT	$0.85\text{Pb}(\text{Mg}_{1/3}\text{Nb}_{2/3})\text{O}_3-0.15\text{PbTiO}_3$
PVA	polyvinyl alcohol
Q	flow rate
r	stoichiometric ratio
rpm	rounds per minute
RT620	Elastosil RT 620 A/B silicone
S184	Sylgard 184 silicone kit
SDS	sodium dodecyl sulfate
SEM	scanning electron microscopy
$s_z$	actuation strain
$\tan \delta$	loss factor
TATATO	triallyl-1,3,5-triazine-2,4,6(1H,3H,5H)-trione
$T_g$	glass transition temperature
U	voltage
UV	ultraviolet light
VHB	very high bonding (refers to commercial VHB adhesive tape from 3M)
XLR630	Powersil XLR 630 A/B silicone
Y	Young's modulus
$Y_{100}$	modulus of elasticity at 100% strain

## Outline

The thesis describes experimental paths leading to the formation of a novel type of hybrid elastomer based on polar liquid-containing silicone composites. This unconventional material was developed in order to validate the potential of high-dielectric constant liquids as fillers for dielectric transducers.

The research conducted during my Ph.D. studies includes two main approaches. Chapter 2 describes the first approach, in which flow-focusing microfluidic technique was used in order to produce water-containing elastomeric microcapsules. The produced soft core-shell microspheres were subsequently embedded into a PDMS matrix, and the mechanical and dielectric properties of the resulting hybrid composites were then evaluated. This experimental path is defined as a two-step procedure involving the preparation of composites through, firstly, the preparation of soft microcapsules and, secondly, embedding them into a silicone elastomer.

Developing a one-step preparation of liquid-silicone composites based on the high-speed mixing of two virtually immiscible liquids (described in Chapter 3) resulted in a breakthrough in how the preparation of such hybrid materials is understood. The approach exhibits many advantages in this straightforward fabrication method and takes into account various parameters when designing composites. Next to attractive dielectric properties, the materials exhibit multiple counterintuitive features, which are meticulously examined and subsequently explained in subsequent sections.

All exploited analytical methods, as well as measurement conditions, are described in Chapter 5 of the thesis.

# 1. Introduction

## 1.1. Electroactive polymers

The desire for new technologies, directed at more efficient, lightweight and silent actuators that drive everyday devices, has become an integral part of science. Consequently, far more attention is centred nowadays on so-called ‘electroactive polymers’ (EAPs), which could potentially revolutionise the transducer industry. The idea of using polymeric materials as transducers stems from back in 1880, when Wilhelm Röntgen designed a simple experiment in which a rubber band was driven by sprayed-on charges that induced the formation of electrostatic forces.<sup>1</sup> This initial research led eventually to material thinning and planar expansion. This phenomenon became an inspiration for the research conducted nowadays on the development of dielectric electroactive polymers. Another groundbreaking discovery was made in the 1970s by Heeger, MacDiarmid and Shirakawa, when the first conductive polymers were synthesised (Nobel Prize in 2000).<sup>2-5</sup> This invention helped researchers to grasp the enormous potential of polymer’s applicability in the electronics industry. Stepping away from conventional polymer applications, at this point polymers became active components of electronics rather than being used only as insulators. Henceforth, research on electroactive polymers, both conductive and dielectric, has become a hot topic and gradually gained in importance in the field of transducers. Studies on this class of material intensified after 1990, and ever since, material scientists have worked on optimising material properties and actuation conditions.<sup>6-8</sup>

Ionic and electronic actuators have so far been the two most thoroughly investigated families of electroactive polymer. Although the principles of operation of these classes are very different, they both need electric potential difference, in order to induce an actuation.

## 1.2. Ionic electroactive actuators

Ionic actuators are usually very thin strips of conductive polymers that require only a few volts to produce an adequate deflection. Converting electrical to mechanical energy is based on a reversible ion transport within the material. An applied voltage induces ion flux within the polymer, provided there is an electrolyte present in the material. The penetrating ions tend to aggregate at an electrode with an opposite charge, thereby generating local macroscopic expansion which consequently leads to bending of the material. The principles behind this operation are depicted in Figure 1.2.1. Ionic actuators usually exhibit moderate strains, while response times vary between a few seconds and fractions thereof.<sup>9</sup>

First-generation actuators were based on exposing the material to gaseous electrolyte environment<sup>10</sup> or immersing it in an electrolyte solution.<sup>11,12</sup> Therefore, the need to encapsulate these materials was frequently reported as one of its main disadvantages. An open-air, tri-layer actuator was presented in 1995 by Kaneto and MacDiarmid.<sup>13</sup> In this approach a porous membrane was swollen with an electrolyte, which was finally entrapped within the applied membrane. Nevertheless, due to high vapour pressure given off by the applied electrolyte (hydrochloric acid),

the actuator had a very limited lifetime, as the concentration of ions decreased rapidly upon exposure to air. This issue was finally overcome when ionic liquids were used as electrolytes in ionic actuators.<sup>14</sup> Due to negligible vapour pressure and tunable ion composition, the application of ionic liquids became one of the main milestones in the development of this class of actuators. Many other approaches were dedicated to improving ion mobility within actuator membranes, including, for example, the preparation of interpenetrating polymer networks (IPNs), which inter alia allowed for the precise designing of cross-linking density of polymer matrix and therefore ensured better control over ion flux was achieved.<sup>15-18</sup> This and many other approaches led research on ionic polymer actuators to the current state, in which they can now operate in solvents and open-air conditions at frequencies approaching 20 Hz, without compromising the induced actuator displacement.<sup>19</sup> Most improvements achieved for this class of actuator led to the miniaturisation of devices, and so mainly micro-size applications are envisioned these days.<sup>20-22</sup>

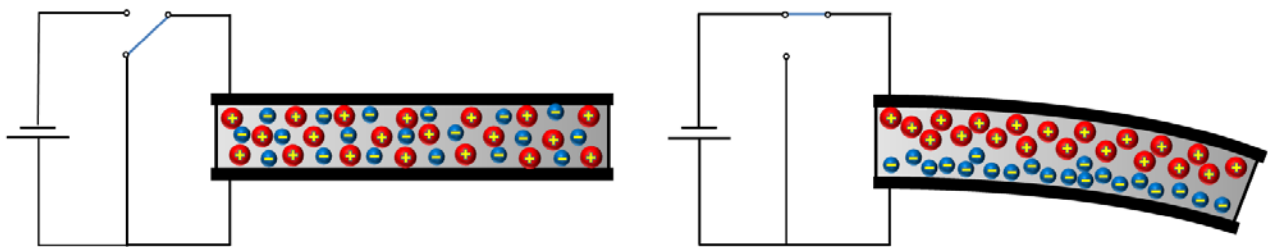


**Figure 1.2.1.** Principle of operation for ionic electroactive actuators.

### 1.3. Dielectric electroactive actuators

Dielectric elastomers (DEs) represent a very unique group of soft materials that respond to an applied electrical field, exhibiting planar expansion. The principle of operation for dielectric elastomeric actuators (DEAs) is presented in Figure 1.3.1. An elastomeric film is sandwiched between two compliant electrodes. After a voltage is applied, an electrical field is built up, which leads to material thinning and thereupon planar expansion.<sup>23,24</sup> Due to very short response times and high strains, this class of actuator has become an important point of discussion within the last two and a half decades.<sup>25-27</sup> Nevertheless, the voltage necessary to drive dielectric actuators is orders of magnitude higher than is required for ionic actuators, and so it is considered that both classes should be developed in parallel, in order to cover as many potential applications as possible.<sup>28</sup>

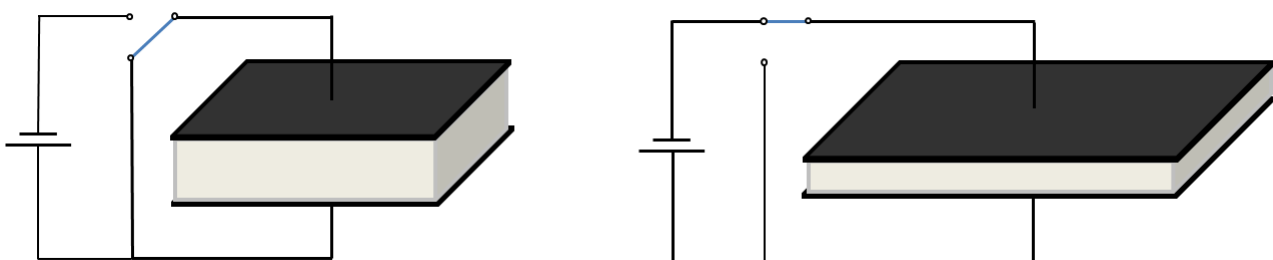


**Figure 1.3.1.** Principle of operation for dielectric electroactive actuators.

Generally speaking, dielectric elastomeric actuators can be considered as parallel plate capacitors with a soft dielectric membrane sandwiched between two compliant electrodes.<sup>29</sup> The ability to conserve energy by using the discussed dielectric is related directly to a dielectric constant of the material, whereas the dielectric constant is often considered as a parameter characterising the ability of a dielectric to polarise and thereupon to store energy. An overall ability to accumulate electrical energy through an elastomeric membrane can be expressed as:<sup>30</sup>

$$C = \frac{\varepsilon_0 \varepsilon A}{d} \quad (1.1)$$

where  $C$  refers to the capacitance of the material,  $\varepsilon_0$  corresponds to vacuum permittivity ( $8.854 \times 10^{-12}$  F/m) and  $\varepsilon$  is a membrane permittivity.  $A$  and  $d$  define the material's area and thickness, respectively.

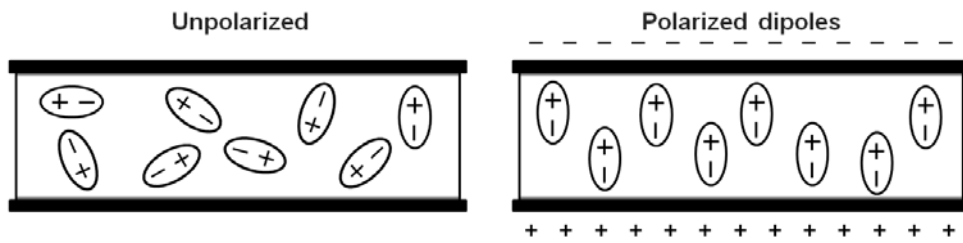


**Figure 1.3.2.** Schematic presentation of dipole polarisation within a dielectric membrane.

In order to understand fully the principle operation of DEAs, the structure of an elastomer at the molecular level has to be visualised. It is well known that all dielectric materials consist, to some extent, of dipolar molecules. When the discussed capacitor is connected to a source of electricity, its plates become charged according to the current's direction, following which an electrical field is built and thus the dipoles present in the dielectric become aligned by facing positive charges towards negative electrodes and vice versa (see Figure 1.3.2). As a result of this process electrostatic pressure is generated, which subsequently induces thinning and planar expansion of the dielectric.<sup>31</sup> Electrostatic pressure, reported often as Maxwell pressure, is defined as:

$$p = \varepsilon_0 \varepsilon E^2 \quad (1.2)$$

where  $p$  is pressure and  $E$  is the electrical field. Assuming that the mechanical properties of the elastomer remain unchanged throughout the actuation cycle, the actuator's performance ( $s_z$ ) can be expressed as a ratio of electrostatic pressure and the Young's modulus ( $Y$ ) of the membrane ( $U$  and  $d$  correspond to applied voltage and membrane thickness, respectively).<sup>32,33</sup>

$$s_z = -\frac{p}{Y} = -\frac{\varepsilon_0 \varepsilon E^2}{Y} = -\frac{\varepsilon_0 \varepsilon}{Y} \left(\frac{U}{d}\right)^2 \quad (1.3)$$

### 1.3.1. Overview on dielectric polymers for DEAs

Already knowing the principle of operation for a dielectric actuator, and the factors influencing its performance, it might appear relatively simple to choose the right membrane for this very specific application. Nevertheless, when looking closer into material requirements, it is evident that the polymer market offers a very broad range of elastomers based on different polymeric structures and with very distinct ultimate properties. Generally speaking, elastomers are soft polymeric materials that undergo elongation or deflection, even at low loadings. After the external stimulus is removed, the material goes back to its original size within a short time frame. This property is of great importance for actuators operating at all frequency ranges, but it becomes crucial when considering actuators operating at a level of mHz.<sup>34,35</sup> Furthermore, the glass transition temperature of the applied material has to be well below the intended temperature of operation, as this will ensure optimal mechanical elastomer properties, even at very low ambient temperatures.<sup>36</sup> When considering the dielectric constant as one of the parameters, it has to be taken into account that more obvious choices with respect to dielectric actuators will be polyacrylates and polyurethanes, since both polymers contain multiple polar groups in the molecular backbone, thus making them very efficient when undergoing polarisation upon exposure to an electrical field.<sup>25</sup> On the other hand, they can both be prone to uncontrollable water condensation induced by the polar groups, leading to the formation of conductive paths throughout the material. Furthermore, water is known to have moderately poor dielectric strength, and therefore the probability of electrical breakdown is increased by the presence of randomly distributed water molecules – and thereby the reliability of dielectric actuators decreases.<sup>37</sup> Polydimethylsiloxanes (PDMS) represent a group of elastomers with relatively high breakdown strength, a property which is additionally enhanced by silica particles being the most common reinforcing agent used in these polymers.<sup>38,39</sup> Additionally, the glass transition temperature of PDMS is usually much lower than the glass transition temperatures of polyurethanes and polyacrylates. Therefore, the temperature range of operation is much broader for PDMS.<sup>25</sup> Moreover, PDMS has been shown to be extremely durable and capable of withstanding millions of stretch-release cycles, unlike the other elastomers discussed here. However, PDMS suffers in general from a very low dielectric constant, usually reported to be in the range of between 2.5 and 3, which limits to some extent its applicability as a dielectric actuator.<sup>40</sup>

There is no incontestable answer to the question of which material works best as an actuator. On the one hand, there are elastomers with very high dielectric constants but which suffer from low breakdown strength and high mechanical losses. On the other hand, there is PDMS – a highly durable elastomer yet exhibiting low relative permittivity. Looking at the vast amount of research being conducted, it can be observed that in spite of its disadvantages, PDMS is the most frequently used material as a DEA. Approaches aiming at enhancing the dielectric constant and to balance the mechanical properties of PDMS are discussed in Chapter 1.3.2.

The abovementioned properties are only the tip of a requirement iceberg for dielectric actuators. In fact, the list is much longer and includes physical and electromechanical properties such as inter alia melting temperature, IR/UV/radiation stability, stability in various environments (gases, liquids, vacuum), material ageing and light transmittance, stiffness, ultimate elongation, tensile



strength, viscosity, electrical resistivity and dielectric loss. Therefore, it can be concluded that material research is a key area of study for obtaining well-operating dielectric transducers.

### 1.3.2. Improving DEA performance

Equation 1.3 suggests that the actuation performance of a DEA depends directly on four variables: applied voltage, dielectric relative permittivity, the Young's modulus and the thickness of the elastomeric membrane.<sup>33</sup> Because of currently over-expensive power supply units, the risks of elastomer electrical breakdown and a risk of exceeding the space charge threshold (resulting in accelerated electrical ageing), the applied voltage has to be kept at the lowest possible level.<sup>41</sup> Approaches aimed at improving DEA performance by modifying the three remaining parameters, as well as other methods, will be discussed herein.

#### Various types of compliant electrodes

Research on compliant electrodes has become one of the main aspects of dielectric actuator development. Compliant electrodes are responsible for the equal distribution of electrical charges across the surface of applied membranes, which in turn directly influences actuation efficiency.<sup>42</sup> Therefore, the choice of electrode for different applications has to be studied carefully, in order to guarantee the optimal operation of actuators. First of all, an electrode material has to be conductive (and uniformly conductive) to ensure fast actuator response and the proper distribution of electrical charges. The high softness and stretchability of an electrode will minimise its influence on the transduction performance of a device. And last but not least, the electrode has to exhibit a long lifetime and be stable over multiple actuation cycles.<sup>42</sup>

The most frequently reported types of electrodes are based on carbon particles, used as a conducting agent. Carbon-based electrodes can be applied onto membranes, for example, as a loose powder, which is the most direct and simplest way of applying electrodes. Nevertheless, this method does not provide good adhesion between the electrode and the membrane, and therefore it is used almost exclusively in actuators based on a commercial adhesive tape, VHB from 3M, as a dielectric membrane.<sup>42</sup> Moreover, at high strains the full coverage of a membrane is very problematic, which additionally limits applicability.<sup>6,43</sup> Furthermore, carbon electrodes can be applied onto a membrane in the form of grease. This technique is commonly used in laboratories due to its simplicity and the negligible mechanical impact of the electrode on actuation. However, carbon grease electrodes have a limited lifetime, due to possible drying of the grease and diffusion into the dielectric membrane. Additionally, such electrodes are highly susceptible to damage, and so they are used almost exclusively in laboratories for basic material testing.<sup>42</sup> The third method is based on mixing carbon black with a curable elastomer composition (e.g. a PDMS pre-elastomer) and applying the mixture onto a membrane. Upon cross-linking of the pre-polymer the electrode solidifies and becomes permanently bonded to the membrane. This approach has been reported to ensure a long lifetime and stability, good adhesion to the substrate and a minimal risk of damaging the electrode. Intuitively, the cross-linked nature of this type of electrode could potentially influence

the actuation performance of the investigated setup and hence a low Young's modulus for these electrodes has to be ensured.<sup>32</sup>

Many approaches aimed at developing and even commercialising metallic electrodes have been presented.<sup>44,45</sup> Methods of patterning materials with metallic layers are already well established and are known to provide very high conductivity on such surfaces. Nonetheless, a relatively high stiffness of metallic layers has to be taken into account when considering applying this technique to DEAs. Moreover, the metallic electrodes have been reported to suffer from cracking when high strains are applied to the material.<sup>46</sup> The latter issue was solved via depositing the metals onto a pre-stretched membrane. After the elastomer was released, a buckled surface structure was obtained, which proved to partially eliminate the problem of cracking.<sup>42</sup> The most prominent approach concerning metallic electrodes was presented and patented by Danfoss PolyPower.<sup>47-50</sup> The company developed elastomeric membranes with corrugated surfaces, which in a separate step were then patterned with metallic electrodes. In this way the problem of pre-stretching prior to metal deposition was eliminated, while the produced DEAs were proved to operate well as transducers. Danfoss PolyPower unfortunately discontinued production of their material, and therefore these promising materials are currently off the market.

To date, there is no clear answer to the question, which electrode performs best? Nevertheless the main focus has fallen on curable carbon electrodes due to their good conductivity, credibility, ease of utilisation and patternability.

### **Film thickness and stacking of membranes**

From equation 1.3 it is obvious that film thicknesses have to be minimised in order to achieve high actuation strains. Nevertheless, along with decreased thickness, the handling of materials becomes very difficult and even impossible at certain levels, which strongly depends on mechanical properties of the applied membrane. Usually, actuator films with thicknesses above 30-50  $\mu\text{m}$  are reported in the literature; however, commercial PDMS membranes of thicknesses as low as 20  $\mu\text{m}$  exist (roll-stock ELASTOSIL<sup>®</sup> films manufactured by Wacker Chemie). The production of such thin films requires cleanroom conditions in order to maintain the homogeneity of the material.

There seems to be a limit for the minimum thickness defined by material handling. However, the idea of stacked actuators presents a solution to this issue. Various groups have reported successful approaches in which thin polymeric films are stacked, whereby the films are separated with soft compliant electrodes providing the equal distribution of electrical charges to all membranes.<sup>51-53</sup> Although the preparation procedure for stacked actuators is rather complicated, much more efficient (significantly higher electrostatic pressure) and easier to handle actuators are obtained in this way.

Furthermore, it has been reported that even submicrometer-thick PDMS dielectric films can be produced via the molecular beam deposition method and successfully actuated through applying voltages in the range between only 1 and 12 V.<sup>54</sup> This certainly offers great potential for minimising membrane thickness, and it broadens the range of applications with biomedical devices and implants.

## Young's modulus

Many scientific groups have focused their research on decreasing the Young's modulus of various elastomers.<sup>55,56</sup> Although it is obvious that low Y values will positively influence actuation strains, it has to be realised that it is electrostatic pressure that truly determines the practical usefulness of actuators. It is believed that through increasing material softness, not only will membrane handling become much more difficult, but additionally the practical aspects of such approaches have certain justified limits. Significant amounts of scientific reports are focused on preparing very low-elastic modulus actuators which exhibit very high strains.<sup>30</sup> It has to be stressed again, though, that for a vast majority of applications, it is pressure that plays the critical role. From the perspective of commercial materials, frequently reported ultra-soft high-strain actuators are unfortunately of a very limited applicability. Consequently, a balance between membrane softness, actuation strain and actuation pressure has to be found when designing an optimal dielectric elastomer.

## Pre-stretching of membranes

It has been proven that actuator performance can be significantly enhanced by pre-stretching membranes.<sup>33</sup> Film thickness is reduced by performing both uniaxial and biaxial pre-stretching. Because the induced Maxwell stress depends on the electrical field, which increases in line with decreasing film thickness, it can be assumed that pre-stretching will directly drive higher actuation strains. Elastomer pre-straining may also induce a perpendicular alignment of molecules toward an electrical field,<sup>57</sup> which results in hindering charge carrier movements and then leads directly to an increase in the dielectric strength of the applied material.

Furthermore, uniaxial pre-stretching leads to the formation of mechanical anisotropy, which might be utilised in order to induce a direction-specific actuation.<sup>58</sup> The uniaxial pre-strain then results in an increase in elastic modulus in the direction of pre-stretch. Therefore, an actuated film will mainly expand in a direction perpendicular to the pre-strain axis, which creates a basis for multiple potential applications.

## Dielectric constant

Although the research on enhancing the dielectric constant has focused mainly on PDMS, there are many alternative and very interesting approaches to investigating polyurethanes and polyacrylates which should not be omitted when discussing the development of dielectric electroactive elastomers. Gallone et al., for instance, presented an approach in which a representative of polyurethanes was modified via blending with various ceramic fillers.<sup>59</sup> The dielectric constant of the applied polyurethane increased significantly after adding 15 wt.% of titanium dioxide ( $\text{TiO}_2$ ), barium titanate ( $\text{BaTiO}_3$ ) and PMN-PT ( $0.85\text{Pb}(\text{Mg}_{1/3}\text{Nb}_{2/3})\text{O}_3-0.15\text{PbTiO}_3$ ) from 6 up to 9, 12 and 14, respectively (permittivity measured at 1 kHz). The values increased even further when additional amounts were added. The same group also reported results on the blending of PDMS with polyurethanes, where the actuation performance of such blends was significantly improved in comparison to neat materials.<sup>59</sup>

The research on polyacrylates concentrated mostly on employing VHB tape, although many other acrylic-based elastomers have been tested extensively as well.<sup>60,61</sup> To date, VHB adhesive is one of the most frequently used materials for actuation experiments and for the investigation of actuation in general.<sup>62–65</sup> Introducing the VHB tape to DEA research can be considered one of the main steps in the development of this technology.<sup>33</sup> The combination of relatively high dielectric constant and a low Young's modulus for this tape has created a fantastic basis for building highly efficient actuators. However, high viscous losses and rather long actuation response times greatly limit its applicability.

Recently, a generator based on VHB tape was reported to exhibit an impressively high power density of 280 W/kg.<sup>65</sup> Yet, the prepared device was only capable of withstanding fewer than 10 cycles, after which energy generation decreased drastically. Therefore, McKay et al.<sup>66</sup> argued whether it is reasonable to conduct research on effective but not mechanically stable polyacrylates. They suggested that investing time in a lower energy density but much more durable PDMS would contribute more significantly to the development of dielectric elastomers.

There have been a number of publications in which the dielectric constant of PDMS was successfully enhanced through simply blending PDMS pre-polymer with high-permittivity fillers. This method, despite being the easiest and most intuitive, offers a broad range of possibilities due to an essentially unlimited selection of fillers, amongst which one can find magnesium niobate-lead titanate,<sup>67</sup> titanium dioxide,<sup>68</sup> graphite,<sup>69</sup> carbon nanotubes,<sup>70</sup> graphene,<sup>71</sup> conductive polymers,<sup>72</sup> etc. Nonetheless, such attempts are usually followed by increasing dielectric loss, decreasing breakdown strength, an increasing Young's modulus or limited durability of the material. Although improved actuation efficiencies compared to initial materials are usually obtained, it is not sufficient for bringing composites to commercialisation.

In parallel with blending-in fillers, a more sophisticated method of increasing elastomer permittivity has been developing, whereby high-dielectric constant dipolar molecules are linked covalently to an elastomer backbone via a novel type of chain extender.<sup>73,74</sup> The grafting reaction is based on a typical “click” chemistry reaction between azide and alkyne groups, which allows for quick and efficient synthesis reactions. This innovative approach makes it possible to graft a variety of polar molecules, and therefore the versatility of this process is considered one of its main strengths. The research has resulted in an increasing dielectric constant with only a minor addition of the modified chain extender to a PDMS composition. It has been reported that by adding only 0.25 wt.% of a pure dipole cross-linker molecule, relative permittivity increases by 35% (an increase from 2.3 to 3.1), thus preserving the favourable properties of neat PDMS.<sup>75</sup> In another approach a copolymer with multiple azide groups has been synthesised which allows for the grafting of significantly higher amounts of dipole molecules onto a polymer backbone, thereupon obtaining materials with higher dielectric constants and high dielectric breakdown strength.<sup>76</sup>

Various synthetic approaches aiming at enhancing the dielectric constant have been presented by other groups.<sup>77,78</sup> In each case significant improvements in relative permittivity were observed, yet the materials suffered from deterioration in dielectric strength or an increase in dielectric loss. Among others, nitrile groups were reported to efficiently enhance the dielectric constant of PDMS.<sup>79–81</sup> Additionally, it was shown that some of these compositions exhibit self-healing properties.<sup>80</sup> It has been discussed that these very soft elastomeric compositions have a unique

capability to self-repair after a dielectric breakdown occurrence. Self-healing dielectric actuators have already been reported, with the effect being attributed to both an applied type of electrode and to the dielectric membrane itself.<sup>82,83</sup> Nevertheless, such phenomena are not yet fully understood, and more research in this direction has to be performed in order to control this fascinating property of elastomeric actuators.

### Encapsulation of fillers

One of the main challenges accompanying blending in fillers is a risk of the formation of particle agglomerates which lead not only to the deterioration of the mechanical uniformity of a composite, but, in the case of conductive fillers, may also result in the formation of conductive paths throughout the material and a significant decrease in dielectric strength. This issue can be eliminated via a process in which each filler particle is encapsulated within a thin dielectric shell. This would minimise a chance of electrical breakdowns and yet allow for the incorporation of considerable amounts of high-permittivity fillers.<sup>84,85</sup> One of the most prominent approaches in which encapsulated high-permittivity fillers were incorporated into silicone elastomers was reported by Opris et al.<sup>30</sup> The proposed method involved coating high-dielectric constant polyaniline (PANI) particles with poly(divinyl benzene) (PDVB). The achieved encapsulation was proved to prevent the occurrence of premature electrical breakdowns, even at higher filler loadings (27.5% by volume). Furthermore, the dielectric constant of the PANI-filled composites was successfully increased. The maximum increase from 2.3 to 7.6 was reported for the sample with 31.7 vol.% of the filler. Nevertheless, most of the samples exhibited the significant enhancement of the elasticity moduli, and thereby no improvements in terms of actuation were observed. However, after modifying the pre-polymer composition, an elastomer with a low Young's modulus was obtained, which remained low even after incorporating 15 vol.% of the filler. The filled soft elastomer exhibited an enhanced dielectric constant ( $\epsilon=3.3$ ) and a more attractive actuation compared to pure PDMS. This improved actuation performance could be attributed to the combined effects of the Young's modulus decrease and the slight dielectric constant enhancement. It is important to stress that the 15 vol.% of microcapsules corresponds to roughly 2.25 vol.% of incorporated PANI (the reported weight percentage of PDVB in the microcapsules was around 85%). This implies that the process of encapsulation was probably not a necessity in this case, as much higher high-permittivity filler (e.g.  $\text{TiO}_2$ ) loadings were reported not to influence the electrical breakdown of PDMS-based composites.<sup>68,86</sup>

A successful attempt to encapsulate aluminum nanoparticles within a soft acrylic shell was presented by Hu et al.<sup>87</sup> In this approach the introduction of the filler increased the dielectric constant from 5.3 up to 8.5 for the sample with 4 vol.% of aluminum, and thereby actuation efficiency was improved significantly. Furthermore, the technique allowed for limiting the leakage current usually occurring at high voltages. Nevertheless, similar approaches concerning PDMS-based elastomers are still missing.

## 1.4. Research motivation

Presently, none of the reported elastomers meets the optimal requirements expected to produce a commercially attractive dielectric elastomer. Therefore, bold approaches have to be undertaken in order to make significant improvements. To date nobody has decided to use (or maybe even thought about using) high-permittivity polar liquids as fillers for DEs. The idea, though, has two very important advantages. Firstly, high-permittivity polar liquids are theoretically capable of enhancing the dielectric constant of a material in the same manner as classical ceramic fillers. Secondly, incorporating polar liquids into a non-polar polymer is envisioned to be realised via introducing discrete microdroplets of the liquid into the polymer, which will introduce zero-stress zones into the elastomer. Ultimately, the Young's modulus of such a material will decrease, and thereby theoretical DEA performance will be enhanced.

The aim of this project is therefore to apply polar liquids as high-dielectric constant fillers. The objective is to encapsulate a selected liquid and subsequently mix the prepared core-shell microspheres with a pre-polymer, in order to obtain the final product. Furthermore, it is intended to design capsules that are mechanically invisible. It has been hypothesised that this could be achieved, providing that the mechanical properties of the capsule shell and the DE basis are comparable. Additionally, capsule-elastomer compatibility is expected to be enhanced via the covalent bonding of the two constituents. This approach is believed to ensure that the encapsulation will become truly invisible mechanically, along with a negligible impact on ultimate mechanical properties.

In summary, the intention of this project is to create an elastomer-liquid hybrid via an encapsulation technique, whereby the encapsulation does not compromise the ultimate mechanical properties of an applied polymer.

When designing these materials, five main aspects have to be realised:

- Selection of the most suitable high-dielectric constant liquid
- Selection of the most promising polymer for the basis of the composite
- Designing a material for the capsule shell
- Choosing the most robust and versatile encapsulation technique
- Optimising the preparation procedure for the membranes.

Within this project a completely new generation of hybrid elastomers is explored and investigated. It has to be comprehended that the availability of related literature is very limited, and actually no reports on liquid-containing elastomers were found. Therefore, the resulting approach is based on the meticulous study of various, often unrelated, fields of science and foremost on intuition and the careful selection of materials and methods.

## 2. Two-step preparation of water-containing PDMS composites

After a comprehensive literature study, no clear guidelines for incorporating polar liquids into silicone elastomers were found. On the other hand, the literature provides a multitude of well-established and thoroughly characterised encapsulation techniques, out of which many are suitable for entrapping liquids within a polymeric shell. A flow-focusing microfluidic technique was selected as a tool, which was expected to allow for the preparation of liquid-core PDMS-shell elastomeric microcapsules.

In this section the preparation of a microfluidic chip, as well as the production of microcapsules, is described. Subsequently, a method for incorporating the capsules into a PDMS elastomer is presented which finally enables the production of free-standing liquid-PDMS composites of a structure presented in Figure 2.0. Furthermore, the mechanical and dielectric properties of the samples are evaluated.

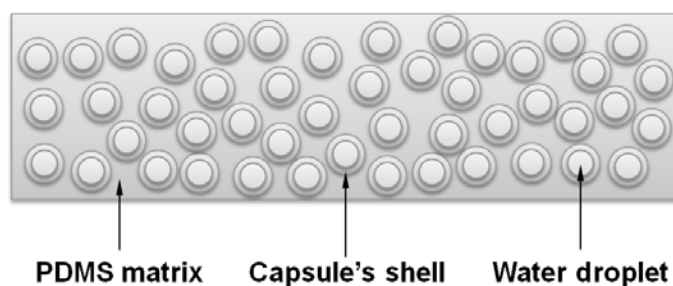


**Figure 2.0.** Schematic visualisation of an elastomer cross-section with incorporated water-containing microcapsules.

## 2.1. Preparing mono-dispersed liquid core PDMS microcapsules from thiol-ene-epoxy-tailored flow-focusing microfluidic devices

### 2.1.1. Introduction

This chapter is based on a paper “*Preparing mono-dispersed liquid core PDMS microcapsules from thiol-ene-epoxy-tailored flow-focusing microfluidic devices*” published in RSC Advances journal. Here a simple method for preparing a flow-focusing microfluidic device by applying thiol-ene click chemistry is discussed. Due to its great versatility and robustness this simple chemistry is being increasingly used for fabricating lab-on-chip devices.<sup>88,89</sup> This fascinating chemistry exhibits a great number of advantages, for example very high reaction efficiency, rapid reactions triggered by exposing compositions to UV-light, low exothermic effects and no byproducts. One of the greatest advantages of these systems is good solvent resistivity, which allows for working with almost any type of material and thereby making thiol-ene systems excellent replacements for the currently most widely used PDMS microfluidic chips.<sup>90</sup>

Thiol-ene chemistry is based on the reaction between vinyl-containing compounds and a mercapto-containing compound. In the first step, a thiyl radical is formed through hydrogen exchange between the thiol group and a radical source (Figure 2.1.1). Subsequently the thiyl radical reacts rapidly with the vinyl group of the second compound, forming a thio-ether covalent bond and transferring the radical to the next thiol group. The reaction mechanism (Figure 2.1.1) implies that only a minimal amount of photoinitiator is necessary for the reaction to progress and to reach maximum conversion. By applying different amounts of initiator and different UV-light intensities the reaction speed can be modified easily. Additionally, when 254 nm light is used, thiol-ene compositions with no photoinitiators can be cross-linked.<sup>91</sup> In this approach the off-stoichiometry thiol-ene (abbreviated OSTE) composition presented by Carlborg et al. is applied,<sup>92</sup> herein a tetrafunctional thiol compound is cross-linked with a trifunctional allyl compound, thus forming a stable matrix which exhibits good solvent resistance and possesses tunable mechanical and chemical properties. Selective surface patterning, necessary for preparing double emulsions in flow-focusing microfluidic systems,<sup>93</sup> is achieved by again applying thiol-ene chemistry, which in turn allows for efficient grafting onto polymer surfaces.

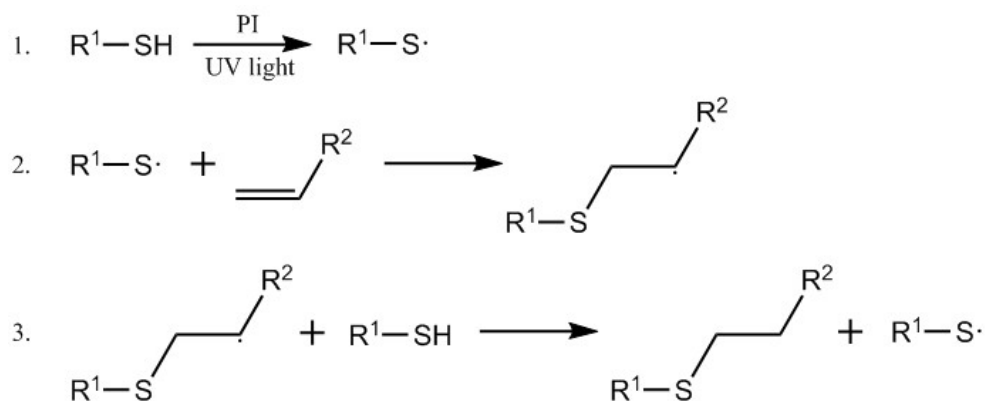


**Figure 2.1.1.** Mechanism of a photoinitiated thiol-ene reaction.<sup>94</sup>



One of the greatest challenges when using flow-focusing microfluidic systems is the prevention of leakages appearing in chips when high pressure is present in microfluidic channels. It is especially intractable when higher-viscosity liquids are introduced to the system, since in such cases higher flow rates are necessary for the dispersed phase stream break-up to occur. Research on bonding strength between wafers made of different OSTE compositions was conducted by Sikanen et al.<sup>95</sup> All combinations of OSTE wafers presented by this group were tested, and none of them appeared to provide adhesion strong enough to eliminate leakages completely, and hence a better method for wafer bonding was required. Herein, a two-step cross-linking method presented by Saharil et al. was modified,<sup>96</sup> which is based on the covalent bonding of the two microfluidic chip wafers through the introduction of an epoxy-containing compound working as a bonding agent. With the help of this method it was possible not only to avoid leakages but it also preserved the possibility of surface modification.

The flow-focusing microfluidic device presented in this chapter was designed in order to enable the encapsulation of any type of liquid, provided that liquids forming the inner/outer phase and the middle phase of produced double emulsions are not miscible.

## 2.1.2. Results and discussion

### 2.1.2.1. Synthesis of 2-hydroxyethylammonium formate

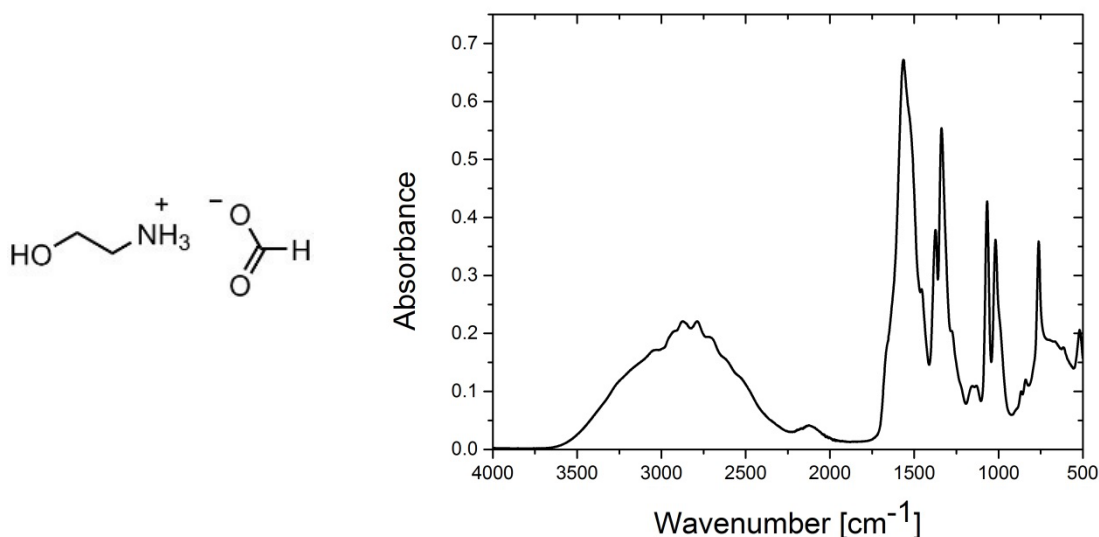


**Figure 2.1.2.** Chemical formula (left) and ATR FTIR spectrum (right) of 2-hydroxyethylammonium formate, with a peak at a wavenumber of around 1565 cm<sup>-1</sup>, thereby indicating a COO<sup>-</sup> stretch, and a peak at a wavenumber of around 2125 cm<sup>-1</sup>, corresponding to an RNH<sub>3</sub><sup>+</sup> bend.

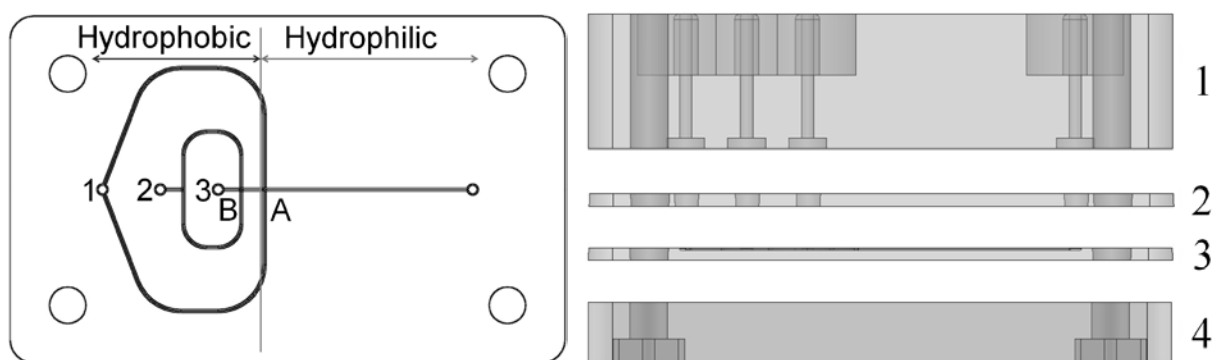
An ionic liquid (IL), 2-hydroxyethylammonium formate (see chemical formula in Figure 2.1.2) was synthesised following a procedure described by Yuan et al.<sup>97</sup> In total, 0.2 mole of 2-

hydroxyethyl amine and formic acid were dissolved in 40 mL of ethanol. Formic acid solution was added drop-wise to a round-bottomed flask equipped with a magnetic stirrer and reflux condenser and containing 2-hydroxyethyl amine solution. The reaction was held for around 4 hours to ensure full conversion. Subsequently obtained ionic liquid was separated from the solvent via vacuum evaporation, dissolved again in ethanol, treated with carbon black and then filtered. The product was kept under low-pressure conditions in order to avoid water condensation. The ATR FTIR spectrum of the ionic liquid confirmed an exchange of protons between Brønsted acid and the base, as shown in Figure 2.1.2.

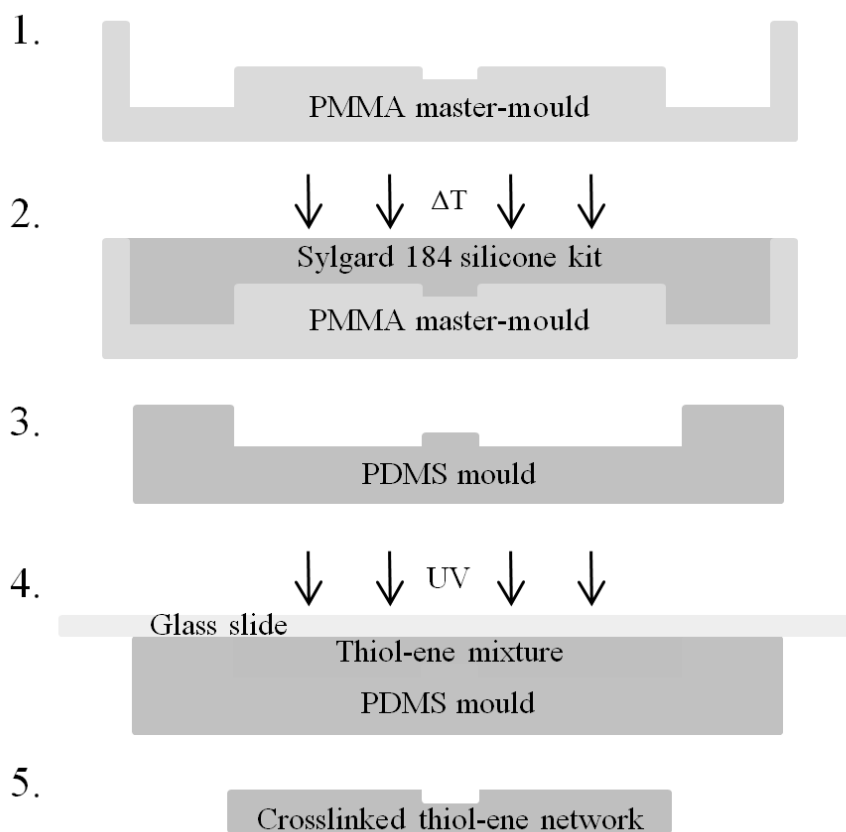
### 2.1.2.2. Preparing microfluidic device

The microfluidic device contained two main units, each consisting of two parts. The microfluidic chip entails a bottom part, with all channels and junctions, and a top part, which seals the chip. The three inlets and one outlet placed in the top part enable liquid transfer throughout the chip. The two wafers of the chip are assembled and sandwiched between bottom and top parts of the holder (see Figure 2.1.3).

The holder wafers were micromilled in polycarbonate. The microfluidic chip was then prepared in a two-step replica moulding process, where all geometries of a master mould were micromilled in a PMMA plate in the first step. Subsequently a Sylgard 184 silicone kit (mixing ratio 10:1) composition was prepared, degassed and cast onto the PMMA master mould, in order to obtain a mirror image PDMS mould. The composition was then cross-linked at 80 °C for 10 hours, after which the mirror image mould was ready to be used for preparing the microfluidic chip. A full scheme for the thiol-ene chip fabrication process is presented in Figure 2.1.4.

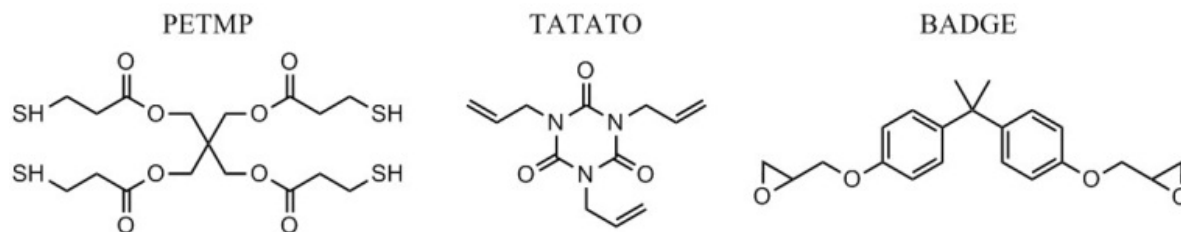


**Figure 2.1.3.** Chip scheme (left) (channel width of 280  $\mu\text{m}$ ) and full microfluidic device (right). 1 – holder top, 2 – chip top, 3 – chip bottom, 4 – holder bottom.

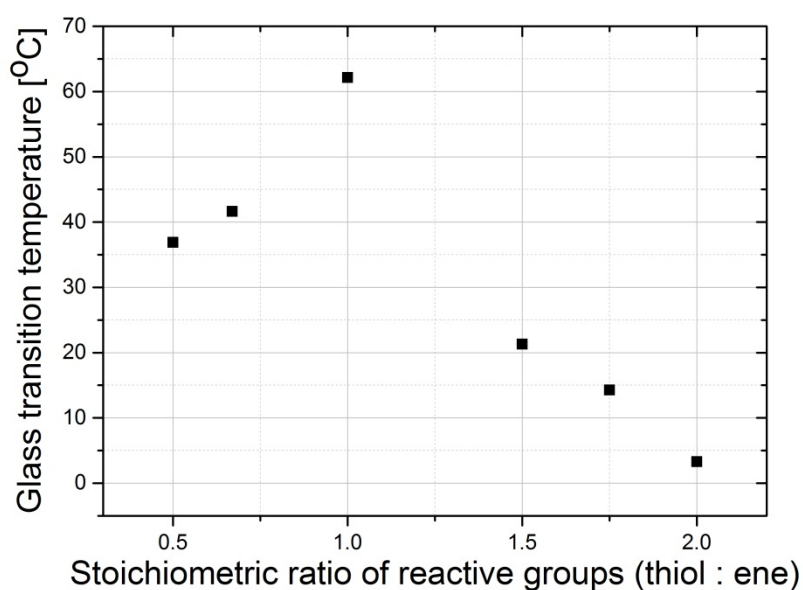


**Figure 2.1.4.** Thiol-ene chip fabrication process scheme.

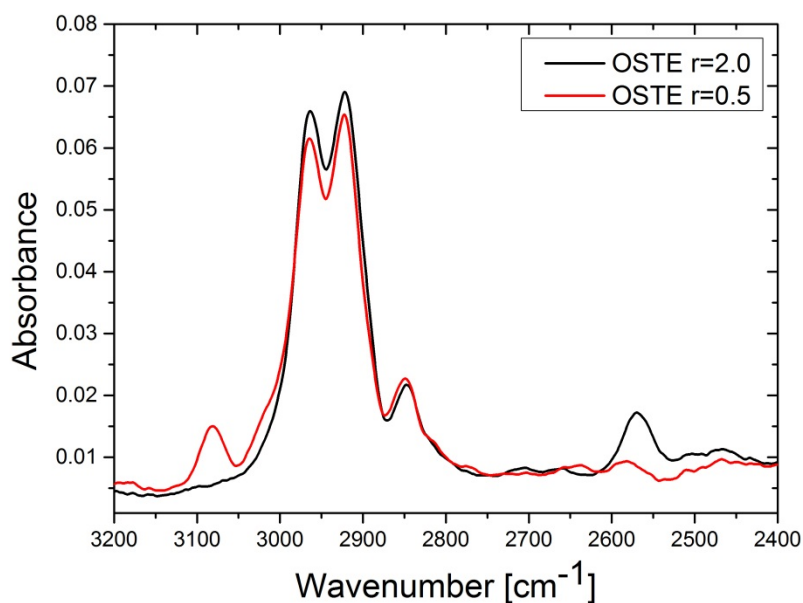
For preparing the microfluidic chip the composition of monomers reported by Carlborg et al. was employed.<sup>92</sup> The off-stoichiometry thiol-ene composition (OSTE) is based on a tetra-functional thiol compound (PETMP) and a tri-functional allyl compound (TATATO) (Figure 2.1.5). The components form a stable network when mixed together with a photoinitiator and following subsequent exposure to UV-light. Depending on the stoichiometric amounts of both components, very different mechanical properties of the material can be obtained. Results for differential scanning calorimetry, presented in Figure 2.1.6, show that when thiol and vinyl groups were used in stoichiometric balance, the glass transition temperature ( $T_g$ ) of the composition reached a maximum 60 °C, which can be attributed to the highest degree of cross-linking in this composition and the presumed absence of dangling chains. On the other hand, when stoichiometric imbalance is introduced, the glass transition temperatures decrease due to an increasing number of dangling chains with unreacted functional groups. It can also be hypothesised that excess triallyl monomer results in the formation of a stiffer structure than in the case of excess thiol monomer, which is finally attributed to the structure of monomers (shorter dangling chains and the cyclic nature of allyl monomer). The presence of both thiol and vinyl groups in different compositions was proven by FTIR tests, which for  $r=2.0$  exhibited a peak at a wavenumber of around  $2550\text{ cm}^{-1}$ , attributed to the S-H stretch of the thiol groups, and no peaks in the range between  $3095$  and  $3010\text{ cm}^{-1}$ , attributed to the  $\text{sp}^2$  C-H stretch of the vinyl group and vice versa in the case of compositions with excess allyl monomer (see Figure 2.1.7).



**Figure 2.1.5.** Structural formulas of compounds used for preparing a flow-focusing microfluidic chip: pentaerythritol tetrakis(3-mercaptopropionate) (PETMP), triallyl-1,3,5-triazine-2,4,6(1H,3H,5H)-trione (TATATO) and bisphenol A diglycidyl ether (BADGE) working as a dual cure agent.



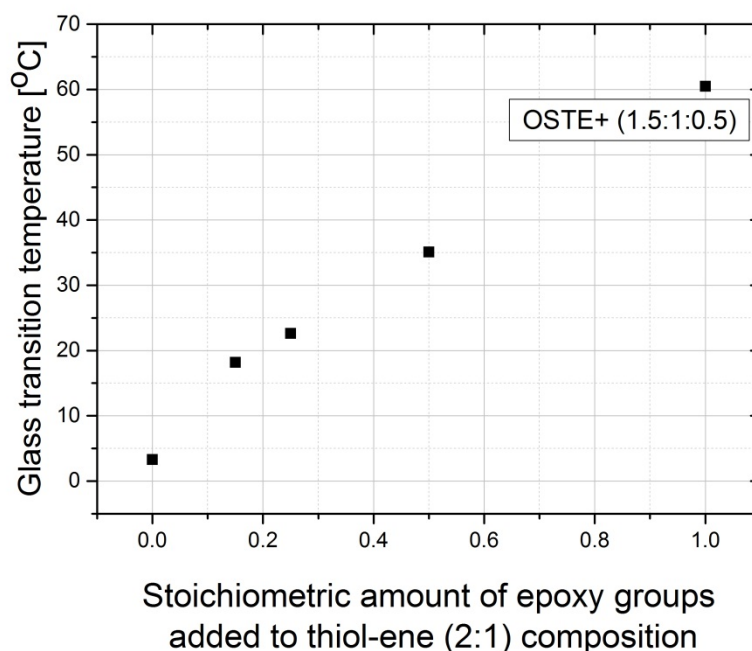
**Figure 2.1.6.** Glass transition temperatures of different OSTE compositions.



**Figure 2.1.7.** FTIR spectra of OSTE compositions with  $r=2.0$  and  $r=0.5$ .

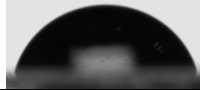


Due to the fact that the thiol-ene reaction is initiated at the mercapto groups, a composition with excess thiol groups was chosen for fabricating microfluidic chips. It is believed that grafting allyl containing compounds onto thiol-containing surfaces provides higher grafting selectivity, since active thiyl radicals, when fixed permanently to the polymer surface, cannot migrate, and hence the grafting reaction will take place on the UV-exposed area exclusively, which is an essential feature for preparing double emulsions in flow-focusing systems. Nevertheless the composition used for preparing the chip did not provide sufficient adhesion between the chip wafers, which in turn caused leakages when pumping liquids through the channels. Adhesion tests between different TATATO and PETMP compositions, as presented by Sikanen et al.,<sup>95</sup> reveal that the highest physical bond strength is achieved for formulations with excess allyl groups and for a combination of two different wafers (one wafer with excess allyl and one with thiol groups). For the intended application, none of the described systems showed sufficient adhesion, and therefore a third compound (BADGE, see Figure 2.1.5) was introduced to the matrix, thereby making it a dual-cure polymer composition – as described by Saharil et al.<sup>96</sup> The new three-component formulation is abbreviated as OSTE+. In the dual-cure process a mixture of monomers was degassed, cast onto a PDMS mirror-image mould and UV-irradiated for a reaction between the thiol and allyl groups to take place. Afterwards, both chip wafers were demoulded and assembled together, thus avoiding the formation of air voids. No heating prior to demoulding was necessary due to the flexible nature of PDMS and the fact that the discussed OSTE+ composition after the UV-cross-linking step has  $T_g$  below room temperature. Therefore separation of chip wafers from the mould did not generate additional preparation steps as described by others.<sup>92</sup> The assembled wafers were then exposed to elevated temperatures (80 °C for 2 hours), where the reaction between the epoxy groups and

the remaining thiol groups took place both in the bulk as well as at the wafer/wafer interface. The thiol-epoxy reaction was catalysed by 1,5-diazabicyclo-[4,3,0]-non-5-ene (DBN), which was added to the system in minor amounts. Different reactive group molar ratios between PETMP, TATATO and BADGE were investigated and analysed in terms of DSC. Bonding strength between the two assembled chip wafers was determined from organoleptic observations. Glass transition temperatures of the tested formulations showed increasing values in line with the increasing addition of BADGE into the initial thiol-ene composition, which was kept at a constant thiol/allyl ratio of  $r=2.0$  (see Figure 2.1.8). It was realised that by adding a small amount of BADGE (stoichiometric ratio of thiol:allyl:epoxy groups 2:1:0.15), the glass transition temperature increased from around 2 °C to almost 20 °C and further to around 25 °C and 35 °C for samples with stoichiometric ratios of 2:1:0.25 and 2:1:0.5, respectively. As a reference point, a composition with molar ratio of 1.5:1:0.5, as reported by Saharil,<sup>96</sup> was prepared and also tested in terms of differential scanning calorimetry. As expected, the glass transition temperature of this formulation showed the highest value (around 60 °C), due to the fact that all functional groups reacted and left no dangling chains in bulk. Analogously, an increase in stiffness was observed in line with an increasing amount of BADGE in the system, followed by improved bonding strength between the wafers. For purposes of this approach optimal properties were obtained for the 2:1:0.15 OSTE+ formulation, which showed improved adhesion between the wafers and additionally provided the highest amount of unreacted thiol groups on the surface – an important factor for further surface patterning.



**Figure 2.1.8.** Glass transition temperatures of different OSTE+ compositions (OSTE+ (1.5:1:0.5) as reference sample).

As presented in Figure 2.1.3, in order to prepare a water-oil-water emulsion it is desirable to create a microfluidic chip with one hydrophobic and one hydrophilic junction. To achieve this aim, thiol groups remaining on the surface of the OSTE+ composition react with different vinyl containing compounds and their influence on surface wettability is investigated. Surface patterning follows the same thiol-ene reaction mechanism, and therefore if more accurate surface modification is desirable, it is more effective to graft vinyl-containing compounds onto thiol-containing surfaces – and not vice versa. The grafting reactions were performed on the OSTE+ films by immersing them in 10 wt.% solutions of different vinyl compounds in absolute ethanol along with the addition of 2,2-dimethoxy-2-phenylacetophenone (DMPA) as a photoinitiator. Reactions were carried out at a UV-light (365 nm) intensity of around 4 mW/cm<sup>2</sup> for 15-20 minutes, to ensure the full conversion of thiol groups. It has been reported that the solvent-mediated thiol-ene grafting reaction can be accelerated significantly by applying UV-light of higher intensities.<sup>98</sup> A series of grafting reactions was performed in order to reveal the most suitable compounds that would effectively and permanently change the wetting properties of the material to the highest possible levels of hydrophobicity and hydrophilicity, respectively. Different grafting conditions were additionally tested in order to determine the most efficient grafting procedure. Experiments showed that increasing the amount of photoinitiator, from 0.5 to 3 wt.%, did not improve grafting efficiency. Furthermore, Lucirin TPO-L proved to be an effective photoinitiator for grafting reactions when ethanol and isopropanol were used as reaction media. Different solvents (e.g. ethanol, isopropanol, toluene, heptane) used for surface modification reactions showed comparable contact angles albeit with one exception, where it was found that acrylic compounds tend to homopolymerise when toluene is used as a solvent. After just 3-4 minutes of UV-irradiation, a grafting solution changed colour from transparent to white, which indicates the progressing homopolymerisation of acrylic monomers. Increased concentrations of grafted compounds also did not improve grafting efficiency in the investigated range. Same water contact angles for concentrations between 3 and 10 wt.% were obtained. Results of the experiments, supported by static contact angle measurements, are presented in Figure 2.1.9, and the structural formulas of the two grafted compounds that alter the surface properties most efficiently are shown in Figure 2.1.10. The best results regarding obtaining the highest hydrophilicity were acquired through grafting allylmalonic acid (AMA). The grafted surface was subsequently flushed with a 0.01 M NaOH solution, performed in order to replace the protons of AMA carboxyl groups with sodium cations, which resulted in a significant increase in hydrophilicity. The highest hydrophobicity was obtained for 2:1:0.15 OSTE+ grafted with 2,2,3,3,4,4,5,5,6,6,7,7-dodecafluoroheptyl acrylate (DFHA), where the static contact angle increased from 74.1° for a neat sample to 100.6° for a modified sample. This value could be increased even further by grafting DFHA onto a 2:1:0.25 OSTE+ sample, which showed a static contact angle of 106.3° ± 0.4°.

		
Neat OSTE+ sample	Grafted with DFHA	Grafted with allyl-malonic sodium salt
$74.1^\circ \pm 0.5^\circ$	$100.6^\circ \pm 1^\circ$	$35.2^\circ \pm 1.2^\circ$

Compound	Contact angle	Compound	Contact angle
ATFA	$88,3^\circ \pm 1,6^\circ$	PFD	$89,8^\circ \pm 1,8^\circ$
APFB	$87,9^\circ \pm 4,5^\circ$	PEG	$49,4^\circ \pm 1,7^\circ$

**Figure 2.1.9.** Wetting properties of 2:1:0.15 OSTE+ samples grafted with different compounds in terms of static contact angle.

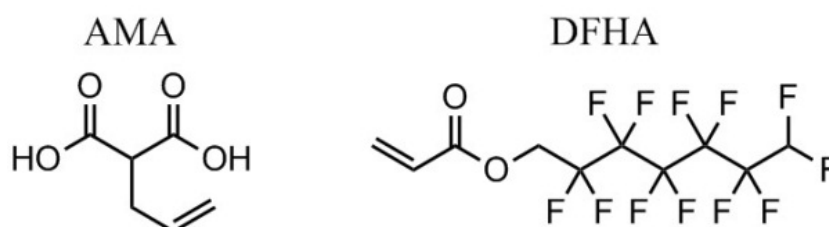


**Figure 2.1.10.** Structural formulas of allylmalonic acid and 2,2,3,3,4,4,5,5,6,6,7,7-dodecafluoroheptyl acrylate.

Surface selectivity of the grafting reactions was finally proved by performing two-step surface patterning. The OSTE+ polymer film was first immersed in the DFHA ethanol solution with the addition of DMPA, while half of the film was covered with a stencil mask (black rubber film), thus preventing it from reacting when the sample was subsequently exposed to UV-light. After the first surface modification step was complete, the polymer film was thoroughly washed with a substantial amount of ethanol and blow-dried with N<sub>2</sub>. In the second step the sample was immersed in AMA solution but this time covering the already grafted half with the stencil mask and exposed to UV-light (a schematic illustration of the full process is in Figure 2.1.11). Afterwards the polymer film was cleaned again, flushed with 0.01 M NaOH solution and then blow-dried. Static contact angle tests performed on both sides of the sample proved the validity of the two-step grafting process, by providing contact angle values comparable to results obtained from the simple surface modification process. The two-step surface patterning process was applied to the modification of the microfluidic chip channel surfaces, though the grafting reactions took place within chip channels exclusively after both wafers were covalently bonded.



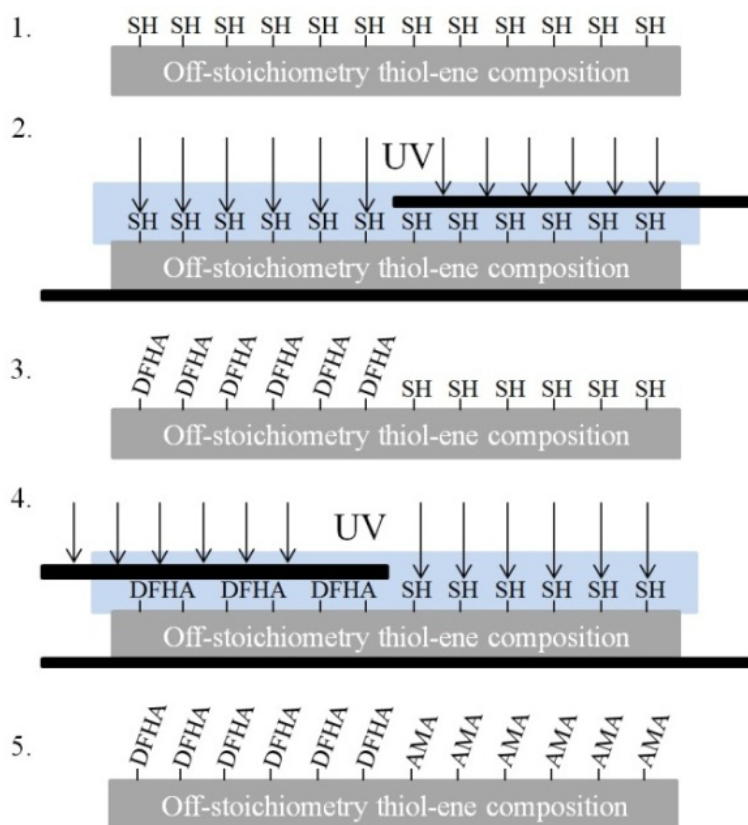


**Figure 2.1.11.** Schematic illustration of the two-step surface patterning of the OSTE+ polymer film. SH represents unreacted thiol groups present on the polymer surface that subsequently react with DFHA and AMA in separate steps of the surface patterning process.

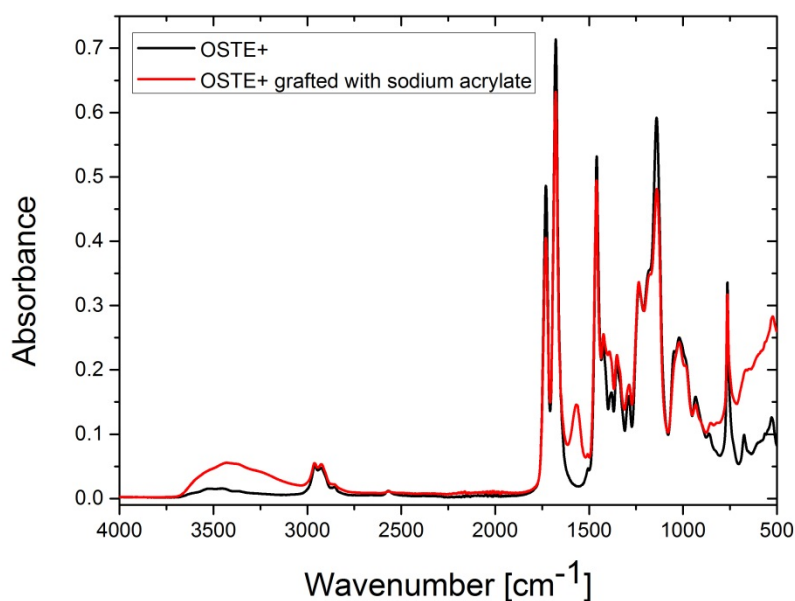


**Figure 2.1.12.** ATR FTIR spectra of OSTE+ and OSTE+ grafted with sodium acrylate, presenting changes in absorbance at wavenumbers of  $2550\text{ cm}^{-1}$ ,  $1565\text{ cm}^{-1}$  and  $1425\text{ cm}^{-1}$ .

The progress of the grafting reactions was monitored by ATR FTIR. It was shown that the grafting reaction of small molecules takes place not only on the surface of the material but also, to some extent, in bulk, which is attributed to the fact that the polymer network contains a substantial amount of dangling chains due to the relatively high off-stoichiometry ratio of the initial composition. The FTIR analyser beam usually penetrates through the first few microns of tested samples, so the spectra obtained should – in principle – show a small peak for the thiol group at the wavenumber of  $2550\text{ cm}^{-1}$ , as it is in the case of the initial network. Spectra obtained, for example, for OSTE+ grafted with sodium acrylate show no peaks in that region. Additionally, other strong peaks are to be observed at different wavenumbers, for example stretches typical for carboxylic salts at around  $1565\text{ cm}^{-1}$  and  $1425\text{ cm}^{-1}$  (Figure 2.1.12), which was shown by Gonzalez et al.<sup>99,100</sup> In the case of grafting larger molecules, such as DFHA, there are no significant changes in FTIR spectra, although contact angle measurements show substantial divergence in wetting properties.

### 2.1.2.3. Formation of a single emulsion

Separately controlled Harvard Apparatus 11 plus syringe pumps were used to introduce liquids to the microfluidic chip. The formation of a single emulsion was performed using inlets 1 and 2. Inlet 3 was plugged, which consequently blocked all liquid transfers through this connector (see Figure 2.1.3). Two component Sylgard 184 silicone kit mixed to a ratio of 3:2 (base:cross-linker), was used as the dispersed phase ( $\eta=1080\text{ mPa}\cdot\text{s}$  at shear rate of  $0.1\text{ 1/s}$ ) and injected into the system through inlet 2, while sodium dodecyl sulfate/polyvinyl alcohol (SDS/PVA) aqueous surfactant solution (3 wt.% and 1 wt.%, respectively) was used as a carrier phase and was injected through inlet 1 ( $Q_1 > Q_2$ , where  $Q$  corresponds to the flow rates of liquids). Droplet formation took place at junction A. Initial flow rates for each experiment were  $10\text{ mL/h}$  and  $1\text{ mL/h}$  for  $Q_1$  and  $Q_2$ , respectively (initial droplet diameter was  $250\text{ }\mu\text{m}$ ). Depending on liquid flow rates single emulsions of different droplet sizes (between  $100$  and  $425\text{ }\mu\text{m}$ ) and very narrow size distributions were obtained (see Figure 2.1.13). In order to obtain smallest droplet size, the outer phase was injected at a flow rate of  $50\text{ mL/h}$ . By increasing the flow rate even higher to  $100 - 200\text{ mL/h}$  the size distribution of spheres was significantly broadened. Nonetheless no leakages were observed. As an alternative method for altering droplet diameters, different carrier phase compositions were applied. Modifying the viscosity of the outer phase, which in this case could be done by increasing surfactant concentrations, works in favour of decreasing sphere sizes. As a result the range of sphere sizes can be shifted towards lower diameters. This effect can be achieved, for example, by increasing the amount of PVA, which substantially influences the viscosity of the solutions.

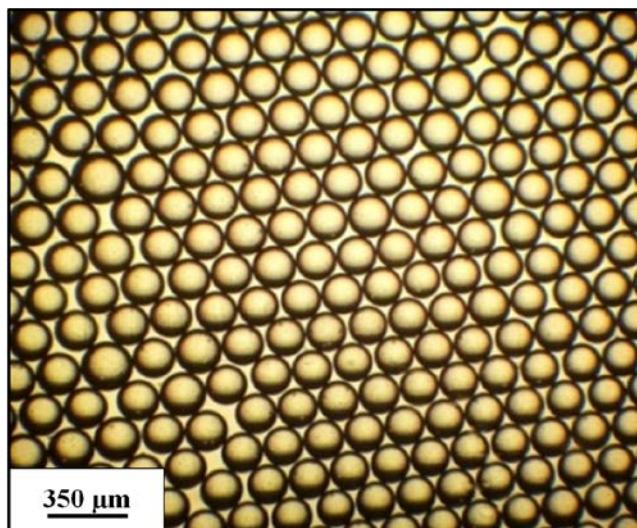


**Figure 2.1.13.** Microscope image of silicone in water single emulsion obtained on junction A.

#### 2.1.2.4. Formation of a double emulsion

Three liquids have to be introduced to the microfluidic chip in order to obtain core-shell microspheres. In this study various approaches are presented where deionised water, ionic liquid (2-hydroxyethylammonium formate), ethanol, isopropanol and different water/glycerol mixtures were used as the inner phase of double emulsions. In each experiment a Sylgard 184 silicone kit, mixed to a weight ratio of 3:2 (base:cross-linker), was used as the middle phase and water with various surfactants as the outer phase.

In the first experiment water was used as the inner phase of the double emulsion and SDS, PVA water solutions (3 wt.% and 1 wt.%, respectively) as the outer phase. In the first step the outer phase liquid is introduced to the chip via inlet 1 (see Figure 2.1.3), followed by introducing the middle phase ( $Q_1 > Q_2$ ). Initial flow rates were  $Q_1=10$  mL/h and  $Q_2=1$  mL/h. As a result silicone droplet formation takes place at junction A and, as in the single emulsion case described paragraph above, droplets size is determined by the outer phase liquid flow rate. After a stable and mono-dispersed single emulsion is obtained, the inner phase is introduced to the chip via inlet 3 ( $Q_1 > Q_2 > Q_3$ ).  $Q_3$  is slowly increased until the desired core-shell morphology with designed core and shell dimensions is obtained. The resulting double emulsion is collected via the outlet of the microfluidic chip and then left for the cross-linking reaction of the PDMS shell to take place. The study confirmed that, as in case of low viscosity liquids,<sup>101,102</sup> the higher viscosity liquids investigated in this approach can also be used successfully in flow-focusing microfluidic chips. Additionally in these systems, core-shell microsphere dimensions can also be altered by varying the flow rates of injected liquids. Results of encapsulating water within a PDMS shell can be seen in Figure 2.1.14.

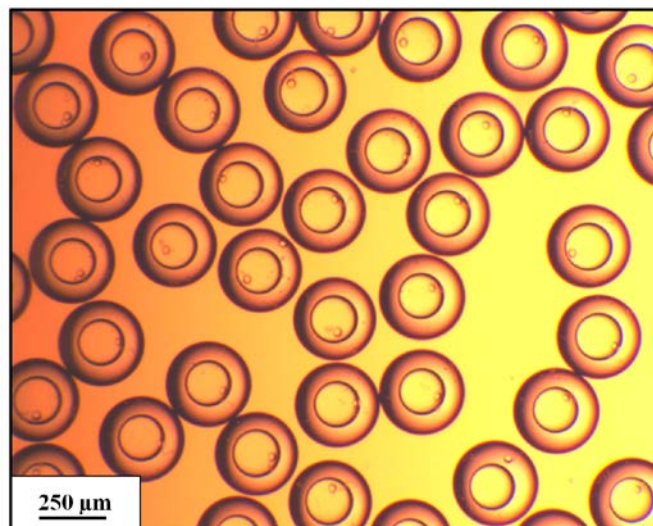


**Figure 2.1.14.** Optical microscopy image of a water-in PDMS-in water double emulsion.

The 2-hydroxyethylammonium formate was then used as a core material for the microcapsules, where PDMS was used as a shell material. The process for preparing the microcapsules followed the same scheme as in the water encapsulation case, whereby injection of the outer phase was followed by injection of the middle and then inner phases. An example of an acquired double emulsion can be seen in Figure 2.1.15. Again, microcapsules of narrow size distribution were obtained, which proves that the flow-focusing microfluidic system presented in this study is a versatile method of encapsulation and can be applied to a broad range of materials. It was observed that by using IL (reported viscosity  $\eta=118$  mPa.s)<sup>97</sup>, microcapsules of smaller diameters in comparison to water-core spheres were obtained. Attempts to encapsulate ethanol, isopropanol and different water and glycerol mixtures within a PDMS shell also resulted in the formation of microcapsules of very narrow size distribution, which again proves the versatility of the microfluidic system.

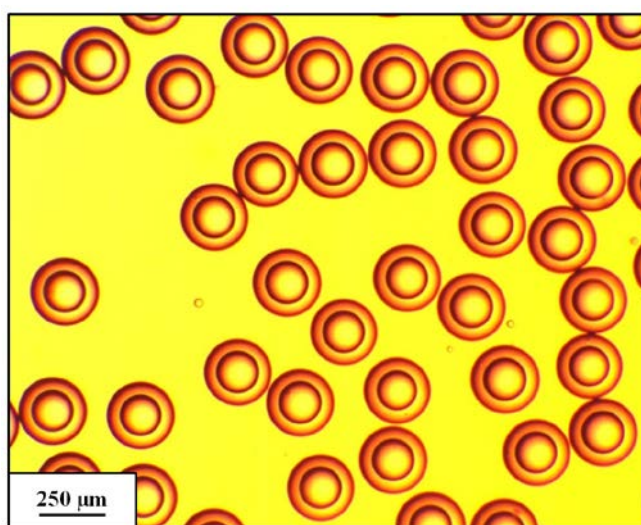


**Figure 2.1.15.** Optical microscopy image of a 2-hydroxyethylammonium formate-in PDMS-in water double emulsion.

Size distribution of spheres in single and double emulsions was obtained by measuring diameters of at least 100 droplets. An average size and standard deviation were determined for each experiment. That allowed for calculations of coefficients of variation (CV), which were proved to be held at substantially low values ( $CV < 3\%$ ) for all experiments. An example of size distribution of water-in PDMS-in water emulsion is presented in Figure 2.1.16.

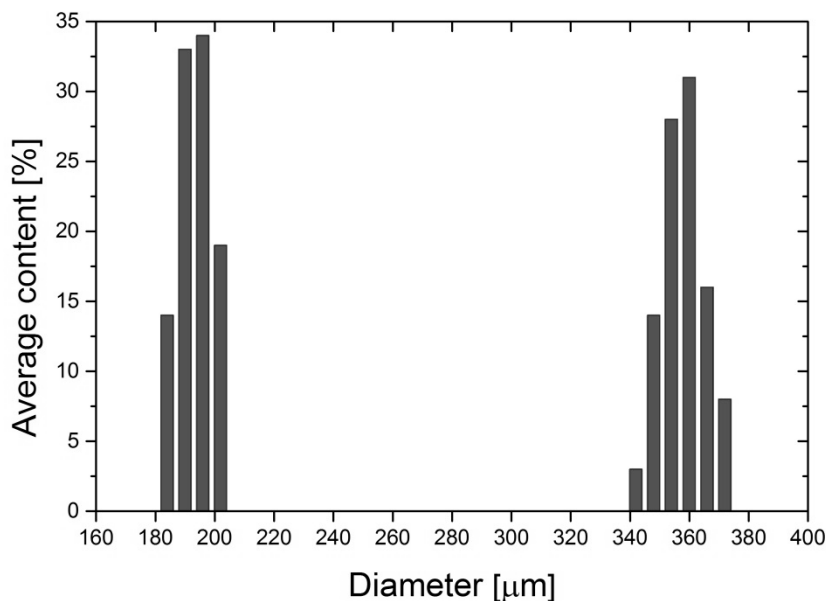


**Figure 2.1.16.** An example of a size distribution of capsule cores (left columns) and capsules (right columns) obtained from the water-in PDMS-in water double emulsion.

The curing process for core-shell microspheres has been tested and optimised at example of water-in PDMS-in water double emulsion. The acquired double emulsion was collected into a beaker containing a water solution of SDS and PVA (3 wt.% and 1 wt.%, respectively) under constant stirring with a magnetic stirrer, which prevents the double emulsion from forming microcapsule aggregates. The collected capsules were left for 24 hours at room temperature for the PDMS composition to be cross-linked and then form a solid shell. Increasing the temperature at this stage effectively accelerates the curing process, although too high temperature results in disruption to the double emulsion and causes a collapse in microcapsules. The solution containing solid-shell capsules was heated up to 70 °C to ensure full cross-linking of the material.

After each use, the microfluidic chip was thoroughly flushed with soap water, ethanol and heptane, and then once again with ethanol in order to remove possible PDMS residues and other impurities from the chip channels. This allows for the multiple use of a single chip and maintains surface properties, even up to several months and potentially longer. Experiments show that flushing the channels with soap water and ethanol only significantly lowers the lifetime of the chip. This appears to be a big advantage of this system over microfluidic devices based on PDMS, where

surface properties and wafer bonding are usually achieved through plasma treatment, thereby causing temporary effects only.

### **2.1.3. Conclusions**

A flow-focusing microfluidic device based on thiol-ene “click” chemistry was designed and fabricated. Due to the applied chemistry, physical and chemical properties of the chip could be adjusted to the intended application of producing elastomeric microcapsules. As a result it was possible to modify chemically the microfluidic chip channel surfaces in a controlled way and additionally to prevent any leakages while pumping liquids through the channels at very high flow rates. The developed system is an efficient tool for preparing core-shell microspheres of extremely narrow size distribution with tunable core diameters and shell thicknesses. The study successfully demonstrated that very different liquids can be encapsulated within a PDMS shell where the only limitations are surface tension between liquids and their viscosities. The developed microfluidic device additionally has a very long lifespan, which efficiently saves time when conducting experiments on double emulsions. The versatility of the design creates a robust basis for fabricating new flow-focusing microfluidic devices for forming any type of core-shell microspheres for various applications. It is believed that encapsulating liquid substances within soft PDMS shells is a great step towards self-healing elastomeric materials.

## **2.2. Dielectric and mechanical properties of water-silicone composites**

### **2.2.1. Introduction**

In this chapter the preparation and characterisation of water-filled PDMS composites is discussed. The produced water-core PDMS-shell microcapsules (described in Chapter 2.1) are used as a high-dielectric constant filler. Consequently, incorporating the capsules is expected to increase the overall relative permittivity of prepared PDMS films. Mechanical and dielectric properties of composites will be discussed with respect to filler content. Additionally, the morphology of the prepared samples will be evaluated with the help of optical microscopy. The results of these experiments were reported in a SPIE 2014 conference proceedings paper “*Novel encapsulation technique for incorporating high-permittivity fillers into silicone elastomers*”.

The presence of water in polymeric materials leads to an increase in conductivity (water itself does not exhibit significant conductivity; however, due to the unavoidable presence of ions, water is a good conductor). On the other hand, it is believed that if an insulating layer around each portion of embedded water is formed, the overall increase in conductivity will be hindered. Therefore, it is expected that the dielectric constant of liquid-filled elastomers will increase as a function of water content, whereas conductivity as well as dielectric losses will remain unaffected.

### **2.2.2. Results and discussion**

#### **2.2.2.1. Morphology of the composites**

The produced core-shell microspheres used for the preparation of composites had an average diameter and a core diameter of 350  $\mu\text{m}$  and 200  $\mu\text{m}$ , respectively (Figure 2.2.1). These relatively large dimensions for the microcapsules, compared to the designed film thickness, result from technical limitations of the microfluidic chip and the viscosity of the middle phase in double emulsion, which in this case was an off-stoichiometric mixture from a Sylgard 184 silicone kit. It is believed that by decreasing the dimensions of microfluidic chip channels and introducing liquids of lower viscosities, smaller microcapsules can be obtained.

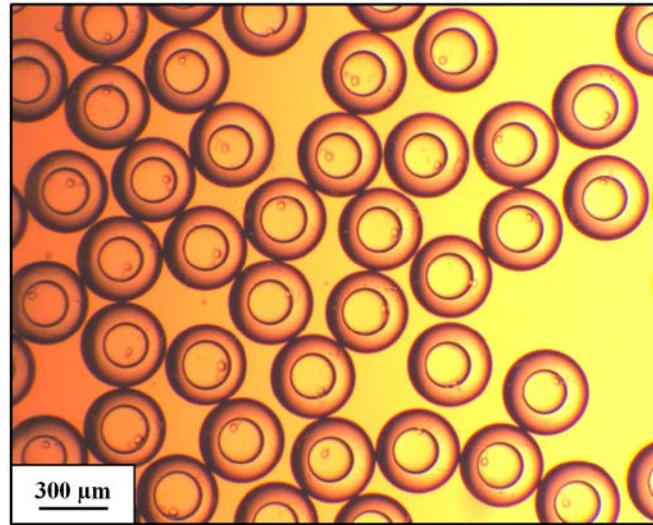


**Figure 2.2.1.** Optical microscopy image of the microcapsules obtained from a water-in silicone-in water double emulsions.

Various amounts of dried liquid core microcapsules were mixed with a commercial PDMS composition (Sylgard 184) and carefully transferred onto a metal mould with a 1 mm thick spacer. The material was finally cured at 40 °C for 5 hours and additionally left overnight at room temperature for possible post-curing to take place. The PDMS cross-linking process was kept at the lowest possible temperatures, in order to avoid evaporating the encapsulated water which, due to relatively high vapour pressure, tends to migrate through the thin silicone shell. The microcapsules were mixed at various weight ratios (10, 20, 30) with a Sylgard 184 silicone kit mixed at a ratio of 13:1 (base:cross-linker) (all formulations are listed in Table 2.2.1), thereby forming free-standing films. Significant excess of vinyl groups in the PDMS composition allows covalent bonding between the PDMS network and the PDMS shell of microcapsules possessing excess silicone hydrides.

**Table 2.2.1.** Sample names of various composites with different amounts of incorporated core-shell microspheres and corresponding amounts of encapsulated filler.

Sample name	Amount of microcapsules incorporated into PDMS film [wt.%]	Amount of filler (water) incorporated into PDMS film [wt.%]
S184_13:1	0	0
S184_13:1_10	10	1.5
S184_13:1_20	20	3
S184_13:1_30	30	4.5

Optical microscopy images confirm that the microcapsules were well distributed and that water was still present in the capsules, although the samples were exposed to elevated temperatures during the PDMS cross-linking process. Black spots that can be seen in Figure 2.2.2 correspond to air bubbles, which indicates that, to some extent, water evaporated from the core of the spheres. This is a result of the relatively high gas permeability of PDMS and high water vapour pressure.<sup>103</sup>



Nonetheless, the fraction of empty capsules is acceptable, and in the case of samples with smaller amounts of filler it becomes negligible. Specimens with higher microcapsule content are influenced more by emerging air voids, since the percentage amount of filler in the polymer film becomes larger.

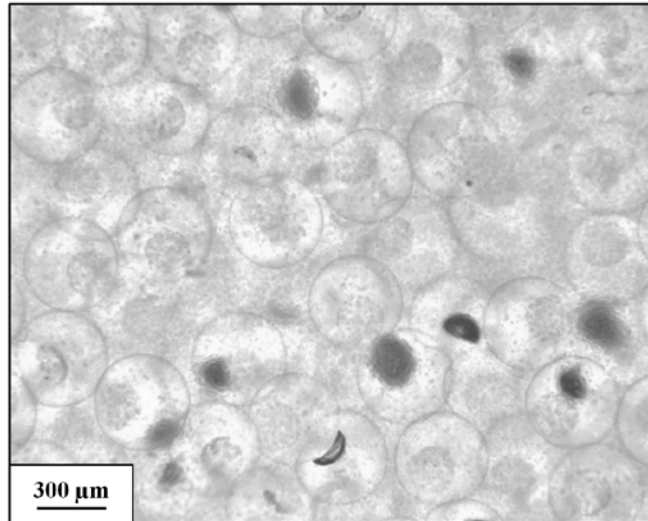


**Figure 2.2.2.** Microscope image of a cross-linked PDMS film with incorporated core-shell microspheres. Dark spots present in the matrix correspond to air voids.

#### 2.2.2.2. Mechanical properties

The prepared films are stable and free-standing at the current film thicknesses and have considerable strength when handling them. This implies that there is a significant cross-linking of the microcapsules into the elastomer. Frequency sweep tests were conducted in order to determine the viscoelastic properties of the prepared composites and to characterise how increasing amounts of core-shell microspheres influence mechanical properties. Rheology measurements were carried out on four different specimens, and results summarising changes in the storage modulus and the loss factor ( $\tan \delta$ ) as a function of frequency were plotted in Figure 2.2.3. The curves representing storage and loss moduli prove nearly identical viscoelastic behaviour for all compositions. In all cases the elastic modulus at the plateau region ( $10^{-1} - 10^{-3}$  Hz) varies from 55 kPa to 60 kPa. These small differences are within the range of measurement error, and so it can be assumed that incorporating core-shell microspheres does not influence significantly the viscoelastic behaviour of the tested PDMS composition. Mechanical properties of the composition forming microcapsule shell (S184\_3:2) is presented in Figure 2.2.3 for comparison.

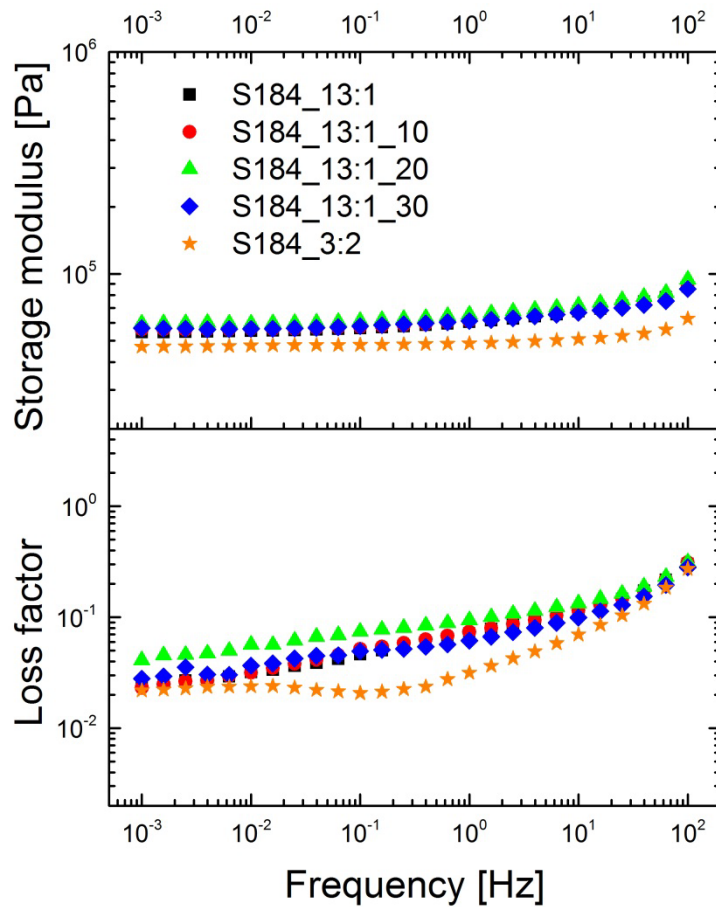


**Figure 2.2.3.** Storage modulus and loss factor for the unfilled elastomer and different PDMS-microcapsule composites obtained from frequency sweep tests performed at a controlled strain mode of 2% strain.

### 2.2.2.3. Dielectric spectroscopy measurements

Results from investigating the dielectric properties of the produced composites are summarised in Figure 2.2.4. The dielectric constant of the PDMS was increased successfully by incorporating water-core microcapsules. Values measured at a frequency of 1 kHz indicate an increase from 2.8 for the unfilled network to 3.6 for a composite containing 30 wt.% of microcapsules (4.5 wt.% of water). These are very promising values in the context of a possible decrease in the dielectric constant, caused by the presence of air voids in the structure – a higher amount of air bubbles for the higher loading of microcapsules in the sample. By eliminating empty microcapsules dielectric permittivity is expected to increase even more, thus making water-PDMS composites competitive against other high-permittivity DEs.

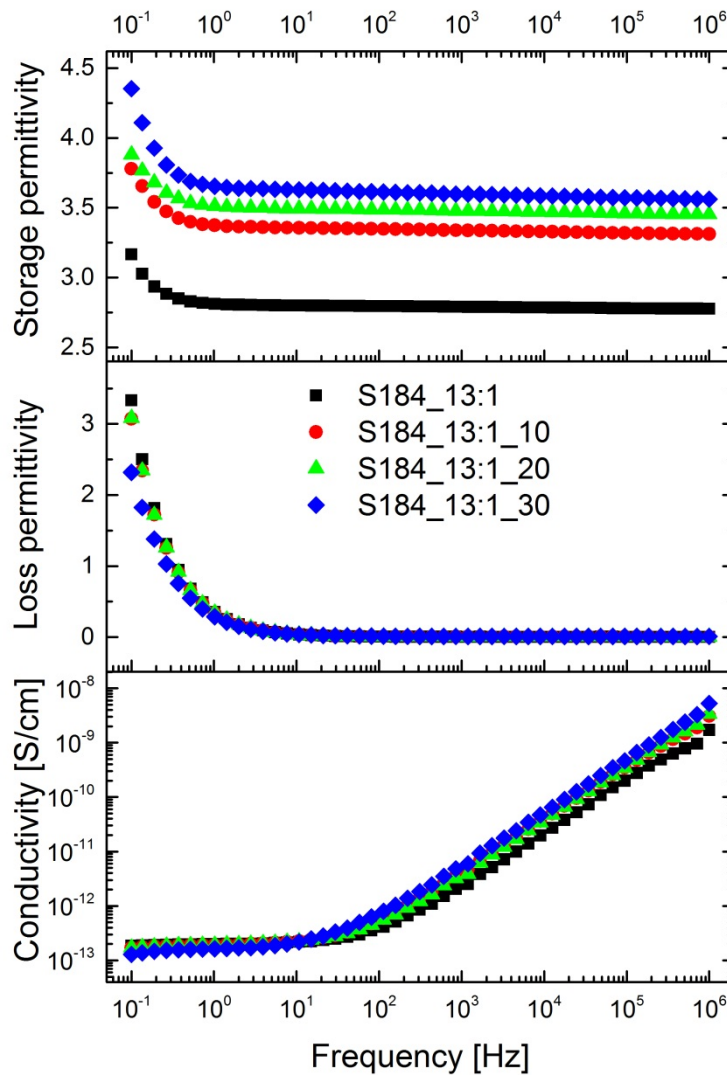


**Figure 2.2.4.** Relative permittivity, dielectric loss and conductivity of the elastomer reference and different water-PDMS composites measured at room temperature.

Conductivity was proven to remain at nearly the same level for all tested compositions (Figure 2.2.4), although small deviations can be observed in the high-frequency region. As expected, the lower the filler loading, the lower the conductivity. Each portion of water in the investigated systems was hermetically encapsulated within a PDMS insulating shell and therefore conductive pathways throughout the material were unlikely to appear and wherefore the overall conductivity remained almost unaffected.

At this point it was decided to refrain from investigating PDMS-microcapsules composites in terms of breakdown strength. It has been reported that the dielectric strength of materials generally decreases in line with increasing film thickness.<sup>68</sup> Additionally, DEA membranes are usually much thinner (even 10 – 20 times) than the films prepared in this approach. Therefore, breakdown strength values would not be comparable with the results presented for thinner films.

### 2.2.3. Conclusions

In this study a method for incorporating water into silicone elastomer, in the form of encapsulated droplets, was presented. The technique proved not to influence the mechanical properties of the resulting composites. Importantly, the discussed results proved the validity of a hypothesis that the dielectric constant of an elastomer can be enhanced by introducing high-permittivity polar liquids to its structure. Furthermore, the presence of water did not significantly influence the dielectric losses and conductivity of the obtained composites. The outcome of this approach is of great importance with respect to future work in which higher amounts of liquids are intended to be incorporated.

Although this pioneering attempt to incorporate polar liquids into a silicone network produced very promising results, there are many parameters and steps in the preparation procedure that require further optimisation. The prepared films suffer from relatively high thicknesses, which is directly determined by the diameters of the produced capsules. It is expected that through incorporating smaller microcapsules with thinner shells, and by eliminating hollow spheres, the overall performance of this type of composite can be enhanced further. Furthermore, a problem with the high water permeability of PDMS was exposed. It is believed that water has to be replaced with a low-vapour pressure liquid, in order to eliminate the problem of filler evaporation.

### 3. One-step preparation of liquid-containing PDMS composites

The potential of water-containing PDMS composites was revealed in Chapter 2. Yet, this proof of concept study was only a first step in the development of elastomers filled with polar liquids in the form of discrete droplets. Importantly, the study made it possible to recognise aspects that need to be considered when designing liquid-containing elastomers. It has been established that the high gas permeability of silicones limits the range of liquids that can be incorporated into the elastomer, which became one of the major parameters when selecting liquids for this particular application. Due to its high-dielectric constant, accessibility, low price and negligible vapour pressure, glycerol became a substance that will be thoroughly investigated in the next sections.

A milestone was reached when a new method for incorporating liquids into PDMS elastomers was discovered. Counterintuitively, it appeared that when a PDMS pre-polymer composition and glycerol were mixed, by applying sufficiently high shear forces, stable glycerol-silicone emulsions were obtained. The emulsions became a basis for creating glycerol-PDMS hybrid elastomers. Upon cross-linking the pre-elastomer, free-standing two-phase materials were obtained, as presented in Figure 3.0. The discovery of this process completely changed the previously envisioned concept of incorporating polar liquids into silicones. The new method was proved to be very simple and robust, thus allowing for incorporating significant amounts of liquids into various PDMS compositions. The technique itself, as well as the multiple counterintuitive properties of the obtained elastomers, are revealed and evaluated in Chapter 3.1, while the dielectric properties and usefulness of liquid-PDMS hybrids are discussed in detail in Chapters 3.2 and 3.3. Various polar liquids and silicone compositions are thoroughly investigated in order to find the best candidates for the DEAs.

The preparation procedure for composites is discussed thoroughly in Chapter 3.1. The same procedure is then applied in approaches described in Chapter 3.2 and Chapter 3.3, unless stated otherwise.

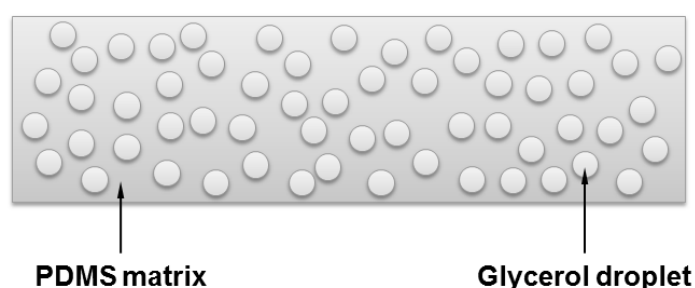


**Figure 3.0.** Schematic visualisation of an elastomer cross-section with incorporated discrete glycerol droplets.

### 3.1. Green silicone elastomer obtained from a counterintuitively stable mixture of glycerol and PDMS

#### 3.1.1. Introduction

Non-toxic, energy saving, biodegradable, made from recycled materials or renewable resources, made from industrial or agroforestry residues – the qualification list for a polymer to be regarded as “green” is very long. Thus, fulfilling more than one of them generally leads to multiple issues in material preparation procedures, and it usually also compromises the material’s ultimate properties.<sup>104</sup> Research on eco-friendly plastics has become one of the main targets of modern industry,<sup>105–108</sup> and the prospect of an oil shortage motivates the material industry to look into innovative sources. Ideal alternatives to traditionally synthesised monomers seem to be substrates of natural origin; therefore, extensive investigations into the usefulness of bio-based monomers, as well as natural fillers (e.g. fibres), have been conducted successfully.<sup>109–113</sup> Nonetheless, not many reports have been presented on green elastomers. The significant extensibility of these materials is a very unique property that requires an uncompromised balance of physical and chemical properties in their structure, and so the task of preparing commercially attractive elastomers is a highly complicated procedure. Nevertheless studies exist representing successful attempts at using bio-based substrates and incorporating them into elastomers. An interesting example was presented by Brook et al., who employed softwood lignin, acting as a cross-linker, and at the same time as a reinforcing agent in silicone elastomers.<sup>114</sup> Furthermore, other approaches have extensively investigated and finally improved the biodegradability of elastomers.<sup>115–118</sup>

Glycerol, as a residue of biodiesel production, offers great potential in the preparation of a new wave of green polymers. Considering the fact that biodiesel production in European Union increased fourfold between 2004 and 2008, and that 100 kg of glycerol is obtained from 1000 kg of biodiesel, it is believed that more attention should be devoted to research on glycerol-based polymers.<sup>119</sup> Thus, so far, multiple research groups have investigated the usefulness of this compound in organic chemistry and material science.<sup>120,121</sup> One common example of applying glycerol in polymer science is using it as one of the monomers in polymer synthesis.<sup>116,122,123</sup> Introducing glycerol into polymers as one of the substrates brings these materials closer to the definition of “green” polymers, although the amounts of glycerol used in such cases are usually insignificant compared to other reactants, whilst in addition the resulting polymers become significantly more expensive.

Adding solid fillers to elastomeric or non-elastomeric polymers is usually intended to improve material properties or decrease the overall price of the product. In either case, adding fillers significantly influences material features over time, i.e. product reliability is reduced.<sup>57</sup> For example, in the case of polydimethylsiloxane, incorporating silica particles is a fundamental process that allows for obtaining highly stretchable materials with good ultimate properties. On the other hand, incorporating rather inexpensive fillers, such as wood-dust, is a common procedure for decreasing a product’s price.<sup>124</sup> In this approach an innovative way of identifying the introduction of fillers into elastomers is presented. Additionally the possibility of using glycerol as a liquid filler of a polar nature incorporated into a commercially available, highly non-polar, silicone elastomer

was investigated. It was found that incorporating glycerol into PDMS does not compromise the ultimate strain of the material, thereby making it much cheaper compared to non-glycerol PDMS. Samples with different amounts of glycerol were prepared and extensively investigated in terms of their morphology and mechanical properties. The conducted experiments revealed and finally proved the great potential of this new type of green and cheap elastomer.

### 3.1.2. Sample preparation

**Table 3.1.1.** Glycerol – PDMS formulations with corresponding volume fractions.

Sample name	Amount of glycerol [phr]	Volume fraction of glycerol in the sample
S184	0	0
G10_S184	10	0.075
G20_S184	20	0.141
G30_S184	30	0.197
G40_S184	40	0.246
G50_S184	50	0.290
G60_S184	60	0.329
G70_S184	70	0.364
G80_S184	80	0.395
G90_S184	90	0.424
G100_S184	100	0.450
G110_S184	110	0.473
G120_S184	120	0.495
G130_S184	130	0.515
G140_S184	140	0.534

A dual asymmetric centrifuge SpeedMixer DAC 150 FVZ-K was used for mixing all of the compounds. The Sylgard 184 silicone kit was mixed in a 10:1 ratio by weight, as recommended by the manufacturer. Subsequently the desired amount of glycerol was added to PDMS and stirred with the help of the speed-mixer for 5 minutes at 3500 rpm, unless mentioned otherwise (3500 rpm is the maximum rotational speed of the device). No additional degassing of the formulations was necessary, due to the dual asymmetric method of mixing, which effectively pushes out entrapped air voids. The amounts of glycerol incorporated by mass, along with corresponding volume fractions, are presented in Table 3.1.1. Volume fractions were calculated based on densities available in the literature, which were  $1.03 \text{ g/cm}^3$  and  $1.26 \text{ g/cm}^3$  for Sylgard 184 and glycerol, respectively. After the mixing step, all compositions were cast onto a metal mould with a 1 mm spacer and cured at  $80 \text{ }^\circ\text{C}$  for 1 hour. Obtained films were then left at room temperature for at least two days, in order for eventual post-curing to take place. The abbreviation ‘phr’, used to describe glycerol content in all compositions, corresponds to glycerol weight amount per hundred weight parts of silicone rubber. Sample names were formed using the following pattern: GX\_Y\_Z, where G and X stand for glycerol and glycerol phr added to a PDMS pre-polymer, respectively. Y corresponds to applied

PDMS composition and Z stands for an additional supplement (e.g. the thinning fluid OS-20 discussed in Chapter 3.2 and Chapter 3.3).

### 3.1.3. Results and discussion

#### 3.1.3.1. Glycerol in PDMS emulsions and the morphology of cured samples

The morphology of glycerol in PDMS emulsions obtained by direct mixing the two virtually immiscible liquids was analysed with the help of optical microscopy. Proper mixing conditions were determined with a simple test, in which a composition of pre-polymer and glycerol was mixed at different speeds and increasing mixing times. It was found that an increase in shear forces has a tremendous impact on glycerol droplet size (see Figure 3.1.1), in that the higher the rotational speed, the more mono-dispersed emulsions are obtained. The maximum droplet diameter decreased from around 30  $\mu\text{m}$  to around 3  $\mu\text{m}$  for the same formulations mixed for 5 minutes at 1000 and 3500 rpm, respectively. Longer mixing times were proved to have a negligible impact on droplet size, though for each glycerol concentration a minimum mixing time that ensures obtaining an agglomeration-free emulsion is required. Therefore, most compositions were mixed for 5 minutes at 3500 rpm, which provided sufficient shear forces for obtaining reasonably mono-dispersed emulsions for a broad range of glycerol incorporated into PDMS.

The images shown in Figure 3.1.2 present various uncured compositions with increasing amounts of incorporated glycerol. Viscosities of the obtained emulsions measured at the shear rate of 0.1 1/s are presented in Figure 3.1.3. Produced mixtures were stable even several hours after mixing.

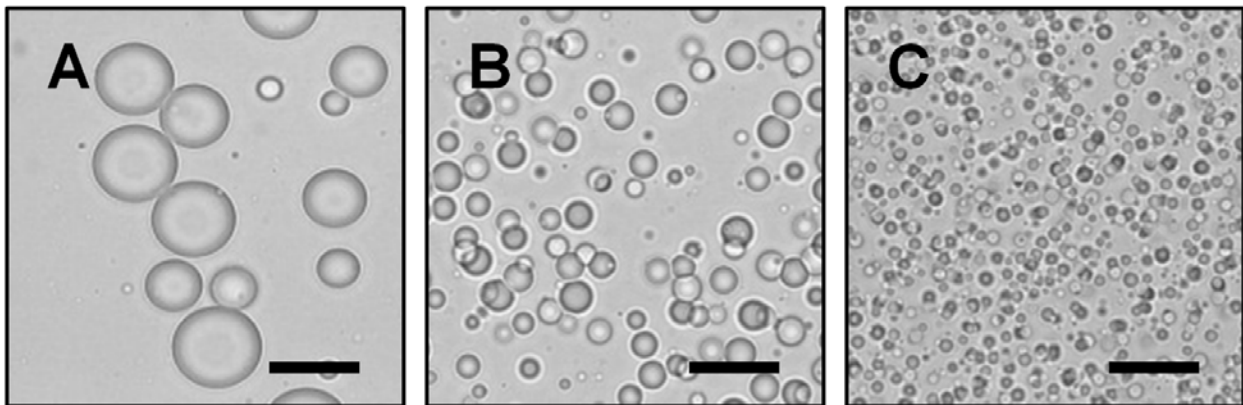


**Figure 3.1.1.** Optical microscopy images of 10 phr glycerol in S184 emulsions obtained after 5 minutes of speed-mixing at 1000 (A), 2000 (B) and 3500 (C) rpm. Scale bars for all images correspond to 25  $\mu\text{m}$ .



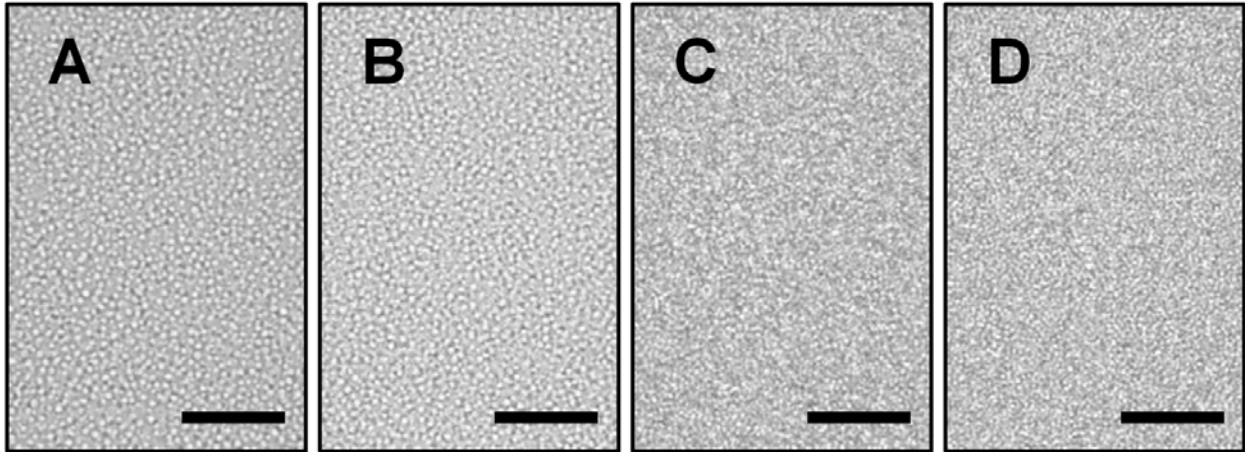


**Figure 3.1.2.** Optical microscopy images of glycerol in PDMS emulsions. A – 10 phr, B – 40 phr, C – 70 phr, D – 100 phr. Scale bars for all images correspond to 50  $\mu\text{m}$ .

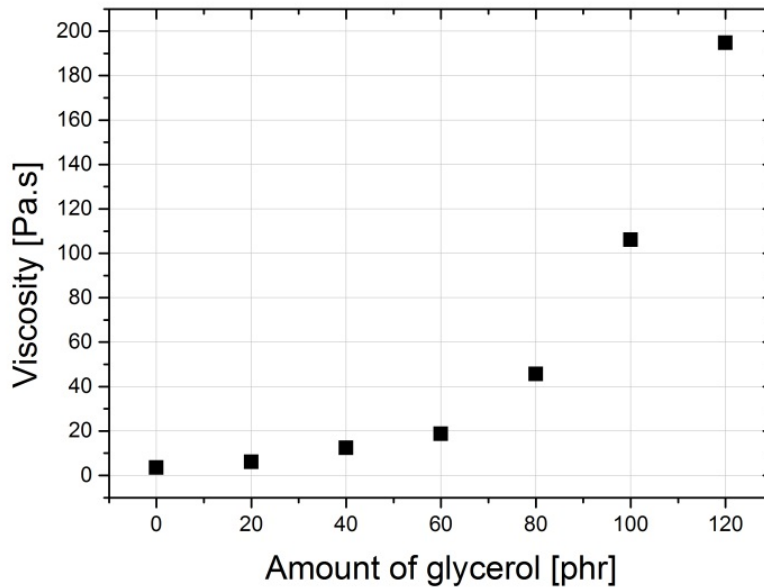


**Figure 3.1.3.** Viscosities of various glycerol-Sylgard 184 formulations measured at the shear rate of 0.1 1/s at room temperature.

Cross-sections of cross-linked composites were investigated through scanning electron microscopy. The images presented in Figure 3.1.4 show the cross-sections of four samples with 10, 50, 90 and 130 phr of incorporated glycerol, respectively. As can be seen, when the amount of glycerol increases, droplet concentration becomes higher; however, the average droplet size remains almost uninfluenced. It was additionally observed that while increasing the glycerol/PDMS ratio of formulations, a threshold concentration is finally reached above which a droplet-like morphology is no longer present in the cross-linked material. Instead, a network with interconnected glycerol channels is formed, which exhibits similarities to a gyroid morphology frequently reported for block copolymers and porous materials.<sup>125,126</sup> This phenomenon was additionally proved by testing the

conductivity of the compositions. Broadband dielectric spectroscopy tests showed that the sample with 140 phr of glycerol exhibited slightly increased conductivity compared to formulations with lower glycerol concentrations (see Figure 3.1.5). This is in agreement with expectations, since it is common knowledge that glycerol exhibits higher electrical conductivity than PDMS. Considering that glycerol molecules are no longer encapsulated by the PDMS matrix, it can be expected that higher conductivity paths will be formed throughout the material. This will lead finally to an overall conductivity increase in the material. Glycerol conductivity is additionally enhanced by the unavoidable presence of impurities such as ion-containing water. The increased conductivity is considered as a direct indication of the formation of a continuous glycerol phase in the elastomer.

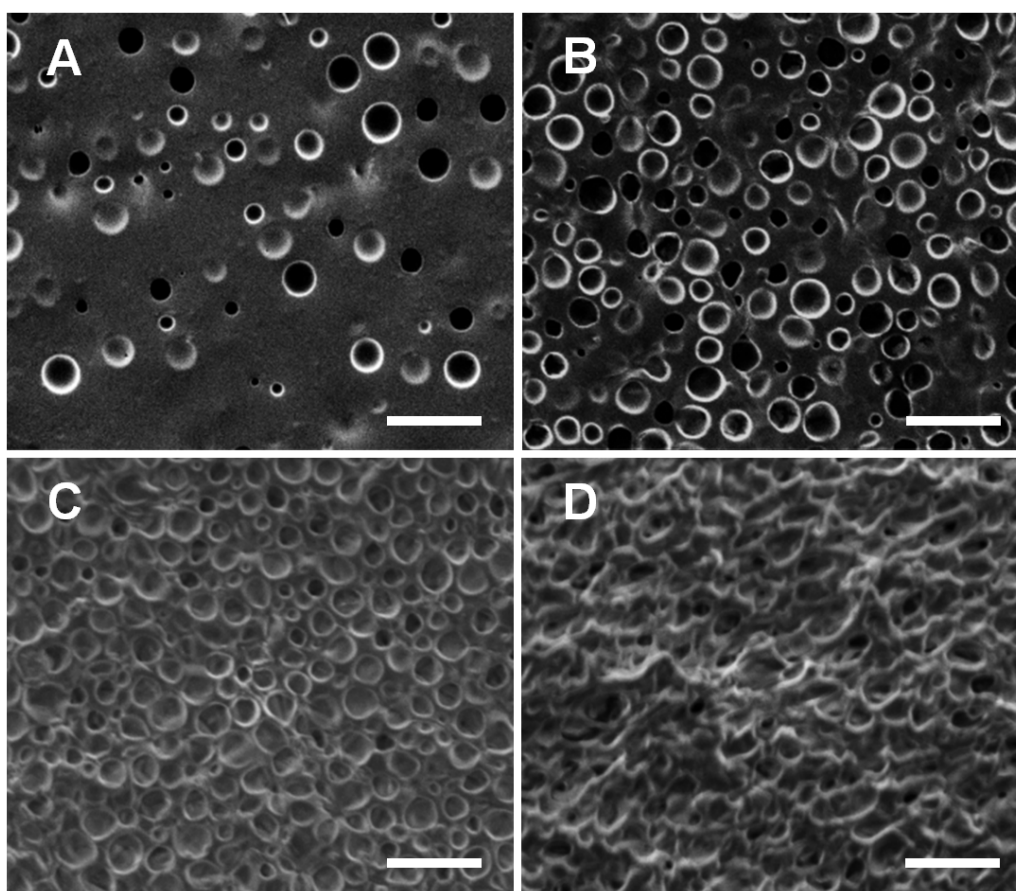


**Figure 3.1.4.** SEM images of cured glycerol-PDMS composite cross-sections. A – 10 phr, B – 50 phr, C – 90 phr, D – 130 phr of glycerol. Scale bars for all images correspond to 10  $\mu\text{m}$ .

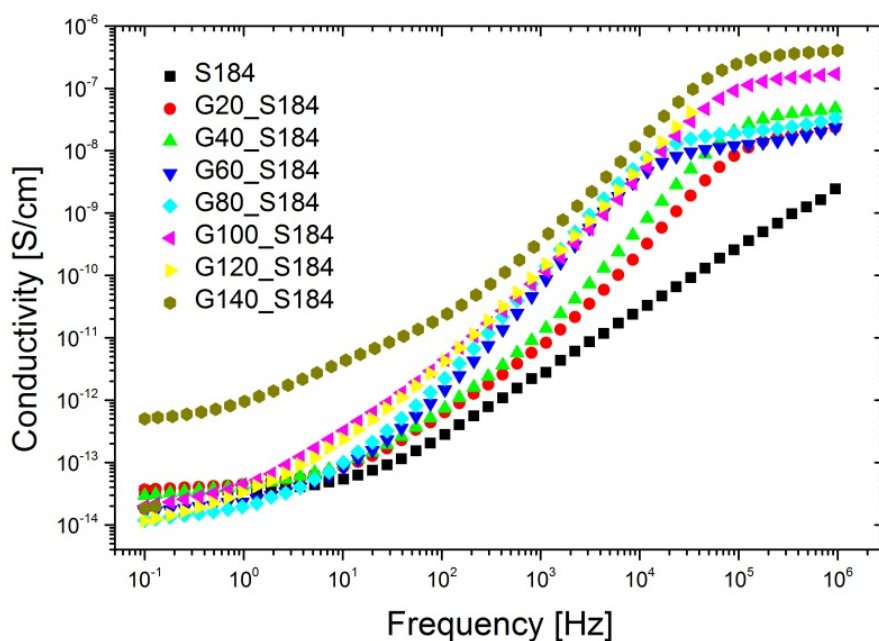


**Figure 3.1.5.** Conductivity of various glycerol-PDMS compositions presented as a function of frequency.

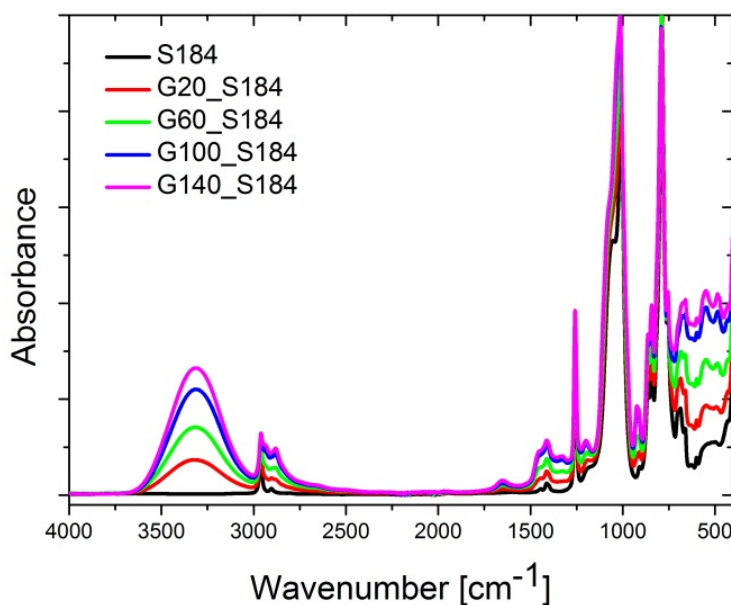


**Figure 3.1.6.** ATR-FTIR spectra of various glycerol-PDMS composite cross-sections.

Different compositions were additionally investigated by means of infrared spectroscopy. Cross-sections of 1 mm thick samples, containing 20, 60, 100 and 140 phr of glycerol, were prepared and tested with the ATR-FTIR technique. Pure Sylgard 184 was tested for reference. The obtained spectra are presented in Figure 3.1.6. A broad peak typical for the O-H band at a wavelength of around  $3400\text{ cm}^{-1}$  becomes more prominent for compositions with increasing amounts of glycerol.

This again indicates the high efficiency of glycerol encapsulation within the PDMS matrix and proves that glycerol remains in the sample.

### 3.1.3.2. Water contact angle

Sylgard 184, as well as its compositions with 20-120 phr of glycerol, was tested for surface wettability. Specimen surfaces were cleaned with ethanol before the analysis and left for 2 hours to equilibrate. Results from at least three separate measurements were averaged and standard deviations were calculated. Contact angle tests showed that surface properties are independent on glycerol content in PDMS. Only slight variations were observed with increasing amounts of glycerol, though no clear trend could be observed. A static water contact angle, averaged from all compositions, was calculated at  $113^\circ \pm 2^\circ$ .

### 3.1.3.3. Water absorption

It was additionally observed that glycerol-PDMS composites exhibit an extraordinary ability to absorb water. Therefore, a series of simple experiments was conducted, in which disc samples (25 mm in diameter and 1 mm thick) were immersed in deionised water for 24 hours and subsequently vacuum-dried. The mass, diameter and thickness of the samples were monitored before the experiment, after water absorption and after 1, 3 and 6 days of drying. Results for the water absorption and drying experiments are presented in Figure 3.1.7 and Figure 3.1.8, respectively. It was found that samples with higher amounts of glycerol absorb water much more effectively than compositions with lower amounts – as expected. Increases in mass, thickness and diameter became more prominent for samples with increasing glycerol content, reaching the maximum level at 100 phr of glycerol. It is most likely due to the relatively high permeability of silicones combined with the hygroscopic nature of glycerol induced by the presence of three hydroxyl groups in each glycerol molecule. For a given glycerol content (140 phr), continuity in the structure of glycerol becomes evident as the glycerol starts to be washed out, which is proved by significant mass loss after immersion in water. This phenomenon can be explained by the fact that the gyroid-like morphology, which becomes more prominent due to an increasing number of interconnected glycerol voids in the structure, allows water to flush out glycerol from the material. As a result, water is not absorbed by glycerol-filled voids and consequently the sample's mass increases only slightly or even – as in the case of the highest concentration – decreases.

Furthermore, an increase in the stiffness of water-absorbed samples was observed. This stiffness gradually increased in line with increasing amounts of incorporated glycerol, caused by the developing stress as a result of expanding water-absorbing glycerol-filled voids in the material. Consequently, the developed stress induced changes in the shape of the samples. An example is presented in Figure 3.1.9, where the sample with 40 phr of glycerol rolled after absorbing water, yet the original sample shape fully recovered after drying.

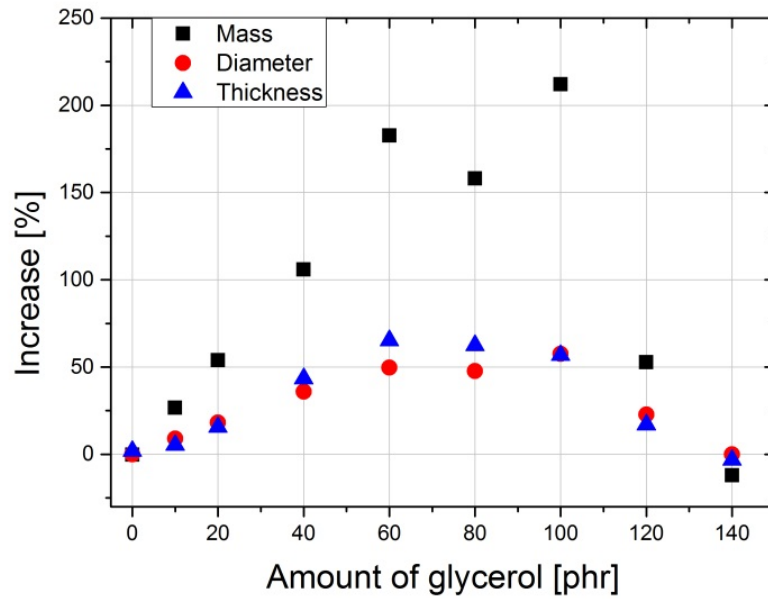


**Figure 3.1.7.** Mass, diameter and thickness changes of various glycerol-PDMS formulations caused by water absorption.

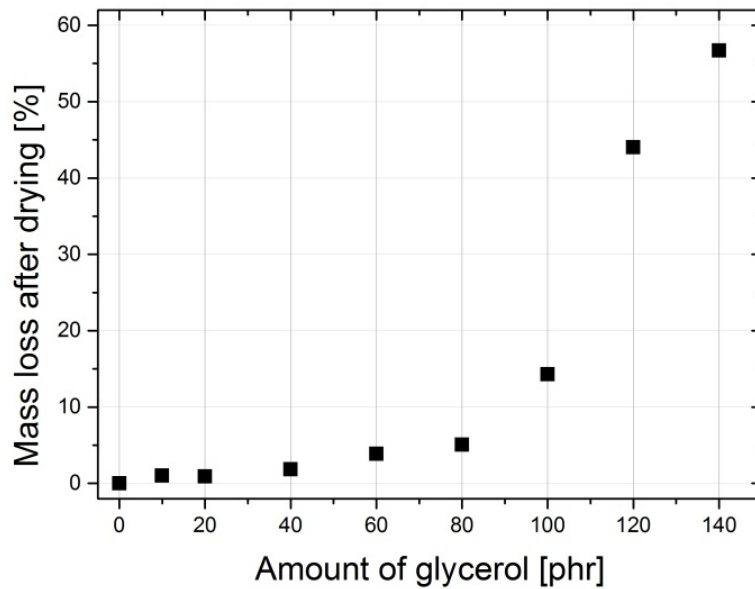


**Figure 3.1.8.** Mass losses of various glycerol-PDMS formulations after 3 days' drying, resulting from water absorption experiments.

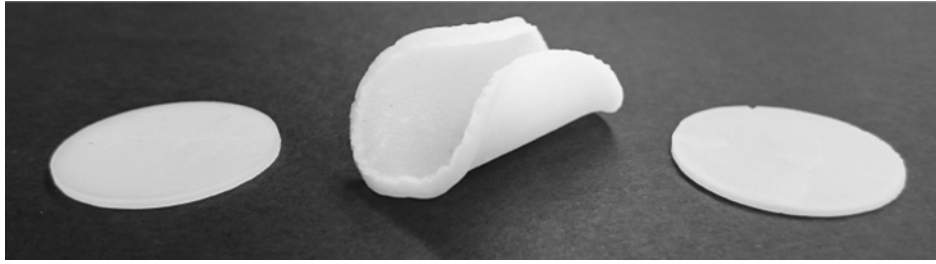


**Figure 3.1.9.** Images of a 25 mm in diameter and 1 mm thick sample, G40\_S184, before the absorption experiment, after absorption and after drying, respectively.

### 3.1.3.4. Dried materials

Ideally, after drying, elastomer should recover to its initial size, due to water being released from the material. Nevertheless, a small decrease in mass was observed for samples with  $\leq 80$  phr of glycerol. In these cases glycerol was partially flushed out from the material and replaced by water. During the drying process water left the voids, which finally led to a mass decrease in the sample. Nevertheless, in the case of samples with  $\geq 100$  phr, the mass decrease became substantial. Since, as it has been hypothesised, glycerol voids are interconnected in the presence of high glycerol content, it was therefore much easier for water to flush out glycerol from the material. It finally led to a mass decrease of 14%, 45% and 57% with respect to initial sample mass for the samples with 100, 120 and 140 phr of glycerol, respectively. Mass sample losses are presented in Figure 3.1.8, in which it is evident that the mass losses become more prominent in line with increasing glycerol content. Nevertheless, the difference between the samples with 80 and 100 phr of glycerol is less significant, whereas samples with 120 and 140 phr exhibit major mass losses, thereby indicating that the vast majority of glycerol was flushed away from the samples. Based on these experiments it can be assumed that glycerol-PDMS composites can be applied, for example, as a tool for controlled drug delivery, where adjustable release rate is required.

### 3.1.2.5. Tensile tests

**Table 3.1.2.** Mechanical properties of various glycerol-Sylgard 184 compositions obtained from tensile measurements.

Sample	Tensile modulus of elasticity [MPa]		Strain at break [%]	Stress at break [MPa]
	Tangent (Y)	Secant ( $Y_{100}$ )		
S184	1.07	3.66	154	8.29
G20_S184	0.80	2.58	160	6.19
G40_S184	0.58	1.76	166	4.60
G60_S184	0.51	1.55	168	4.04
G80_S184	0.43	1.32	161	3.17
G100_S184	0.38	1.14	159	2.71
G120_S184	0.33	0.97	116	1.30

Samples with various amounts of glycerol incorporated into PDMS were tested. The mechanical behaviour of Sylgard 184 was investigated for reference purposes. Five specimens from each composition were tested, and average values were calculated and used for evaluating the mechanical properties of the material. Values of tensile modulus of elasticity as well as ultimate stresses and strains are listed in Table 3.1.2, and averaged curves for each tested composition are presented in Figure 3.1.10.

From the curves in Figure 3.1.10 it can be seen clearly that stress produced on samples through mechanical displacement decreases in line with increasing amounts of incorporated glycerol. All compositions exhibit typical linear elastic behaviour up to strain values of around 40%, as reported also by other groups investigating PDMS systems.<sup>127,128</sup> The ultimate stress as a function of glycerol content is presented in Figure 3.1.11. Pure Sylgard 184 exhibits the highest stress, which dramatically decreases when incorporating 20 phr of glycerol, while incorporating 40 phr of glycerol decreases the stress even further. Nevertheless, an additional increase in glycerol content influences stress less significantly but preserves the same tendency as in the case of lower glycerol loadings. In general the decrease in stress is attributed to the presence of glycerol droplets in the material's structure, which introduces zones of zero stress and finally leads to an overall decrease in stress. On the other hand, it is believed that the glycerol voids, to some extent, can absorb tension produced while stretching the material and act as a plasticiser by partially decreasing friction in the material. Therefore a sharp decrease in mechanical strength and a slight increase in maximum strain are observed. Glycerol has no inhibiting effect on the platinum catalyzed cross-linking reaction and is thus not supposed to alter the cross-linking density. Moreover it has been reported that PDMS does not swell in the presence of glycerol.<sup>129</sup> This fact is additionally supported by comparing solubility parameters, which are  $\delta=7.3 \text{ cal}^{1/2}\text{cm}^{-3/2}$  and  $\delta=21.1 \text{ cal}^{1/2}\text{cm}^{-3/2}$  for PDMS and glycerol, respectively.<sup>129</sup> This can be considered as a direct indication that glycerol does not interfere chemically or physically during the cross-linking process and that ultimate composite properties are not influenced thereupon.

From Figure 3.1.11 it is evident that the ultimate strain increases in line with increasing glycerol loading and reaches its maximum at 60 phr of glycerol in PDMS. This phenomenon can be attributed to the fact that the stress exerted on samples can partially be overcome by glycerol voids, which most likely absorb some of the tension. A further increase in the amount of glycerol decreases maximum strain, which in turn drops drastically after exceeding 100 phr of glycerol. The results suggest that incorporating  $\geq 80$  phr of glycerol negatively influences material integrity, which is not significant for samples with 80 and 100 phr of glycerol but becomes prominent at 120 phr of glycerol.

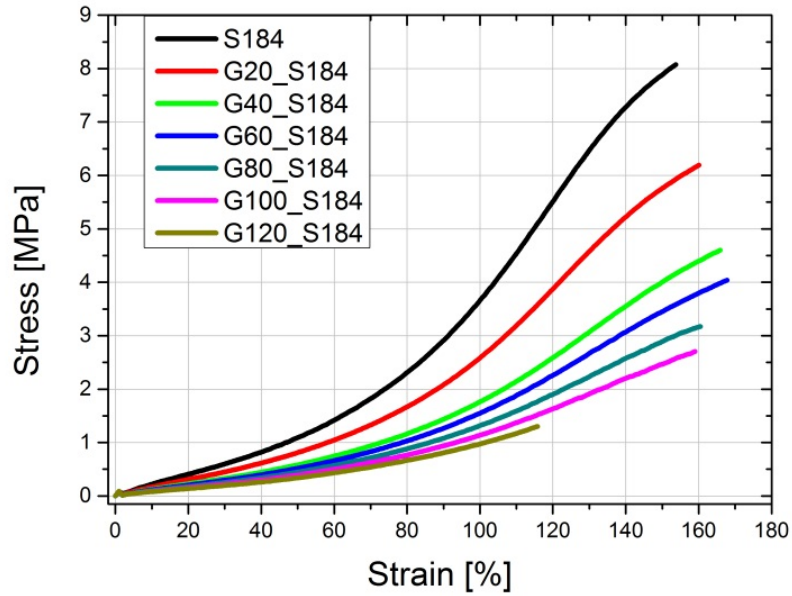


Figure 3.1.10. Stress-strain behaviour of various compositions obtained from tensile measurements.

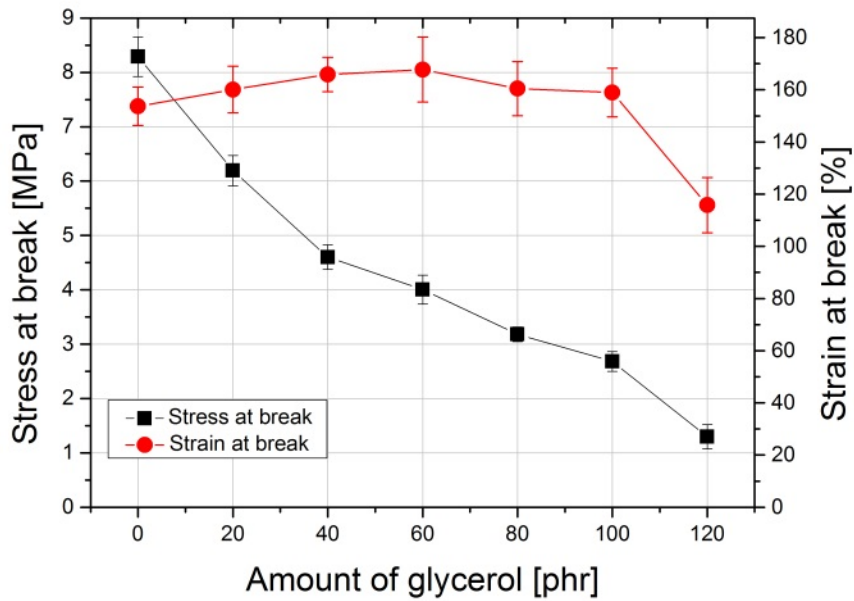
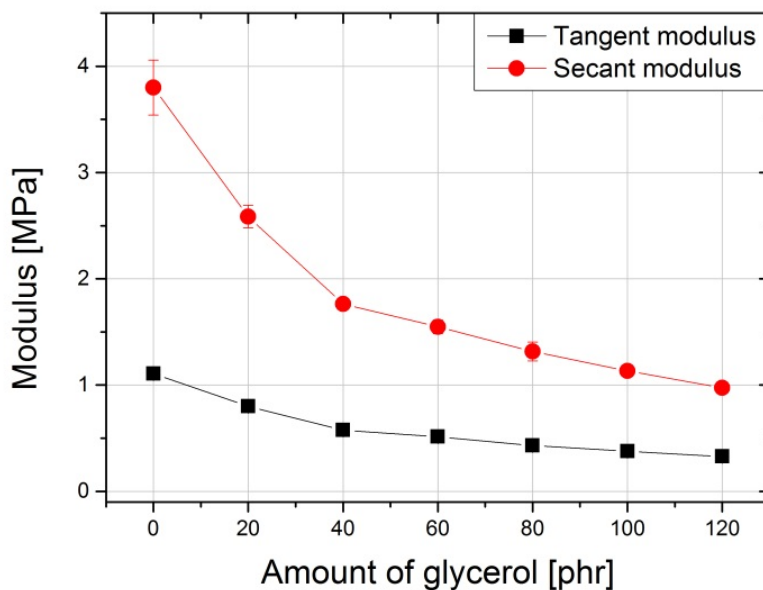


Figure 3.1.11. Ultimate properties of various glycerol-S184 compositions.





**Figure 3.1.12.** Tensional tangent ( $Y$ ) and secant ( $Y_{100}$ ) moduli of elasticity of various glycerol-S184 compositions.

The tensional tangent modulus of elasticity ( $Y$ ) was calculated from a slope of averaged stress-strain curves, while the tensional secant modulus of elasticity ( $Y_{100}$ ) was calculated from a stress/strain quotient at 100% strain. All calculated values are summarised in Figure 3.1.12. It can be seen clearly that the values of both moduli decrease in line with increasing glycerol loading in Sylgard 184. The most prominent loss can be observed again for samples in the range 0 phr to 40 phr of glycerol, whereas changes in moduli at higher loadings are less substantial, which is in agreement with previous observations.

Optical inspection of the stretched material was performed on 50  $\mu\text{m}$  thick PDMS films containing 5 phr of glycerol. The samples were stretched up to 100% and 150% strain values, in order to investigate the behaviour of glycerol-filled voids under applied mechanical stress. An optical microscopy image presented in Figure 3.1.13-A shows that glycerol beads present in the sample and stretched by 100% become elongated in the stretch direction. Glycerol droplets remain stable at this point and do not interconnect with each other. Nevertheless, when the 150% strain is applied, the stress produced on the elastomer forces the glycerol to leave the voids. This phenomenon is depicted in Figure 3.1.13-B, where small glycerol droplets can be observed on the sample's surface. This unique behaviour indicates that the composite, to some extent, loses its integrity at very high stretch ratios. This phenomenon is considered as a materials feature that may potentially lead to various applications where stress-induced substance release is required.

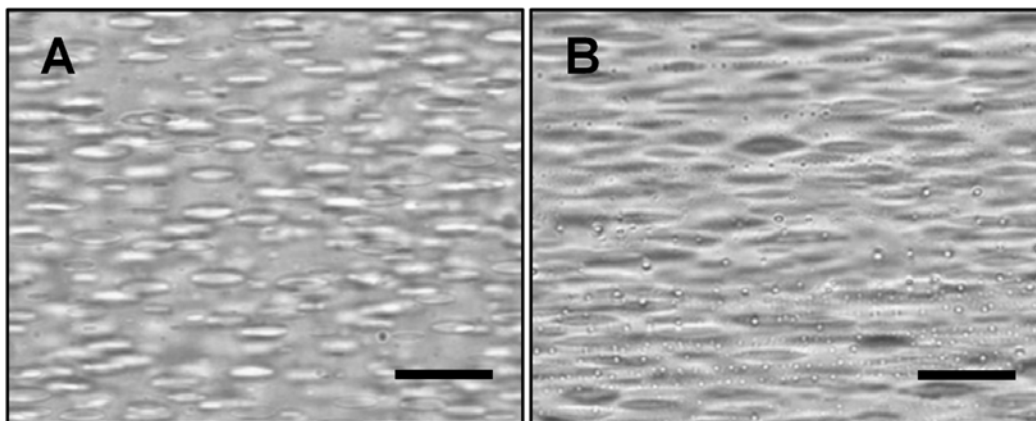


**Figure 3.1.13.** Optical microscopy images of stretched glycerol-PDMS composites (5 phr). A – 100% strain, B – 150% strain. Scale bars for all images correspond to 25  $\mu\text{m}$ .

### 3.1.4. Conclusions

An innovative type of elastomeric material was prepared and tested. In this approach a counterintuitive mixture of hydrophilic glycerol and hydrophobic PDMS was prepared as the basis for a green and cheap elastomer. The obtained glycerol-in-PDMS emulsion was very stable in a broad range of concentrations, even while processing the pre-polymer formulations. The ultimate strain of the elastomer was not compromised by incorporating glycerol, even at higher loadings. Furthermore, material properties like Young's modulus can be modified easily by altering the amount of incorporated glycerol. Additionally, the price of the material is significantly cheaper compared to pure PDMS, due to negligible costs of glycerol as a by-product in biodiesel production. Considering that the glycerol contents described herein substantially exceed 100% by weight, the material's overall price can be reduced at least twofold.

Apart from its promising mechanical properties, the investigated composition exhibits very particular behaviour in the presence of water. Water is absorbed by the material, and additionally glycerol (and potentially other substances) is released from its structure. From the perspective of designing smart materials, this invention could be of a great importance, for example, in the field of controlled drug delivery, water absorbing elastomers and sealants. Furthermore the material may be designed into functional patches with applications for wound care or vehicles for skin therapeutics.<sup>130,131</sup> Based on the presented discussion, it can be assumed that by modifying the PDMS matrix, glycerol-PDMS composites can exhibit different release rates which can potentially lead to broadening the application spectrum.

## **3.2. Glycerol-PDMS composites as very high-dielectric constant DEA candidates**

### **3.2.1. Introduction**

In this chapter the dielectric properties of glycerol-silicone composites are evaluated. The research focuses ostensibly on the dielectric constant, as it is a crucial parameter influencing the actuation performance of membranes. Experimental data from permittivity measurements are compared to various theoretical models predicting changes in relative permittivity as a function of filler loading, and the applicability of the models is also discussed. Furthermore, the influence of average filler diameter on the dielectric constant of a composite is investigated.

Conductivity is the second thoroughly investigated parameter. The samples were subjected to various AC voltages, ranging from 1 V to 350 V, and any changes in conductivities were monitored. These experiments are expected to provide valuable information about the ability of composites to withstand high voltages, and hence determine the usefulness of the materials.

Two commercial PDMS compositions, Sylgard 184 from Dow Corning (referred as S184) and Powersil XLR 630 A/B from Wacker Chemie (referred as XLR630), were filled with glycerol and their properties were evaluated. The preparation procedure followed the pattern presented in Chapter 3.1. Compositions based on XLR630 were additionally extended with 40 phr of a methylsiloxane volatile fluid OS-20 acting as a thinning agent. Subsequently, the samples were left for at least seven days at room temperature, in order to ensure full cross-linking of the material and also evaporation of the remaining OS-20.

### **3.2.2. Results and discussion**

#### **SEM analysis of glycerol-PDMS composites**

Cross-sections of cross-linked composites were investigated by scanning electron microscopy (SEM). Images I and II, presented in Figure 3.2.1, correspond to cross-sections of samples G20\_S184 and G80\_S184, respectively. As can be seen, with an increasing amount of glycerol, droplet concentration becomes higher. However, the average droplet size remains almost uninfluenced. Furthermore, it was observed that while increasing the glycerol/PDMS ratio of formulations, a threshold concentration is finally reached (G130\_S184), above which a droplet-like morphology is no longer present in the cross-linked material. As discussed in the previous chapter, a network of interconnected glycerol channels is obtained which leads to the presence of higher conductivity paths in the material. Therefore, samples with more than 120 phr of glycerol are not discussed in this section.

The morphology of spherical droplets embedded within PDMS is not present in samples G20\_XLR630 and G80\_XLR630, as presented in Figure 3.2.1 (images III-IV). Elongated, ellipsoid-like glycerol droplets were formed instead. It is hypothesised that this is an effect of using the thinning agent OS-20, which was rapidly evaporating from the hydrophobic phase of the samples during the cross-linking process. Intuitively, the fluid was evaporating

upwards, which led to the orientation of the glycerol droplets in the direction of evaporation. The longest semi-axis of the ellipsoid-like droplets was proved, via SEM analysis, to be parallel to the theoretical direction of evaporation. Despite this anomaly, glycerol droplets were successfully encapsulated within the XLR630 PDMS composition, which was substantiated further by the dielectric spectroscopy results. Adding thinning fluids is a common practice, since it greatly simplifies the processability of high-viscosity polymeric compositions. Importantly, the SEM analysis showed that introducing thinning agents might lead to the introduction of anisotropy into the produced material. Consequently, this might induce the deterioration of the ultimate properties of the material and eventually limit its usefulness. Therefore, a proper balance between the evaporation rate and PDMS curing conditions has to be examined for each PDMS system.

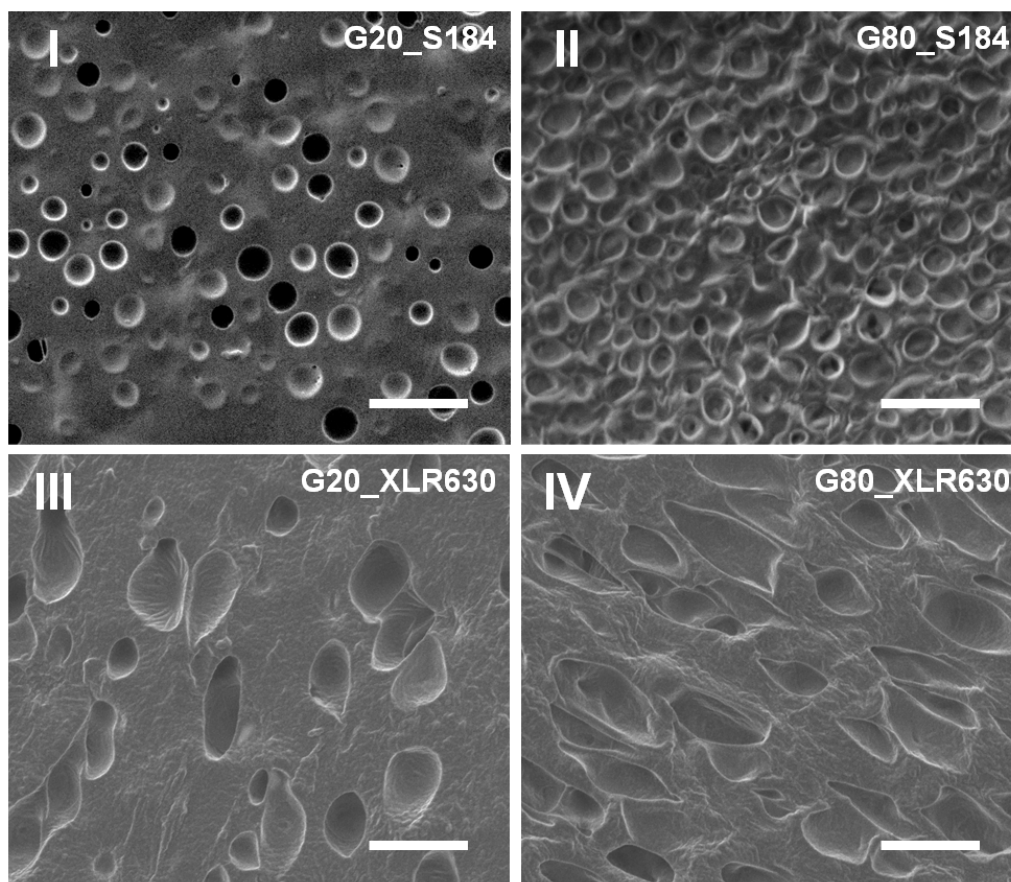


**Figure 3.2.1.** SEM images of cured glycerol-PDMS composite cross-sections. I – G20\_S184, II – G80\_S184, III – G20\_XLR630, IV – G80\_XLR630. Scale bars in all images correspond to 10  $\mu\text{m}$ .

### Dielectric spectroscopy

Broadband dielectric spectroscopy tests were conducted in order to determine the dielectric properties of compositions with different amounts of incorporated glycerol. In this study, a two-phase system is described in which a higher conductivity material is distributed within a lower conductivity material in the form of discrete droplets. The droplets were expected to act as high-permittivity filler uniformly distributed throughout the dielectric

polymer matrix. Since the material is based on a glycerol-PDMS emulsion, it can be assumed that the glycerol droplets are effectively encapsulated within a PDMS insulating layer. Intuitively, this effect should eliminate the probability of the formation of conductive paths throughout the material and consequently keep the conductivity unaffected by increased amounts of the filler. The advantages of filler encapsulation have been thoroughly explained by other groups.<sup>30,87</sup>

As can be seen in Figure 3.2.2, a significant increase in dielectric constant is observed in line with increasing glycerol loading. Permittivity measured at 1 kHz increases from around 3 for neat Sylgard 184 up to around 16 for a sample of G120\_S184. Importantly, already a composition with 20 phr of the filler exhibits a significant enhancement of permittivity compared to the neat sample. Consequently, the G20\_S184 and G40\_S184 samples have a dielectric constant of 5.1 and 7.1, respectively. It has to be noted that all of the curves of samples with incorporated glycerol exhibit a characteristic inflection in the frequency region of between  $10^4 - 10^6$  Hz, which might be evidence of the dipolar relaxation of the incorporated high-permittivity filler. The higher the glycerol loading, the steeper the inflection. In line with the increasing steepness of the storage permittivity curves, a characteristic peak in loss permittivity occurs in the same frequency region. This is an additional indication of the presence of dipolar relaxation. Importantly, dielectric losses are considered to be exceptionally low for all of the investigated compositions, reaching a maximum of around 2.5 in the higher frequency region. As expected, conductivities are not significantly altered by increasing additions of filler, proving the concept of a proper encapsulation of glycerol. The conductivity curves also exhibit characteristic deflection, corresponding to the alleged dipole relaxation.

The samples based on XLR630 also exhibit significant enhancements to the dielectric constant (see Figure 3.2.3). On the other hand, this increase is more prominent than in the case of S184. The maximum dielectric constant of 21 was reached by the G120\_XLR630 sample. S184 and XLR630 have comparable dielectric constants, and so the higher values for composites based on XLR630 are unexpected. The applied thinning agent is not anticipated to influence directly the dielectric constant, due to the presumed complete evaporation. It can be hypothesised that the difference comes from the shape of the embedded filler, as this might alter interactions between adjacent glycerol droplets. The characteristic relaxation can also be observed in the samples based on XLR630, analogously to samples based on S184.

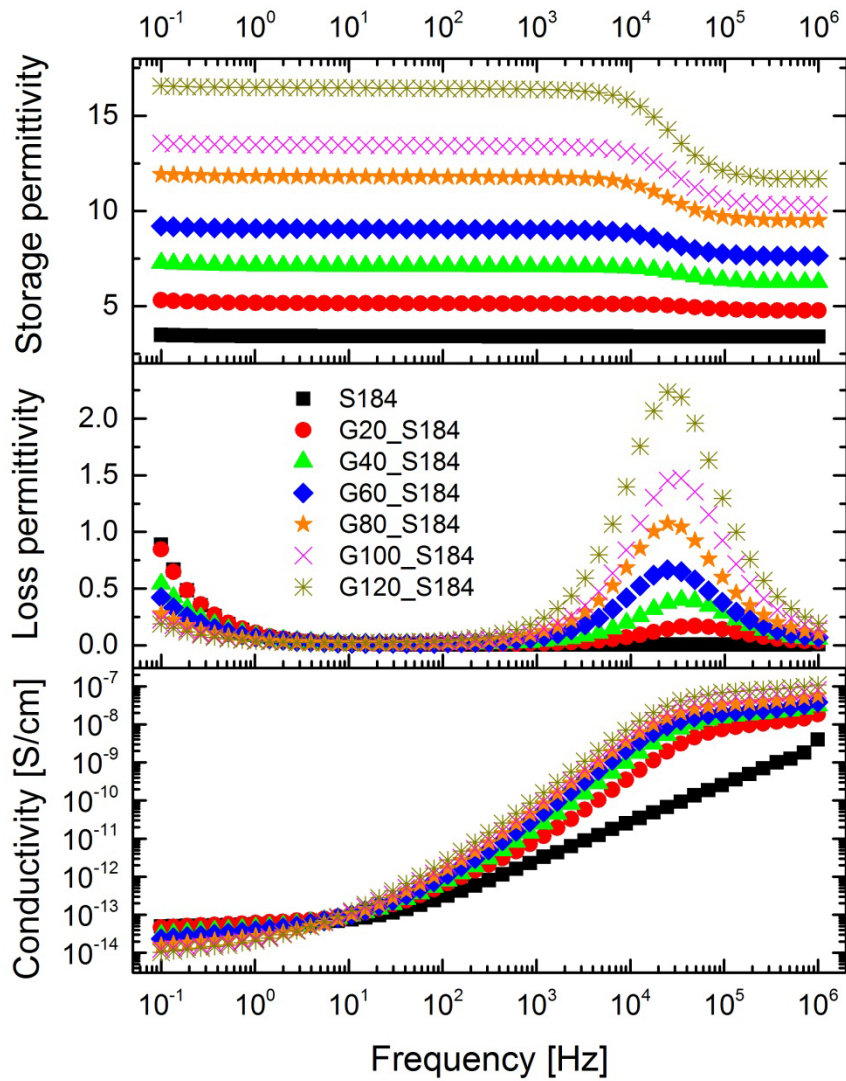


**Figure 3.2.2.** Storage permittivity, loss permittivity and conductivity of various glycerol-S184 composites at room temperature.

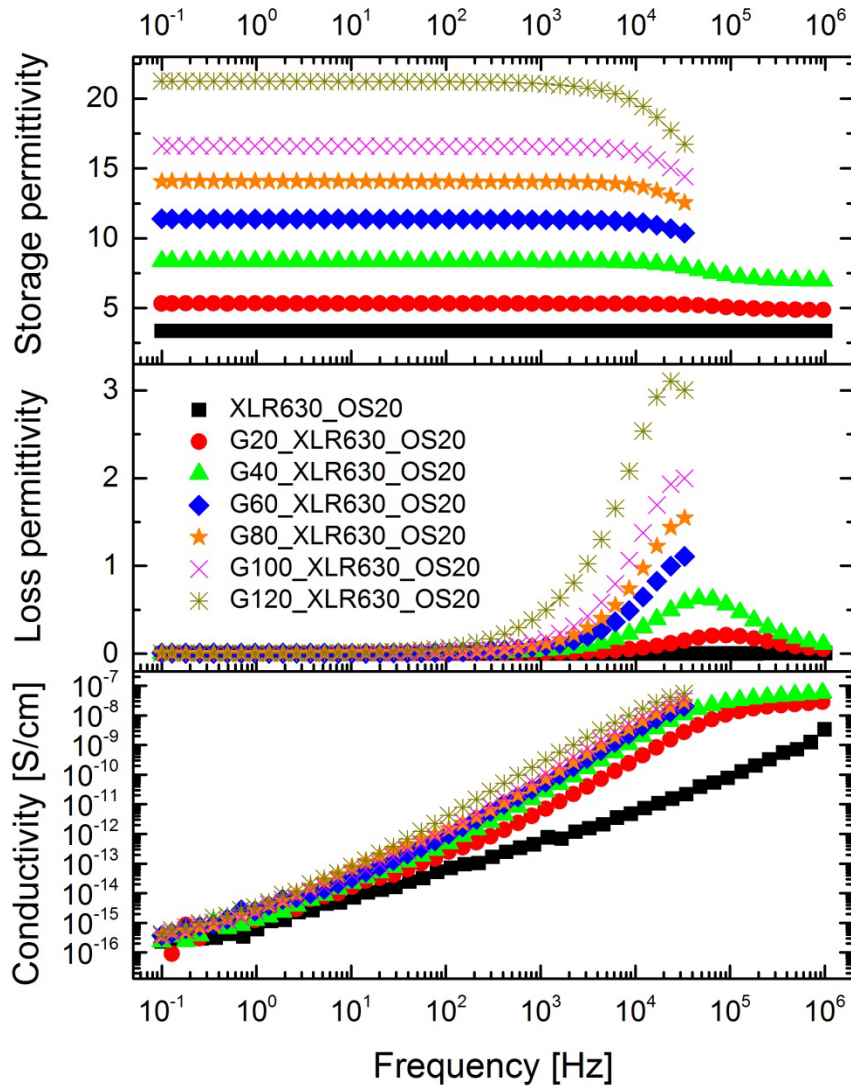


**Figure 3.2.3.** Storage permittivity, loss permittivity and conductivity of various glycerol-XLR630 composites at room temperature.

The gradual increase in relative permittivity as a function of filler concentration was additionally compared to various theoretical models predicting the behaviour of composites of low-permittivity polymers blended with high-permittivity fillers. All models were created for binary systems, where the inclusion has a spherical form. For this reason only composites based on Sylgard 184 were investigated, as only in this case is the spherical shape of the filler present. Firstly, a simple mixing rule, presuming the existence of approximate lower (3.1) and upper (3.2) limits for such binary systems, was applied:<sup>132</sup>

$$\varepsilon_{c,min} = \frac{\varepsilon_m \varepsilon_f}{\varepsilon_m \nu_f + \varepsilon_f \nu_m} \quad (3.1)$$

$$\varepsilon_{c,max} = \varepsilon_m \nu_m + \varepsilon_f \nu_f \quad (3.2)$$

where  $\varepsilon_c$ ,  $\varepsilon_m$  and  $\varepsilon_f$  describe the permittivity of the composite, matrix and filler, respectively, while  $v_m$  and  $v_f$  refer to volume fractions of the matrix and filler in the described binary composites. The experimental data fit well within the presumed limits. Yet, a more accurate model is necessary in order to define precisely the described trends. More meticulous predictions can be obtained with one of the first formulas of this type, namely the Maxwell-Garnett equation (3.3), which holds for a relatively broad range of volume fractions:<sup>133,134</sup>

$$\varepsilon_c = \varepsilon_m \left[ 1 + \frac{3v_f(\varepsilon_f - \varepsilon_m)}{v_m(\varepsilon_f - \varepsilon_m) + 3\varepsilon_m} \right] \quad (3.3)$$

Corrections to the abovementioned equations were introduced by Bruggeman (equation 3.4).<sup>135</sup> The developed model covers inclusion volume fractions up to 0.5, therefore becoming frequently reported as one of the better tools for precisely describing composites with very high filler loadings.<sup>67</sup> The model tolerates the formation of agglomerates, provided the percolation threshold is not exceeded. The equation is usually reported in the following form:

$$\frac{\varepsilon_f - \varepsilon_c}{\varepsilon_c^{1/3}} = \frac{(1 - v_f)(\varepsilon_f - \varepsilon_m)}{\varepsilon_c^{1/3}} \quad (3.4)$$

Subsequently, the validity of the well-known Jayasundere-Smith model (equation 3.5) was verified.<sup>136,137</sup> The expression presumes that the dielectric constant of the inclusion is substantially higher than that of a dielectric continuum. Additionally, the formula takes into consideration polarisation-based interactions occurring between adjacent particles. Intuitively, the probability of particle-particle interactions is much higher at high filler loadings. Therefore, it is expected that the experimental dataset will fit better to the predictions, especially at very high inclusion volume fractions. The model is represented by the following equation:

$$\varepsilon_c = \frac{\varepsilon_m v_m + \varepsilon_f v_f \frac{3\varepsilon_m}{(2\varepsilon_m + \varepsilon_f)} \left[ 1 + 3v_f \frac{(\varepsilon_f - \varepsilon_m)}{2\varepsilon_m + \varepsilon_f} \right]}{v_m + v_f \frac{3\varepsilon_m}{(2\varepsilon_m + \varepsilon_f)} \left[ 1 + 3v_f \frac{(\varepsilon_f - \varepsilon_m)}{2\varepsilon_m + \varepsilon_f} \right]} \quad (3.5)$$

Last but not least, a model suggested by Poon and Shin (3.6) was investigated. The formula was developed, in order to find a model fitting to as broad range of systems as possible.<sup>138</sup> The formula is not limited by a condition of  $\varepsilon_f \gg \varepsilon_m$  (as in the case of equation 3.5, Jayasundere-Smith) and allows even for situations where  $\varepsilon_f < \varepsilon_m$ . Furthermore, the simplicity of this formula is one of its strengths. As the authors argue, more complicated



non-linear equations (like equation 3.4, Bruggeman) have limited usefulness in situations where a simple formula, like the following, is anticipated:

$$\varepsilon_c = \varepsilon_m + \frac{v_f(\varepsilon_f - \varepsilon_m)}{v_f + v_m \frac{\varepsilon_f + 2\varepsilon_m - v_f(\varepsilon_f - \varepsilon_m)}{3\varepsilon_m}} \quad (3.6)$$

Storage permittivity data points at a frequency of 1 kHz were used for comparisons between the discussed models. Nevertheless, between 0.1 Hz and 10 kHz the curves reach a plateau, and therefore the analysis is assumed to be valid for a broad frequency range. As can be seen in Figure 3.2.4, the model proposed by Jayasundere and Smith fits the experimental data most accurately. The theoretical estimation precisely fits the data from lower glycerol loadings up to loadings of around 100 phr. The sample with 120 phr of glycerol deviates slightly from the model. As discussed previously, at very high inclusion loadings (>120 phr) the material becomes more conductive. Here, the aberration is not significant but might be attributed to the creation of the continuous glycerol phase and thereby the formation of conductive paths.<sup>126</sup> All discussed models are presumed for so-called 0-3 composites (spherical filler particles embedded in a continuous material), and so this phenomenon restricts the validity of the formulas at loadings of 120 phr and higher.

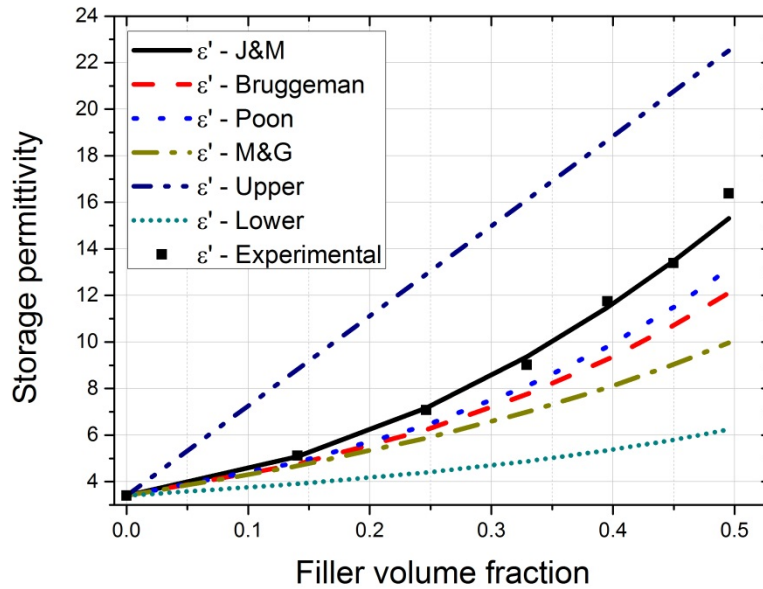


**Figure 3.2.4.** Experimental data and theoretical estimations of the relative permittivity of composites measured at 1 kHz as a function of glycerol loading.

As can be seen in Figures 3.2.2 and 3.2.3, the conductivities of the glycerol-PDMS composites do not change significantly with increasing inclusion loadings. However, the SEM analysis showed that the insulating layer between the glycerol droplets becomes

thinner in line with increasing amounts of incorporated filler, as expected. Therefore, the chance for charge migration between the droplets is enhanced. Although this phenomenon is not to be expected at 1 V, tests at higher voltages were conducted in order to validate the usefulness of the material for high-voltage applications. Various samples, based on S184 and XLR630, were subjected to increasing AC voltages, and the results for these experiments are presented in Figure 3.2.5. The conductivity of sample G100\_S184 increases significantly when increasing the voltage, while the conductivity of G100\_XLR630\_OS20 remains almost unaffected. The conductivity of unmodified XLR630, tested at 1 V, is lower compared to S184, investigated under the same conditions (see Figure 3.2.2 and Figure 3.2.3). As the amount of inclusion in both samples is exactly the same, it can be concluded that the matrix type is a key parameter for determining the conductivity of glycerol-PDMS composites. Intuitively, materials with higher resistivity (resistivity is the reciprocal mode of conductivity) will insulate the glycerol droplets more efficiently and block charge transfer between adjacent spheres. Ultimately, the probability of forming conductive paths will be greatly restricted when using a dielectric with higher resistivity.

As discussed, the thinner the insulating layer between the inclusion droplets, the higher the conductivity. This is additionally proven by the results presented in Figure 3.2.6, in which the conductivities of samples G80\_S184 and G100\_S184 are compared. As can be observed, the conductivity of the sample with 80 phr is not influenced by the voltage increase from 1 V to 350 V, whereas for the sample with 100 phr it drastically increases at 350 V. This suggests the existence of a minimum insulating spacing which separates adjacent glycerol droplets. It is believed that threshold thickness would be lower for materials with higher electrical resistivity.

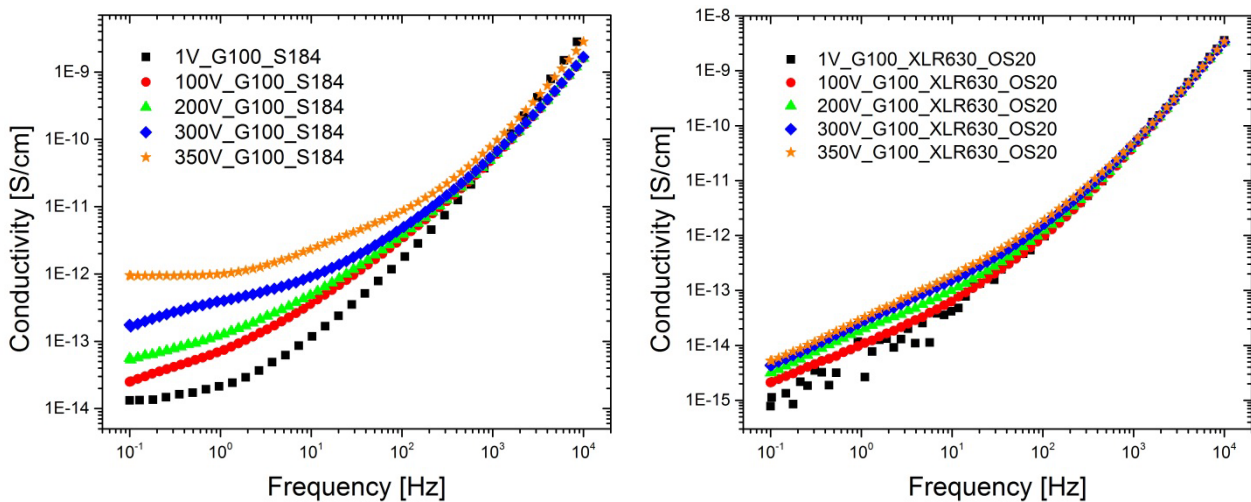


**Figure 3.2.5.** Conductivities of composites based on S184 (left) and XLR630 (right), containing 100 phr of glycerol at various AC voltages at room temperature.

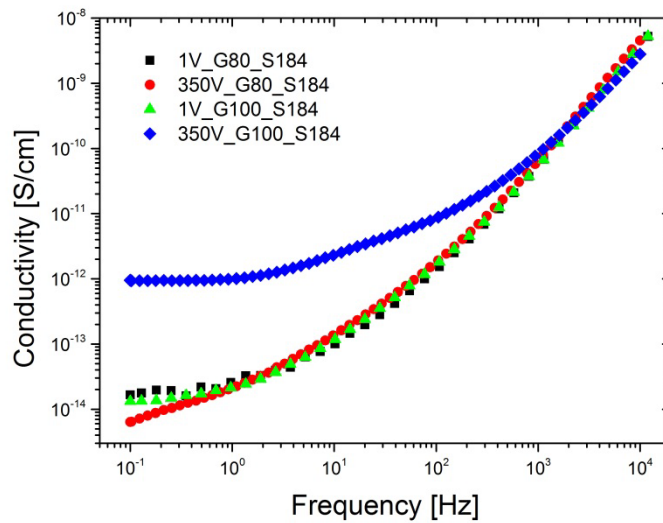


**Figure 3.2.6.** Conductivity of various glycerol-S184 composites at 1 V and 350 V at room temperature.

### Modification of droplet size and its influence on the dielectric constant of glycerol-PDMS composites

In the previous section some common theoretical models for predicting the dielectric constants of composites were evaluated. Other reports can be found in the literature which emphasise the necessity of considering a polymer-filler interphase as an additional parameter influencing the final dielectric constant of a material.<sup>139,140</sup> Furthermore, Vo and Shi discuss the presence of molecular polarisability at the filler-polymer interphase, which also might influence the resulting permittivity.<sup>141</sup> As the filler-polymer interphase increases in line with a decrease in filler size at a given loading, it is expected that a change in relative permittivity will be observed.

Various surfactants in different amounts were added to the G10\_S184 pre-elastomer composition, and its influence on droplet diameter was investigated. Firstly, 1 mm-thick samples of PDMS, containing 10 phr of glycerol with the addition of Tween 20 (a glycerol miscible, polysorbate based surfactant), were prepared following the standard procedure used in this study. SEM images of samples with 0.1 and 5 parts by weight of the surfactant are illustrated in Figure 3.2.7a. Data presented in Figure 3.2.7b indicate that an increasing amount of surfactant in a composition leads to the formation of smaller glycerol droplets, along with a narrower size distribution. The average droplet diameter decreases from 2.3  $\mu\text{m}$  for the non-surfactant sample to 0.8  $\mu\text{m}$  for the highest investigated Tween 20 loading. The dielectric constant increased from 4.2 for pure G10\_S184 to 5.0 with the addition of 5 phr. Nevertheless, the sharpest increase was observed for smaller additions of Tween 20, which corresponds well with the more intensive decrease in droplet diameter at lower surfactant loadings. Remarkably, the dielectric constant of the sample G20\_S184 was measured at 5.1, whereas the sample G10\_S184 with the addition of only 3 phr of Tween 20 reached a dielectric constant of 4.9. This implies that a strong dependence exists between dielectric constant and filler size.

A significant decrease in the average droplet diameter was observed also after incorporating two PEG-PDMS surfactants (block copolymer-based surfactants with molecular weights of 400 g/mol and 3000 g/mol with comparable ratios between PEG and PDMS blocks) into the G10\_S184 composition. The influence on the droplet diameters was similar to the effects of Tween 20; however, no clear increase in the dielectric constant was observed for these compositions.

The aim of this approach was to investigate how the volume of the filler-polymer interphase influences the dielectric constant of composites. The contradictory results herein indicate that the properties vary depending on the constituents forming the interphase, thus suggesting a high complexity of processes occurring at the interphase. It is therefore necessary to consider each system as a separate case.

It has to be stressed that the diameters obtained from evaluating the cross-sections do not correspond to actual droplet diameters, as it is not possible to prepare sample cross-sections by cutting each inclusion droplet through the middle. Nevertheless, for the comparative study this approach is considered to be sufficiently accurate.

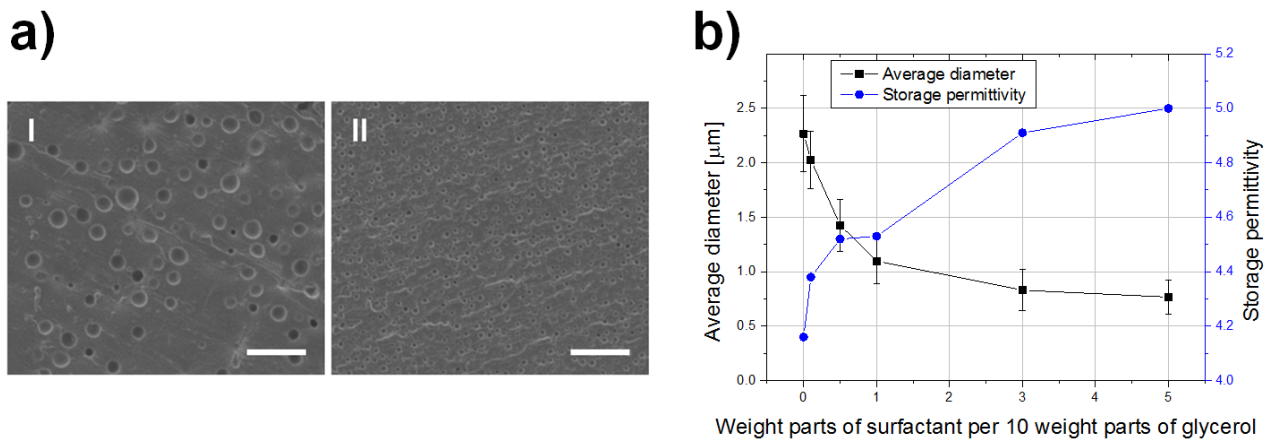


**Figure 3.2.7.** Effect of surfactant on droplet size. a) SEM images of cured samples G10\_S184 with 0.1 (I) and 5 (II) phr of Tween 20. Scale bars for both images correspond to 10 μm. b) Average glycerol droplet diameter and storage permittivity at 1 kHz as a function of surfactant content in various Tween 20-glycerol-PDMS compositions.

### 3.2.3. Conclusions

The approach discusses the use of glycerol-PDMS green elastomers and their potential applicability as dielectric electroactive polymers. This novel class of materials was proven to exhibit very low dielectric losses and relatively high-dielectric constants. The experimental dataset was compared with a few of the most popular theoretical models used to predict changes in relative permittivity as a function of filler content. The results indicated that the formula suggested by Jayasundere and Smith fits the data most accurately. The theory takes into account the presence of interactions between adjacent filler particles, which intuitively

intensify at high glycerol loadings. This factor is considered to be the main advantage of the model.

The high-voltage dielectric spectroscopy measurements indicated that conductivity tends to increase in line with increasing voltage and filler loading. Nonetheless, the experimental results indirectly indicate that this problem can be overcome by using the best possible dielectric material as a basis for composites. It is believed that a highly resistive dielectric matrix would be capable of eliminating the charge transfer between adjacent glycerol droplets. This is especially important at high filler contents, where spacing between the droplets becomes very small.

### 3.3. Overview of PDMS compositions containing various polar liquids

#### 3.3.1. Introduction

In the previous chapters the potential of hydrophobic elastomers with incorporated polar liquids was revealed. That said, a material candidate for dielectric actuators has to meet various requirements in order to be useful commercially. Most of these parameters are thoroughly discussed in Chapter 1 of the thesis, so this section focuses solely on identifying and optimising liquid-PDMS composition parameters that are critical from the point of view of dielectric actuators. Therefore, the research aims at finding a PDMS matrix that would provide the most efficient insulation for the embedded droplets. Furthermore, various high-permittivity polar liquids are taken into consideration when designing composites. Based on a thorough literature research a comparison of liquid properties is performed, which is expected to enable the selection of the most promising candidates for composites.

The materials were tested in terms of dielectric properties and physical morphology. Finally a simple test was performed, aimed at evaluating the actuation performance of the investigated compositions.

#### 3.3.2. Results and discussion

##### Various compositions based on glycerol as a high-dielectric constant filler

The results of the study presented in Chapter 3.2 showed that glycerol incorporated into silicone elastomer effectively enhances the permittivity of a base elastomer, even at lower loadings such as 10 phr. Although noticeably high permittivities were obtained, the investigated materials suffered from increased conductivity when the filler loadings and applied voltages were increased. This generated further approaches in which various commercial PDMS compositions were tested. It has been hypothesised that for liquid-elastomer dielectric composites the best possible performance will be achieved by applying a low-viscosity, high resistivity and moderately soft PDMS composition. After a thorough search two commercial PDMS systems were selected as candidates – Elastosil RT 620 A/B (referred to later as ‘RT620’) and Elastosil P 7684/60 A/B (referred to later as ‘P7684’), both produced by Wacker Chemie AG. For a more detailed specification of the materials’ properties given by the manufacturer, see Table 3.3.1 below.

**Table 3.3.1.** Selected mechanical properties of various commercial PDMS systems reported by the materials’ manufacturer.

Composition	Mixing ratio (A:B)	Viscosity [Pa.s]	Elongation at break [%]	Hardness Shore A	Tear strength [N/mm]	Tensile strength [N/mm <sup>2</sup> ]	Pot life at 25°C
S184	10 : 1	3.9	–	50	–	6.7	> 2 h
XLR630	1 : 1	13	450	35	25	7	2 days
RT620	10 : 1	6	900	17	> 12	5	35 min
P7684	1 : 1	2.5	600	12	13	3	60 min

The sample preparation followed the same procedure as applied in previous cases described in Chapter 3.1. A maximum of 80 phr of glycerol could be incorporated to the RT620 while the lower viscosity P7684 composition produced emulsions with a maximum of 60 phr of glycerol. Considering the rather low viscosity of the P7684 base composition this outcome was unexpected as low viscosities of silicone pre-elastomers were expected to facilitate the formation of highly concentrated emulsions. As can be seen in Figure 3.3.1, the samples with 20 phr and 40 phr of glycerol formed uniform emulsions, while the sample with 60 phr produced a structure with much larger glycerol droplets and a significantly broader size distribution. This implies that the maximum concentration of glycerol in the pre-polymer is being approached. After reaching a critical point, the inclusion liquid separates completely from the emulsion. In the ideal case the phase split does not occur; instead, a reversed (PDMS-in-glycerol) emulsion is formed, which was observed, for example, for the G150\_S184 sample.

Upon analysis of these results it can be hypothesised that the efficiency of emulsion formation depends not only on the viscosities of the constituents, but most likely also on the molecular structure of PDMS pre-polymer chains, the amount of incorporated silica and possibly on the presence of other compounds facilitating or restricting the formation of emulsions. As the exact composition of commercial silicone systems is usually not known, it is not possible to indicate which factors play a significant role in any particular case.

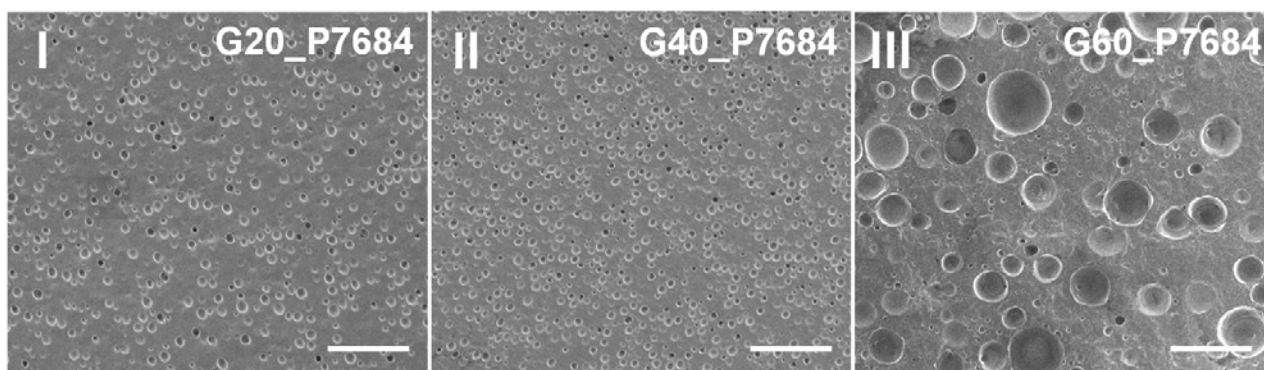


**Figure 3.3.1.** SEM images of cross-sections of cured glycerol-PDMS composites. I – G20\_P7684, II – G40\_P7684, III – G60\_P7684. Scale bars for all images correspond to 50  $\mu\text{m}$ .

The broadband dielectric spectroscopy measurements revealed that the dielectric constants of the RT620 and P7684 formulations were successfully enhanced by incorporating glycerol. In both cases permittivity increased from around 3 (pure PDMS) to around 5, 7 and 11 for samples with 20, 40 and 60 phr of glycerol, respectively, as can be seen in Figure 3.3.2 and Figure 3.3.3 ( $\epsilon=15$  was exhibited by sample G80\_RT620). The obtained values are significantly higher than in the case of S184-based composites, but they are comparable with XLR630. Importantly, dielectric losses in all cases remained low compared to the dielectric constant, whilst conductivity at lower frequency ranges also remained almost uninfluenced by the increasing glycerol loadings. The unfavourable dielectric loss increase at higher frequencies is considered to be of lower significance, due to the fact that the vast majority of reported dielectric transducers operate at frequencies below 1 kHz.<sup>34</sup> The conductivities of both pure PDMS compositions can be considered as low, yet the composition

RT620 exhibits almost one order of magnitude lower values. Consequently, this PDMS system appears more promising with respect to the preparation of dielectric transducers. As argued in Chapter 3.2, the most important property regarding the base material is resistivity, while the dielectric constant is of lower significance, as it can be easily enhanced by incorporating glycerol.

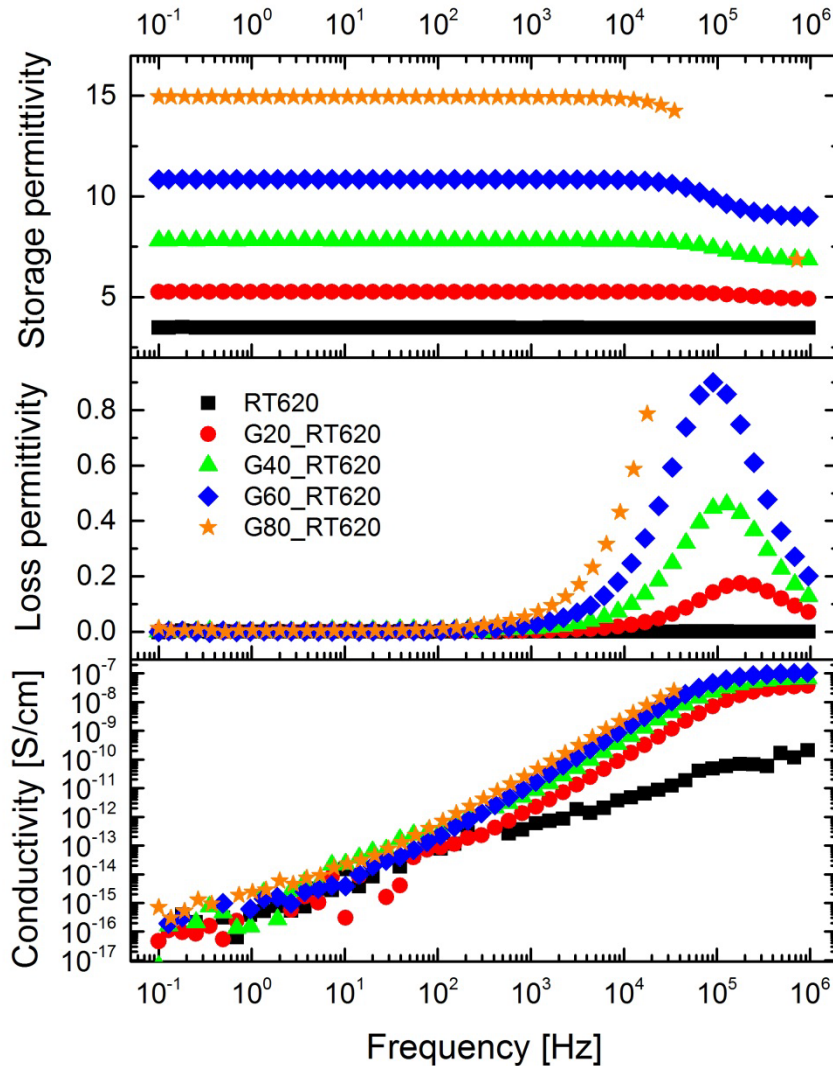


**Figure 3.3.2.** Storage permittivity, loss permittivity and conductivity of various glycerol-RT620 composites at room temperature.



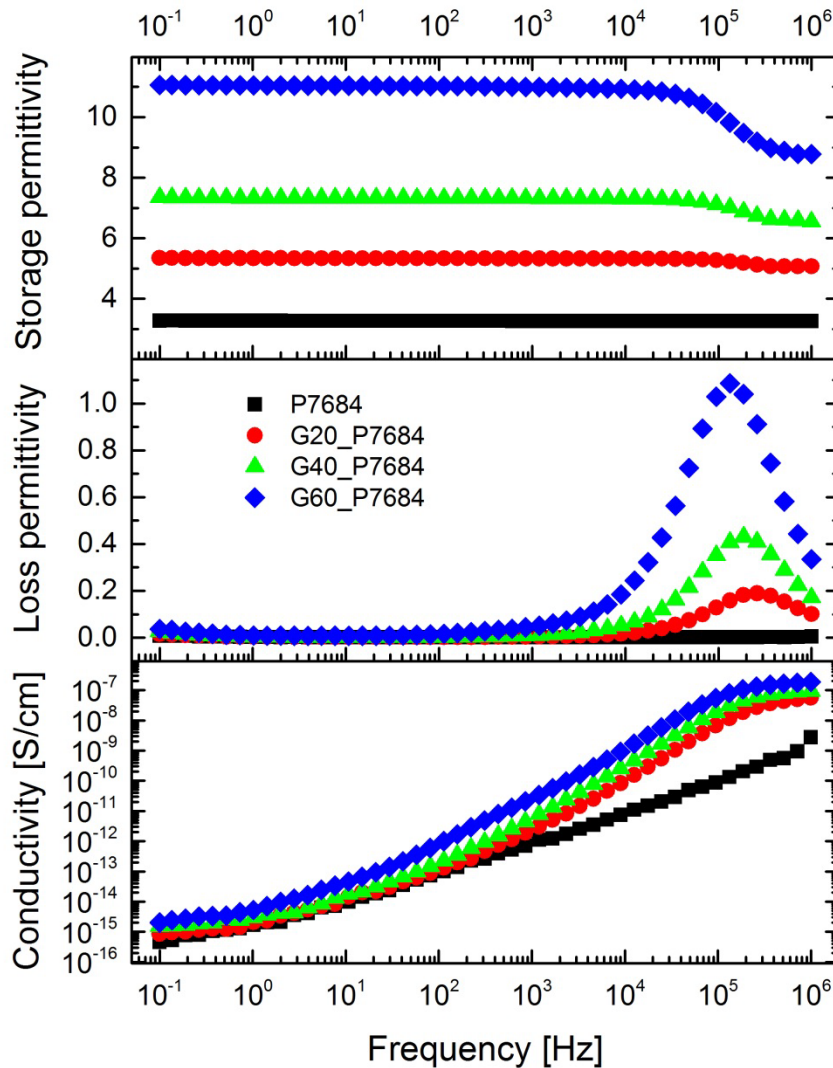


**Figure 3.3.3.** Storage permittivity, loss permittivity and conductivity of various glycerol-P7684 composites at room temperature.

### Various compositions based on propylene carbonate as a high-dielectric constant filler

The choice of high-permittivity polar liquids is very broad; however, for this specific application the liquid had to fulfill a number of criteria. Table 3.3.2 represents selected high-permittivity liquids, along with various critical properties determining their usefulness as fillers in dielectric transducers industry. Next to a high-dielectric constant, the liquid should have low volatility (here represented as vapour pressure at a given temperature). This parameter is crucial, as silicones are known to possess high gas permeability, thereby allowing for the evaporation of substances embedded in the material.<sup>103</sup> It has to be stressed that volatility increases rapidly in line with increasing temperature, which usually occurs when dielectric actuator membranes are exposed to high voltages. Additionally, the solubility parameter (and consequently the swelling degree) determines whether an embedded liquid will penetrate the PDMS structure or not. If the investigated PDMS formulation swells in the presence of a given liquid, the combination cannot be

used as a material for dielectric elastomer transducers, as the conductivity of such materials is expected to be greatly increased. Another restriction comes from a temperature range at which a given liquid retains its favourable properties. A rough estimation can be attained from the melting and boiling points. Relatively high melting points of certain liquids eliminate them from low-temperature applications, as the mechanical properties of the liquid-PDMS composites deteriorate upon liquid crystallisation.

**Table 3.3.2.** Various physical properties of selected high-permittivity polar liquids.<sup>129,142,143</sup> The marked values correspond to unfavourable properties which eliminate a given liquid from its use as a filler for PDMS-based dielectric elastomers.

	Dielectric constant at 20 °C	Vapour pressure at 20 °C [Pa]	Melting point [°C]	Boiling point [°C]	Solubility parameter $\delta$ [cal <sup>1/2</sup> cm <sup>-3/2</sup> ] <sup>a</sup>	Swelling ratio <sup>b</sup>
Water	80	<b>2340</b>	<b>0</b>	<b>100</b>	23.4	1.00
Glycerol	42	0.4 (at 50 °C)	18 <sup>c</sup>	290	21.1	1.00
Propylene carbonate	64	17	-49	242	13.3	<b>1.01</b>
Ethylene glycol	37	8	<b>-13</b>	197	14.6	1.00
DMSO	48	56	<b>19</b>	189	13.0	1.00
DMF	38	<b>516</b>	-61	153	12.1	1.02
Ethanol	24	<b>5950</b>	-114	<b>78</b>	12.7	<b>1.04</b>

<sup>a</sup>  $\delta_{\text{PDMS}}=7.3 \text{ cal}^{1/2}\text{cm}^{-3/2}$ , <sup>b</sup> swelling ratio is the ratio between sample lengths in swollen and dry states, <sup>c</sup> crystallisation only under very specific conditions (normally does not crystallise)

Data presented in Table 3.3.2 suggest that only the glycerol seems to completely fulfill all of the requirements. However, propylene carbonate (PC) and ethylene glycol seem to be applicable as well, with only minor shortcomings. According to Lee et al., silicones swell in the presence of propylene carbonate, yet the swelling ratio is very slight.<sup>129</sup> On the other hand, the relatively high melting point of ethylene glycol eliminates it from using this liquid at low ambient temperatures. Experiments on ethylene glycol were not conducted, as the permittivity of this liquid is lower than that of glycerol. The research focused on propylene carbonate instead, which has a very high dielectric constant ( $\epsilon=64$ ) and is a well-known and widely used liquid in electrochemistry.<sup>144–146</sup>

In the first step propylene carbonate was embedded within Sylgard 184. The sample preparation followed the same procedure as in the case of the glycerol-silicone composites. SEM images of cross-sections of the cured composites are presented in Figure 3.3.4. Rough calculations of the average droplet diameter (based on measurements of at least a hundred adjacent droplets, and assuming that the droplets are spherical) showed that the droplet size of propylene carbonate is smaller than that of glycerol in the investigated silicone. Sample PC20\_S184 has an average droplet diameter of 1.8  $\mu\text{m}$  (coefficient of variation  $CV = 39\%$ ), while droplets in glycerol-S184 compositions have an average diameter of 2.3  $\mu\text{m}$  ( $CV = 35\%$ ). The observed decrease might come from the fact that propylene carbonate exhibits significantly lower viscosity than glycerol, and therefore droplet breakup is more efficient at a given shear force. Additionally, it can be observed that the propylene carbonate droplets do not form spherical shapes as in the case of glycerol. Especially at higher loadings the droplets become less spherical-like, which might lead to a conductivity increase in the resulting composites.

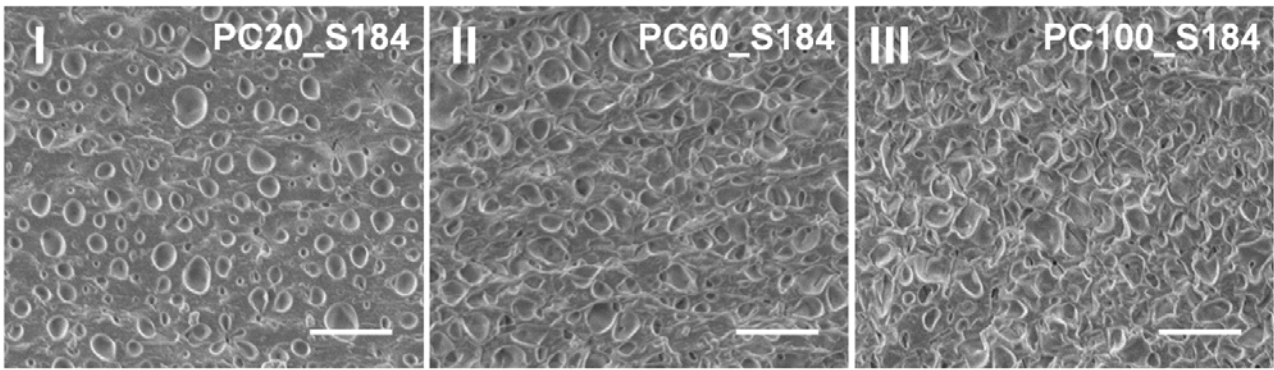


**Figure 3.3.4.** SEM images of cross-sections of cured PC-S184 composites. I – PC20\_S184, II – PC60\_S184, III – PC100\_S184. Scale bars for all images correspond to 10  $\mu\text{m}$ .

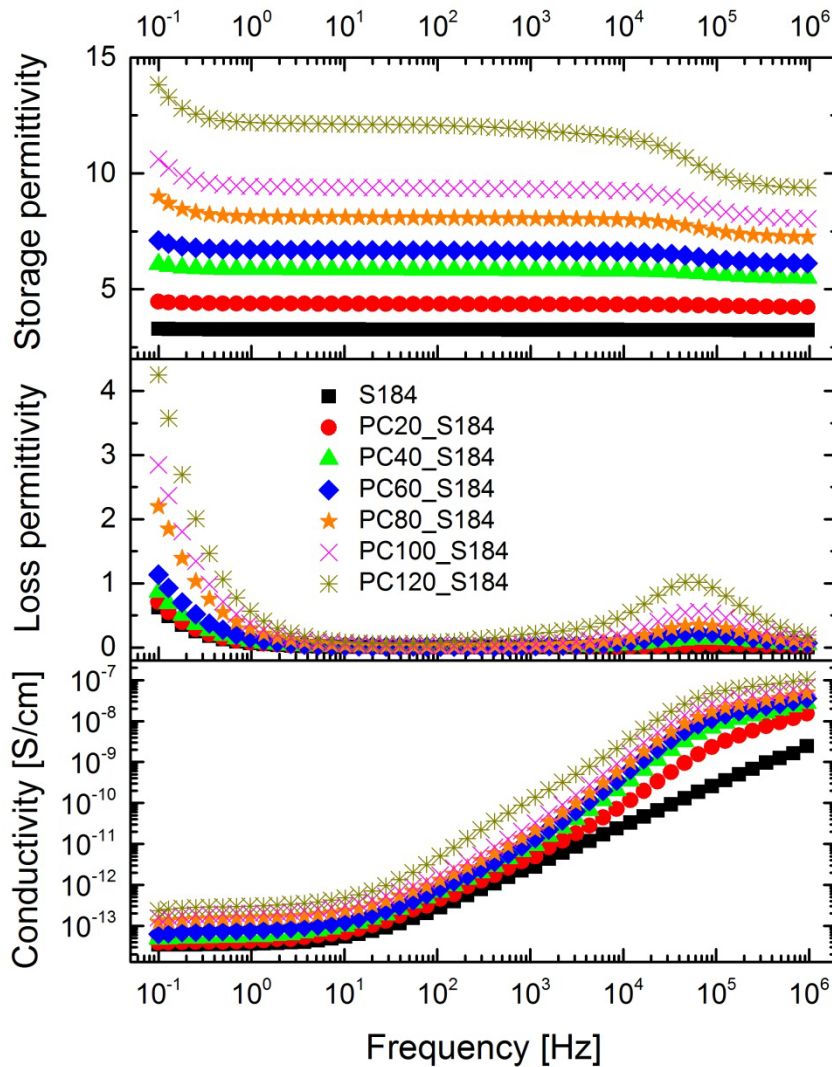


**Figure 3.3.5.** Storage permittivity, loss permittivity and conductivity of various PC-S184 composites at room temperature.

As can be seen in Figure 3.3.5, the dielectric constant of Sylgard 184 was enhanced efficiently by adding propylene carbonate. Nonetheless, the increase was lower than in the case of the glycerol-S184 composites. Maximum permittivity of around 12.5 was reached by the sample PC120\_S184, whereas the sample G120\_S184 exhibited permittivity of 16 at 1kHz. Considering the difference in dielectric constants between the two liquids, the slight increase in the permittivity of the PC-S184 composites was unexpected. Moreover, the dielectric loss exhibited by these composites increased in the low frequency range, and this became more prominent in line with increases in liquid loading. Similar tendencies were observed in the case of the conductivity, which also increased with increasing propylene carbonate content. It might be argued that this phenomenon is caused by the poor encapsulation of propylene carbonate by PDMS. Interestingly, though, conductivity increased at lower filler loadings (unlike glycerol-S184 composites), which might be evidence for PDMS swelling in the presence of propylene carbonate.

Multiple issues were encountered when preparing composites based on propylene carbonate and other PDMS formulations (XLR630, RT620 and P7684). All three PDMS systems allowed for the preparation of PC-PDMS emulsions with a maximum loading of 20 phr. Above this level, though, a clear phase split was observed, which is especially counterintuitive when the low viscosity of the P7684 is considered. The thinning agent OS-20 was used in order to produce high propylene carbonate loading composites, as it was expected that it might promote emulsion formation. Firstly, XLR630 was investigated and 40 phr of OS-20 was added to each composition. Although the emulsion formation was satisfactory, the obtained cross-linked films did not exhibit any enhancement of permittivity. SEM analysis showed that propylene carbonate was not present in the structure of XLR630 after the curing reaction was completed. It can be hypothesised that OS-20 facilitated the evaporation of propylene carbonate, resulting in a major decrease in the inclusion content in the final material. XLR630 requires a high-temperature environment for the cross-linking reaction to occur, and so lowering the curing temperature was not an option in this case. Subsequently, samples based on RT620 and propylene carbonate with the addition of 40 phr of OS-20 were prepared. As RT620 is a room-temperature vulcanisable silicone, it allows one to decrease the temperature of the cross-linking reaction. The prepared samples were cured at around 20 °C in order to eliminate the issue of propylene carbonate evaporation. As can be seen in Figure 3.3.6, a slight enhancement of dielectric constant was achieved. On the other hand, the increase is much lower than expected, thereby indicating that the negative effect of OS-20 on the propylene carbonate evaporation was not eliminated, although curing temperature was significantly decreased. In addition, the conductivities of the produced composites increased by around three orders of magnitude when propylene carbonate was added. Data presented in Table 3.3.1 suggest that RT620 is much softer than S184. It is believed that a balance between cross-linking density and silica loading in softer materials facilitates the swelling of the elastomer when it is exposed to solvents, such as propylene carbonate. This is considered a direct factor influencing the conductivity enhancement and thereby eliminating propylene carbonate from using it as a filler for dielectric elastomer transducers.

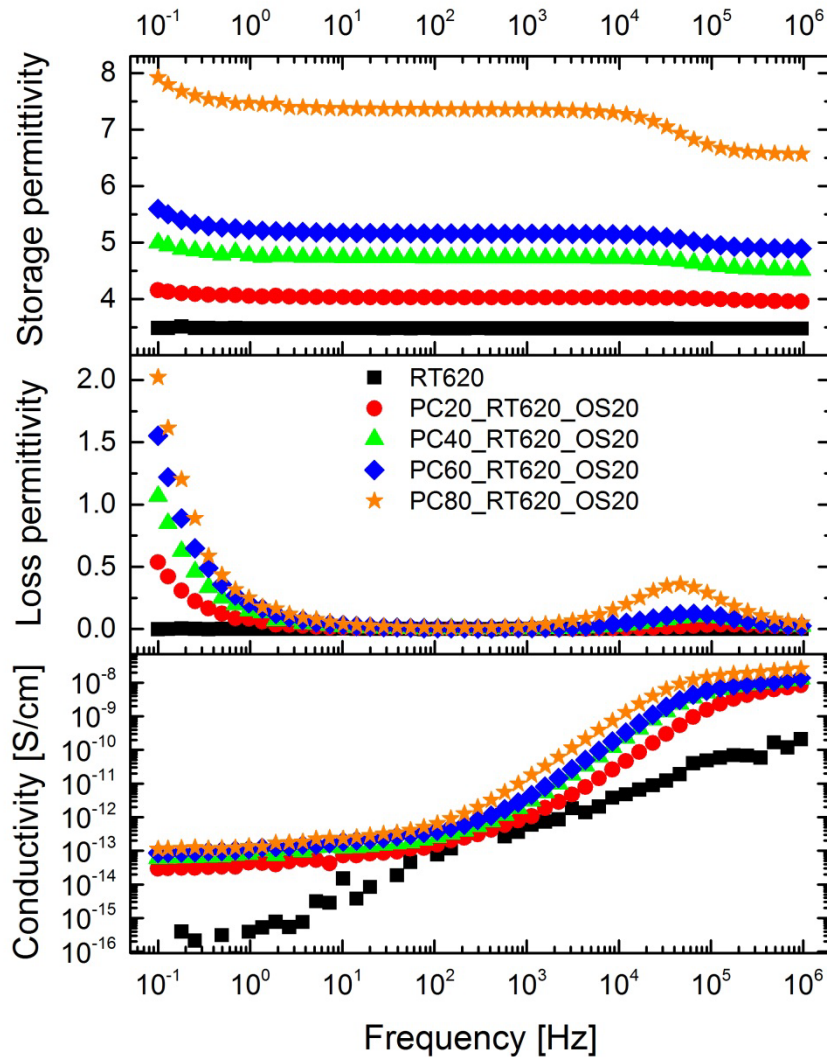


**Figure 3.3.6.** Storage permittivity, loss permittivity and conductivity of various PC-RT620 composites at room temperature.

### Breakdown strength and actuation performance of various liquid-PDMS composites

Breakdown strength measurements were performed on glycerol-PDMS composites, using a home-built device equipped with a 20 kV voltage source. In the first step, the thicknesses of the previously prepared films were measured with the help of an optical microscope. The sample thicknesses were around  $100\ \mu\text{m}$  ( $\pm 10\ \mu\text{m}$ ) unless mentioned otherwise. The investigated films were placed between two semi-spherical electrodes with adjustable spacing, as seen in Figure 3.3.7, and subjected to voltage increasing with a rate of 200 V/s. Measurements were interrupted when an electrical breakdown event occurred. Each sample was tested 12 times, and an average breakdown voltage was calculated. This procedure is considered to provide reliable data with good reproducibility.<sup>57,68</sup>

All investigated samples (starting with 10 phr of incorporated glycerol) exhibited current leakage before the occurrence of electrical breakdown. The higher the glycerol loading, the lower electrical

field could be withstood and the higher the subsequent leaking current was. The samples exhibited conductive behaviour in the electrical fields, starting between 10 and 20 V/ $\mu\text{m}$ , whereas breakdown occurred at around 40 V/ $\mu\text{m}$ . Although dielectric strength appears satisfactory, current leakages eliminated composites at the present state from applications at voltages exceeding 10 – 20 V/ $\mu\text{m}$ .

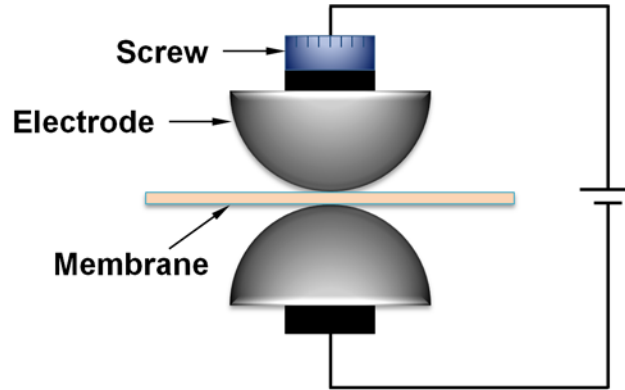


**Figure 3.3.7.** Schematic representation of the electrical breakdown test setup.

Despite issues with current leakages, actuation tests were conducted in order to investigate actuation performance at relatively low voltages. As the high-loading composites exhibited very high values of dielectric constants and low elastic moduli, it was believed that the prepared membranes might exhibit actuation in low electrical fields. The investigated films were placed and clamped to a round frame, as presented in Figure 3.3.8. Carbon grease electrodes were smeared on both sides of the sample and wired to a voltage source. Each of the investigated formulations was tested with 30% pre-stretching and without pre-stretching.

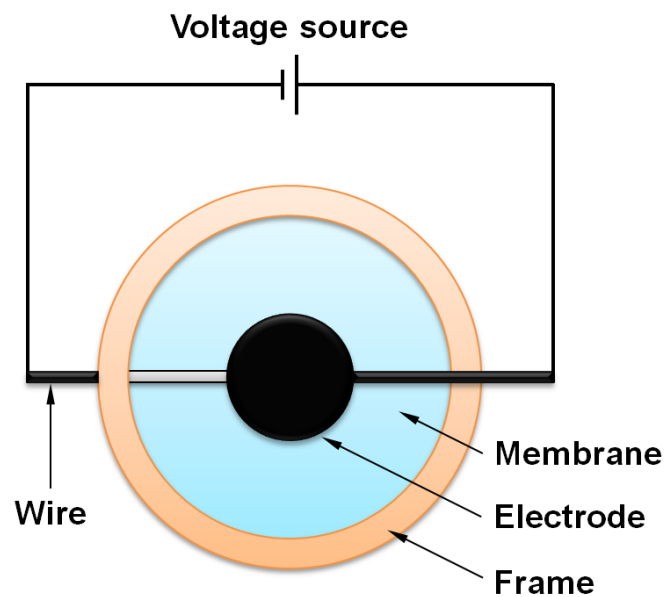


**Figure 3.3.8.** Schematic representation of the actuation experiment.

All pre-stretched membranes exhibited current leakage before any actuation occurred. This might be explained by the fact that upon stretching the distance between adjacent droplets decreased significantly, which finally led to minimising the effect of droplet insulation and resulted in increased conductivity. On the other hand, some of the non-pre-stretched composites exhibited actuation in the electrical fields lower than in the case of the pure PDMS samples, most likely due to the higher dielectric constant and the lower Young's modulus of the liquid-PDMS compositions. However, these results exhibited poor reproducibility, implying that the material is very sensitive to any inhomogeneity. Sample preparation in cleanroom conditions might potentially solve this issue.

Up to this point, none of the investigated liquid-PDMS composites had withstood electrical fields comparable to the applied base PDMS matrix, so the reliability of such materials was considered to be insufficient in the current state. However, the actuation performance experiments exhibited some potential for the liquid-PDMS composites, because in some cases actuation at relatively low voltages was obtained. It is obvious that the liquid-PDMS compositions require further optimisation, but the conducted research resulted in significant progress and exposed the parameters that need to be considered when designing such materials. It is believed that additional research on the development of an elastomeric matrix might facilitate a breakthrough and allow for the preparation of commercially attractive dielectric elastomers.

### **3.3.3. Conclusions**

In this chapter the most important parameters influencing actuation performance of liquid-silicone composites were recognised and discussed. The applicability of various PDMS matrices as well as high-permittivity polar liquids was discussed in detail, and the most promising candidates were evaluated experimentally. It is believed that the meticulous investigation of the matrix and inclusion parameters defined precisely the requirements that need to be fulfilled in order to produce an attractive dielectric elastomer. Consequently, the necessity to conduct thorough experiments, aiming at finding the polymeric matrix with the highest possible resistivity, was exposed.

## 4. Conclusions and future work

Enhancing the relative permittivity of silicone elastomers was achieved through two different methods. Both approaches involved incorporating polar liquids in the form of discrete droplets which acted as high-dielectric constant fillers.

In the first part of the research a versatile and robust flow-focusing microfluidic device, based on thiol-ene-epoxy “click” chemistry, was designed and developed. It allowed for the formation of elastomeric in nature core-shell microspheres with a narrow size distribution, which then became a carrier for embedding water into a silicone matrix. This rather complicated and time-consuming approach proved the concept that the dielectric constant of polymers can be enhanced efficiently via the controlled introduction of water droplets into polymeric materials. Incorporating only 4.5 wt.% of water resulted in a 30% increase in the dielectric constant. Although the approach was considered to be successful, it exhibited many challenges that had to be faced and overcome in order to obtain an attractive material. The main disadvantages and limitations of the developed composites were fast water evaporation from the PDMS matrix and relatively high film thicknesses, which were directly determined by the diameters of the produced capsules.

In the second part of the project the research focused solely on exploiting a new technique for composite preparation. The developed method was based on the direct mixing of two virtually immiscible liquids which formed stable emulsions (e.g. glycerol-PDMS emulsions) upon exposure to sufficiently high shear forces. This rather counterintuitive but at the same time very simple method allowed for the fast preparation of films consisting of even 50% by volume of a liquid phase in a form of discrete droplets. Furthermore, the preparation of very thin (even 50  $\mu\text{m}$ ) free-standing films with controllable filler droplet diameters (down to sub-micrometer sizes) was possible. Polar liquid droplets acted as high-permittivity fillers and were proven to efficiently enhance the dielectric constant and at the same time decrease the modulus of elasticity of various silicone matrices. Incorporating 120 phr of glycerol into Sylgard 184 resulted in increasing permittivity by 380% and a more than three-fold decrease in the Young’s modulus. Multiple compositions were investigated in terms of their performance as dielectric actuators, and hence a thorough evaluation of the concept of incorporating high-permittivity polar liquids into silicone elastomers was performed. Nonetheless, in the current state none of the prepared liquid-silicone composites exhibits promising actuation upon exposure to high electrical fields. On the other hand, it is believed that further research on the optimisation of an applied polymeric matrix might potentially solve the identified problem of leakage current. The research conducted within this Ph.D. project revealed the potential of this class of dielectric elastomer and exposed directions for further – and exciting – study.

Although the dielectric properties of the developed hybrid materials need further optimisation, it emerged that glycerol-silicone composites have many appealing properties. Water absorption and release followed by substance release, described thoroughly in Chapter 3.1, are properties that appear promising from the perspective of applications such as sealants, functional patches or active substance delivery vehicles. Their green profile and low price are additional factors that might attract the attention of the silicone society. It is envisioned that any future research on these novel



elastomers will focus largely on developing biomedical products, as both PDMS and glycerol are considered as biocompatible substances. One possible application, showcasing the potential of the material, could focus on developing functional catheters that would be capable of adjusting their thickness in relation to a ureter's diameter. In this way the usual discomfort accompanying catheter insertion would be reduced significantly. Furthermore, the catheter would be able to release active substances into the ureter's tissue (such as disinfectant), which would benefit many and lead to improved quality of life.

## 5. Experimental methods

### Infrared spectroscopy

Nicolet iS50 FT-IR was used to obtain ATR FTIR spectra of neat and surface-modified polymers, synthesised ionic liquids and cross-sections of liquid-silicone composites.

### Differential Scanning Calorimetry

A TA Instruments Differential Scanning Calorimeter (DSC) Q1000 was used to determine the thermal behaviour of the samples. All tests were performed at a heating rate of 10 °C/min across a temperature range between -30 °C and 120 °C in an N<sub>2</sub> atmosphere. Reported glass transition temperatures of OSTE formulations were based on at least two independent measurements, where deviations from individual tests were no higher than 2 °C, whereas for OSTE+ formulations one measurement was conducted.

### Water contact angle

The water wettability properties of the polymers were investigated through the use of DataPhysics OCA20. Samples were tested using the sessile drop method, and the average water contact angle was calculated from at least three measurements.

### Viscosimetry

Viscosities of the investigated pre-polymer formulations were determined with the help of an Ares AR2000ex rheometer from TA Instruments, using a conical concentric cylinder geometry at a steady state flow measurement.

### Optical microscopy

A Leica DM LB optical microscope was applied, in order to determine the morphology of produced microspheres, microcapsules, glycerol-silicone emulsions and cured glycerol-silicone composites.

### Rheology

Frequency sweep tests performed on an ARES G2 rheometer from TA Instruments were conducted, in order to determine both the storage and loss moduli of the investigated compositions. Disc samples 25 mm in diameter and 1 mm thick were tested in the frequency range between 100 Hz and 0.001 Hz and under controlled strain mode (2% strain) at room temperature.

### Broadband Dielectric Spectroscopy

A Novocontrol broadband dielectric spectrometer was used to investigate the dielectric permittivity, dielectric losses and conductivity of samples. Disc specimens 20 mm in diameter and 1 mm thick were tested in the frequency range between 10<sup>6</sup> Hz and 10<sup>-1</sup> Hz. While discussing the resulting dielectric constants of composites, values at 1 kHz were used (unless stated otherwise), as in all cases all samples reach a plateau at this frequency.

**Scanning Electron Microscopy**

An FEI Inspect S scanning electron microscope (SEM) was used to obtain images of cured liquid-silicone composite cross-sections. Samples were gold-sputtered prior to testing, in order to obtain higher quality images.

**Tensile tests**

Tensile measurements were performed at room temperature using an Instron 4301 universal tester at a strain rate of 500 mm/min – as stipulated by ASTM D412-C standards. All specimens were cut with a custom-made die.

**High-voltage broadband dielectric spectroscopy**

A high-voltage broadband dielectric spectroscopy was performed on a Novocontrol Alpha-A device equipped with a high-voltage booster HVB1000. Specimens were tested in a frequency range between  $10^4$  and  $10^{-1}$  Hz (a narrower frequency range as in case of 1 V measurements, due to apparatus limitations).

**Dielectric strength measurements**

Measurements were performed on an in-house-built apparatus following international standards (IEC 60243-1 and IEC 60243-2). The voltage increase was 50-100 V/step at a rate 0.5-1 steps/s.

## Bibliography

- 1 C. Keplinger, M. Kaltenbrunner, N. Arnold and S. Bauer, *Proc. Natl. Acad. Sci. U. S. A.*, 2010, **107**, 4505–4510.
- 2 C. K. Chiang, C. R. Fincher, Y. W. Park, A. J. Heeger, H. Shirakawa, E. J. Louis, S. C. Gau and A. G. MacDiarmid, *Phys. Rev. Lett.*, 1977, **39**, 1098–1101.
- 3 H. Shirakawa, E. J. Louis, A. G. MacDiarmid, C. K. Chiang and A. J. Heeger, *J. Chem. Soc. Chem. Commun.*, 1977, 578–580.
- 4 W. P. Su, J. R. Schrieffer and A. J. Heeger, *Phys. Rev. Lett.*, 1979, **42**, 1698–1701.
- 5 W. P. Su, J. R. Schrieffer and A. J. Heeger, *Phys. Rev. B*, 1980, **22**, 2099–2111.
- 6 R. Pelrine, R. Kornbluh, J. Joseph, R. Heydt, Q. Pei and S. Chiba, *Mater. Sci. Eng. C*, 2000, **11**, 89–100.
- 7 M. Zhenyi, J. I. Scheinbeim, J. W. Lee and B. A. Newman, *J. Polym. Sci. Part B Polym. Phys.*, 1994, **32**, 2721–2731.
- 8 Y. M. Shkel and D. J. Klingenberg, *J. Appl. Phys.*, 1996, **80**, 4566–4572.
- 9 U. Kosidlo, M. Omastová, M. Micusik, G. Ćirić-Marjanović, H. Randriamahazaka, T. Wallmersperger, A. Aabloo, I. Kolaric and T. Bauernhansl, *Smart Mater. Struct.*, 2013, **22**, 104022.
- 10 Q. Pei and O. Inganäs, *Synth. Met.*, 1993, **57**, 3730–3735.
- 11 R. H. Baughman, *Synth. Met.*, 1996, **78**, 339–353.
- 12 T. F. Otero, R. J. E. Angulo and C. Santamaria, *Synth. Met.*, 1993, **57**, 3713–3717.
- 13 K. Kaneto, M. Kaneko, Y. Min and A. G. MacDiarmid, *Synth. Met.*, 1995, **71**, 2211–2212.
- 14 W. Lu, A. G. Fadeev, B. Qi, E. Smela, B. R. Mattes, J. Ding, G. M. Spinks, J. Mazurkiewicz, D. Zhou, G. G. Wallace, D. R. MacFarlane, S. A. Forsyth and M. Forsyth, *Science*, 2002, **297**, 983–987.
- 15 F. Vidal, C. Plesse, D. Teyssié and C. Chevrot, *Synth. Met.*, 2004, **142**, 287–291.
- 16 J. Arias-Pardilla, C. Plesse, A. Khaldi, F. Vidal, C. Chevrot and T. F. Otero, *J. Electroanal. Chem.*, 2011, **652**, 37–43.
- 17 A. Khaldi, C. Plesse, C. Soyer, E. Cattan, F. Vidal, C. Legrand and D. Teyssié, *Appl. Phys. Lett.*, 2011, **98**, 164101.
- 18 N. Festin, A. Maziz, C. Plesse, D. Teyssié, C. Chevrot and F. Vidal, *Smart Mater. Struct.*, 2013, **22**, 104005.
- 19 A. Maziz, C. Plesse, C. Soyer, E. Cattan and F. Vidal, *Proc. SPIE*, 2015, **9430**, 943000–1.
- 20 E. W. H. Jager, E. Smela and O. Inganäs, *Science*, 2000, **290**, 1540–1545.
- 21 E. W. H. Jager, O. Inganäs and I. Lundström, *Science*, 2000, **288**, 2335–2338.
- 22 S. A. Wilson, R. P. J. Jourdain, Q. Zhang, R. A. Dorey, C. R. Bowen, M. Willander, Q. U. Wahab, M. A. H. Safaa, O. Nur, E. Quandt, C. Johansson, E. Pagounis, M. Kohl, J. Matovic, B. Samel, W. van der Wijngaart, E. W. H. Jager, D. Carlsson, Z. Djinovic, M. Wegener, C. Moldovan, R. Iosub, E. Abad, M. Wendlandt, C. Rusu and K. Persson, *Mater. Sci. Eng. R-Reports*, 2007, **56**, 1–129.
- 23 R. Pelrine, R. Kornbluh, J. Joseph, S. Chiba and M. Park, *IEEE Micro Electro Mech. Syst.*, 1997, **1**, 238–243.
- 24 F. Carpi, S. Bauer and D. De Rossi, *Science*, 2010, **330**, 1759–1761.
- 25 P. Brochu and Q. Pei, *Macromol. Rapid Commun.*, 2010, **31**, 10–36.
- 26 R. Kornbluh, R. Pelrine, J. Eckerle and J. Joseph, *Proceedings. 1998 IEEE Int. Conf. Robot. Autom.*, 1998, **3**, 2147–2154.
- 27 R. Pelrine, R. Kornbluh and G. Kofod, *Adv. Mater.*, 2000, **12**, 1223–1225.
- 28 J. D. W. Madden, N. A. Vandesteeg, P. A. Anquetil, P. G. A. Madden, A. Takshi, R. Z.

- Pytel, S. R. Lafontaine, P. A. Wieringa and I. W. Hunter, *IEEE J. Ocean. Eng.*, 2004, **29**, 706–728.
- 29 K. Ahnert, M. Abel, M. Kollosche, P. J. Jørgensen and G. Kofod, *J. Mater. Chem.*, 2011, **21**, 14492–14497.
- 30 M. Molberg, D. Crespy, P. Rupper, F. Nüesch, J. A. E. Månson, C. Löwe and D. M. Opris, *Adv. Funct. Mater.*, 2010, **20**, 3280–3291.
- 31 C. Löwe, X. Zhang and G. Kovacs, *Adv. Eng. Mater.*, 2005, **7**, 361–367.
- 32 R. E. Pelrine, R. D. Kornbluh and J. P. Joseph, *Sens. Actuators A Phys.*, 1998, **64**, 77–85.
- 33 R. Pelrine, *Science*, 2000, **287**, 836–839.
- 34 L. Maffli, S. Rosset, M. Ghilardi, F. Carpi and H. Shea, *Adv. Funct. Mater.*, 2015, **25**, 1656–1665.
- 35 S. Michel, X. Q. Zhang, M. Wissler, C. Löwe and G. Kovacs, *Polym. Int.*, 2009, **59**, 391–399.
- 36 Z. Yu, W. Yuan, P. Brochu, B. Chen, Z. Liu and Q. Pei, *Appl. Phys. Lett.*, 2009, **95**, 15–18.
- 37 Y. Torijama and U. Shinohara, *Phys. Rev.*, 1937, **51**, 680.
- 38 L. Bokobza, *J. Appl. Polym. Sci.*, 2004, **93**, 2095–2104.
- 39 I. Stevenson, L. David, C. Gauthier, L. Arambourg, J. Davenas and G. Vigier, *Polymer*, 2001, **42**, 9287–9292.
- 40 D. M. Opris, M. Molberg, C. Walder, Y. S. Ko, B. Fischer and F. A. Nüesch, *Adv. Funct. Mater.*, 2011, **21**, 3531–3539.
- 41 R. Kochetov, I. A. Tsekmes and P. H. F. Morshuis, *Smart Mater. Struct.*, 2015, **24**, 075019.
- 42 S. Rosset and H. R. Shea, *Appl. Phys. A*, 2013, **110**, 281–307.
- 43 R. D. Kornbluh, R. Pelrine, J. Joseph, R. Heydt, Q. Pei and S. Chiba, *Proc. SPIE*, 1999, **3669**, 149–161.
- 44 N. Bowden, S. Brittain and A. Evans, *Nature*, 1998, **393**, 146–149.
- 45 A. Pimpin, Y. Suzuki and N. Kasagi, *J. Microelectromech. Syst.*, 2007, **16**, 753–764.
- 46 I. M. Graz, D. P. J. Cotton and S. P. Lacour, *Appl. Phys. Lett.*, 2009, **94**, 071902.
- 47 M. Benslimane, P. Gravesen and P. Sommer-Larsen, *Proc. SPIE*, 2002, **4695**, 150–157.
- 48 M. Y. Benslimane, H. E. Kiil and M. J. Tryson, *Polym. Int.*, 2010, **59**, 415–421.
- 49 H. E. Kiil and M. Benslimane, *Proc. SPIE*, 2009, **7287**, 72870R–1.
- 50 M. Benslimane, H. E. Kiil and M. J. Tryson, *Proc. SPIE*, 2010, **7642**, 764231–1.
- 51 H. Haus, M. Matysek, H. Mossinger and H. F. Schlaak, *Smart Mater. Struct.*, 2013, **22**, 104009.
- 52 G. Kovacs, L. Düring, S. Michel and G. Terrasi, *Sens. Actuators A Phys.*, 2009, **155**, 299–307.
- 53 G. Kovacs and L. Düring, *Proc. SPIE*, 2009, **7287**, 72870A–1.
- 54 T. Töpfer, F. Weiss, B. Osmani, C. Bippes, V. Leung and B. Müller, *Sens. Actuators A Phys.*, 2015, **233**, 32–41.
- 55 A. L. Larsen, P. Sommer-Larsen and O. Hassager, *Proc. SPIE*, 2004, **5385**, 108–117.
- 56 A. G. Bejenariu, L. Yu and A. L. Skov, *Soft Matter*, 2012, **8**, 3917–3923.
- 57 S. Zakaria, L. Yu, G. Kofod and A. L. Skov, *Mater. Today Commun.*, 2015, **4**, 204–213.
- 58 S. Akbari, S. Rosset and H. R. Shea, *Appl. Phys. Lett.*, 2013, **102**, 2011–2016.
- 59 G. Gallone, F. Galantini and F. Carpi, *Polym. Int.*, 2010, **59**, 400–406.
- 60 W. Hu, Z. Ren, J. Li, E. Askounis, Z. Xie and Q. Pei, *Adv. Funct. Mater.*, 2015, **25**, 4827–4836.
- 61 W. Hu, X. Niu, X. Yang, N. Zhang and Q. Pei, *Proc. SPIE*, 2013, **8687**, 86872U–1.
- 62 C. Jean-Mistral, A. Sylvestre, S. Basrouer and J. Chaillout, *Smart Mater. Struct.*, 2010, **19**, 075019.

- 63 J. Sheng, H. Chen, B. Li and L. Chang, *Appl. Phys. A*, 2013, **110**, 511–515.
- 64 M. Wissler and E. Mazza, *Sens. Actuators A Phys.*, 2007, **134**, 494–504.
- 65 J. Huang, S. Shian, Z. Suo and D. R. Clarke, *Adv. Funct. Mater.*, 2013, **23**, 5056–5061.
- 66 T. G. McKay, S. Rosset, I. A. Anderson and H. Shea, *Smart Mater. Struct.*, 2015, **24**, 015014.
- 67 G. Gallone, F. Carpi, D. De Rossi, G. Levita and A. Marchetti, *Mater. Sci. Eng. C*, 2007, **27**, 110–116.
- 68 S. Vudayagiri, S. Zakaria, L. Yu, S. S. Hassouneh, M. Benslimane and A. L. Skov, *Smart Mater. Struct.*, 2014, **23**, 105017.
- 69 A. E. Daugaard, S. S. Hassouneh, M. Kostrzewska, A. G. Bejenariu and A. L. Skov, *Proc. SPIE*, 2013, **8687**, 868729–1.
- 70 K. Goswami, A. E. Daugaard and A. L. Skov, *RSC Adv.*, 2015, **5**, 12792–12799.
- 71 A. Javadi, Y. Xiao, W. Xu and S. Gong, *J. Mater. Chem.*, 2012, **22**, 830–834.
- 72 F. Carpi, G. Gallone, F. Galantini and D. De Rossi, *Adv. Funct. Mater.*, 2008, **18**, 235–241.
- 73 F. B. Madsen, A. E. Daugaard, C. Fleury, S. Hvilsted and A. L. Skov, *RSC Adv.*, 2014, **4**, 6939–6945.
- 74 F. B. Madsen, A. E. Daugaard, S. Hvilsted, M. Y. Benslimane and A. L. Skov, *Smart Mater. Struct.*, 2013, **22**, 104002.
- 75 F. B. Madsen, I. Dimitrov, A. E. Daugaard, S. Hvilsted and A. L. Skov, *Polym. Chem.*, 2013, **4**, 1700–1707.
- 76 F. B. Madsen, L. Yu, A. E. Daugaard, S. Hvilsted and A. L. Skov, *Polymer*, 2014, **55**, 6212–6219.
- 77 B. Kussmaul, S. Risse, M. Wegener, G. Kofod and H. Krüger, *Smart Mater. Struct.*, 2012, **21**, 064005.
- 78 B. Kussmaul, S. Risse, G. Kofod, R. Waché, M. Wegener, D. N. McCarthy, H. Krüger and R. Gerhard, *Adv. Funct. Mater.*, 2011, **21**, 4589–4594.
- 79 S. J. Dünki, M. Tress, F. Kremer, S. Y. Ko, F. A. Nüesch, C. D. Varganici, C. Racles and D. M. Opris, *RSC Adv.*, 2015, **5**, 50054–50062.
- 80 S. J. Dünki, Y. S. Ko, F. A. Nüesch and D. M. Opris, *Adv. Funct. Mater.*, 2015, **25**, 2467–2475.
- 81 C. Racles, M. Cazacu, B. Fischer and D. M. Opris, *Smart Mater. Struct.*, 2013, **22**, 104004.
- 82 S. Michel, B. T. T. Chu, S. Grimm, F. A. Nüesch, A. Borgschulte and D. M. Opris, *J. Mater. Chem.*, 2012, **22**, 20736–20741.
- 83 S. Hunt, T. G. McKay and I. A. Anderson, *Appl. Phys. Lett.*, 2014, **104**, 2013–2016.
- 84 D. M. Opris, D. Crespy, C. Löwe, M. Molberg and F. Nüesch, *Proc. SPIE*, 2009, **7287**, 72870L–1.
- 85 J. E. Quinsaat, M. Alexandru, F. Nüesch, H. Hofmann, A. Borgschulte and D. Opris, *J. Mater. Chem. A*, 2015, **3**, 14675–14685.
- 86 L. Yu, S. Vudayagiri, S. Zakaria, M. Y. Benslimane and A. L. Skov, *Proc. SPIE*, 2014, **9056**, 90560S–1.
- 87 W. Hu, S. N. Zhang, X. Niu, C. Liu and Q. Pei, *J. Mater. Chem. C*, 2014, **2**, 1658–1666.
- 88 A. B. Lowe, *Polym. Chem.*, 2010, **1**, 17–36.
- 89 C. E. Hoyle and C. N. Bowman, *Angew. Chem. Int. Ed.*, 2010, **49**, 1540–1573.
- 90 G. T. Vladislavljević, I. Kobayashi and M. Nakajima, *Microfluid. Nanofluidics*, 2012, **13**, 151–178.
- 91 N. B. Cramer, S. K. Reddy, M. Cole, C. Hoyle and C. N. Bowman, *J. Polym. Sci. A Polym. Chem.*, 2004, **42**, 5817–5826.
- 92 C. F. Carlborg, T. Haraldsson, K. Öberg, M. Malkoch and W. van der Wijngaart, *Lab Chip*,

- 2011, **11**, 3136–3147.
- 93 W. C. Jeong, M. Choi, C. H. Lim and S. M. Yang, *Lab Chip*, 2012, **12**, 5262–5271.
- 94 J. A. Carioscia, J. W. Stansbury and C. N. Bowman, *Polymer*, 2007, **48**, 1526–1532.
- 95 T. M. Sikanen, J. P. Lafleur, M. E. Moilanen, G. Zhuang, T. G. Jensen and J. P. Kutter, *J. Micromech. Microeng.*, 2013, **23**, 037002.
- 96 F. Saharil, F. Forsberg, Y. Liu, P. Bettotti, N. Kumar, F. Niklaus, T. Haraldsson, W. van der Wijngaart and K. B. Gylfason, *J. Micromech. Microeng.*, 2013, **23**, 025021.
- 97 X. L. Yuan, S. J. Zhang and X. M. Lu, *J. Chem. Eng. Data*, 2007, **52**, 596–599.
- 98 G. Pardon, F. Saharil, J. M. Karlsson, O. Supekar, C. F. Carlborg, W. van der Wijngaart and T. Haraldsson, *Microfluid. Nanofluidics*, 2014, **17**, 773–779.
- 99 L. González, A. L. Skov and S. Hvilsted, *J. Polym. Sci. A Polym. Chem.*, 2013, **51**, 1359–1371.
- 100 L. González, A. L. Skov and S. Hvilsted, *Macromol. Symp.*, 2014, **342**, 8–20.
- 101 N. N. Deng, Z. J. Meng, R. Xie, X. J. Ju, C. L. Mou, W. Wang and L. Y. Chu, *Lab Chip*, 2011, **11**, 3963–3969.
- 102 F. C. Chang and Y. C. Su, *J. Micromech. Microeng.*, 2008, **18**, 065018.
- 103 Y. Zhang, M. Ishida, Y. Kazoe, Y. Sato and N. Miki, *IEEJ Trans. Electr. Electron. Eng.*, 2009, **4**, 442–449.
- 104 C. Cazan and A. Duta, *Advances in Elastomers I*, Springer, Berlin, 2013, vol. 11.
- 105 K. Madhavan Nampoothiri, N. R. Nair and R. P. John, *Bioresour. Technol.*, 2010, **101**, 8493–8501.
- 106 S. S. Ray and M. Bousmina, *Prog. Mater. Sci.*, 2005, **50**, 962–1079.
- 107 M. Avella, A. Buzarovska, M. E. Errico, G. Gentile and A. Grozdanov, *Materials*, 2009, **2**, 911–925.
- 108 T. Mekonnen, P. Mussone, K. Alemaskin, L. Sopkow, J. Wolodko, P. Choi and D. Bressler, *J. Mater. Chem. A*, 2013, **1**, 13186.
- 109 G. Mehta, A. K. Mohanty, M. Misra and L. T. Drzal, *Green Chem.*, 2004, **6**, 254–258.
- 110 N. Supanchaiyamat, P. S. Shuttleworth, A. J. Hunt, J. H. Clark and A. S. Matharu, *Green Chem.*, 2012, **14**, 1759–1765.
- 111 H. S. Kim, H. J. Kim, J. W. Lee and I. G. Choi, *Polym. Degrad. Stab.*, 2006, **91**, 1117–1127.
- 112 E. Chiellini, P. Cinelli, V. I. Ilieva and M. Martera, *Biomacromolecules*, 2008, **9**, 1007–1013.
- 113 Y. Sun, L. Yang, X. Lu and C. He, *J. Mater. Chem. A*, 2015, **3**, 3699–3709.
- 114 J. Zhang, Y. Chen, P. Sewell and M. A. Brook, *Green Chem.*, 2015, **17**, 1811–1819.
- 115 M. J. N. Pereira, B. Ouyang, C. A. Sundback, N. Lang, I. Friehs, S. Mureli, I. Pomerantseva, J. McFadden, M. C. Mochel, O. Mwizerwa, P. Del Nido, D. Sarkar, P. T. Masiakos, R. Langer, L. S. Ferreira and J. M. Karp, *Adv. Mater.*, 2013, **25**, 1209–1215.
- 116 Y. Wang, G. A. Ameer, B. J. Sheppard and R. Langer, *Nat. Biotechnol.*, 2002, **20**, 602–606.
- 117 B. G. Amsden, G. Misra, F. Gu and H. M. Younes, *Biomacromolecules*, 2004, **5**, 2479–2486.
- 118 R. Singh and A. J. Varma, *Green Chem.*, 2012, **14**, 348–356.
- 119 A. Takagaki, K. Iwatani, S. Nishimura and K. Ebitani, *Green Chem.*, 2010, **12**, 578–581.
- 120 B. Katryniok, H. Kimura, E. Skrzyńska, J. S. Girardon, P. Fongarland, M. Capron, R. Ducoulombier, N. Mimura, S. Paul and F. Dumeignil, *Green Chem.*, 2011, **13**, 1960–1979.
- 121 C. Della Pina, E. Falletta and M. Rossi, *Green Chem.*, 2011, **13**, 1624–1632.
- 122 A. Celli, P. Marchese, S. Sullalti, C. Berti, G. Barbiroli, S. Commereuc and V. Verney, *Green Chem.*, 2012, **14**, 182–187.
- 123 T. Mekonnen, P. Mussone, H. Khalil and D. Bressler, *J. Mater. Chem. A*, 2013, **1**, 13379–13398.
- 124 S. Sa'adon and A. Z. M. Rus, *Appl. Mech. Mater.*, 2014, **465-466**, 1039–1043.

- 125 B. F. S. Matsen M.W., *J. Chem. Phys.*, 1997, **106**, 2436–2448.
- 126 L. Li, L. Schulte, L. D. Clausen, K. M. Hansen, G. E. Jonsson and S. Ndoni, *ACS Nano*, 2011, **5**, 7754–7766.
- 127 I. D. Johnston, D. K. McCluskey, C. K. L. Tan and M. C. Tracey, *J. Micromech. Microeng.*, 2014, **24**, 035017.
- 128 A. L. Larsen, K. Hansen, P. Sommer-Larsen, O. Hassager, A. Bach, S. Ndoni and M. Jørgensen, *Macromolecules*, 2003, **36**, 10063–10070.
- 129 J. N. Lee, C. Park and G. M. Whitesides, *Anal. Chem.*, 2003, **75**, 6544–6554.
- 130 T. G. Kim, H. Shin and D. W. Lim, *Adv. Funct. Mater.*, 2012, **22**, 2446–2468.
- 131 I. C. Liao, F. T. Moutos, B. T. Estes, X. Zhao and F. Guilak, *Adv. Funct. Mater.*, 2013, **23**, 5833–5839.
- 132 F. Carpi, D. De Rossi, R. Kornbluh, R. Pelrine and P. Sommer-Larsen, *Dielectric Elastomers as Electromechanical Transducers*, Elsevier, Amsterdam, 2008.
- 133 J. C. M. Garnett, *Philos. Trans. R. Soc. A Math. Phys. Eng. Sci.*, 1906, **205**, 237–288.
- 134 E. Tuncer, S. M. Gubański and B. Nettelblad, *J. Appl. Phys.*, 2001, **89**, 8092–8100.
- 135 S. O. Nelson and T. S. You, *J. Phys. D. Appl. Phys.*, 1990, **23**, 346–353.
- 136 N. Jayasundere and B. V. Smith, *J. Appl. Phys.*, 1993, **73**, 2462–2466.
- 137 N. Jayasundere, B. V. Smith and J. R. Dunn, *J. Appl. Phys.*, 1994, **76**, 2993–2998.
- 138 Y. M. Poon and F. G. Shi, *J. Mater. Sci.*, 2004, **39**, 1277–1281.
- 139 M. Ezzat, N. A. Sabiha and M. Izzularab, *Appl. Nanosci.*, 2013, **4**, 331–338.
- 140 M. G. Todd and F. G. Shi, *J. Appl. Phys.*, 2003, **94**, 4551–4557.
- 141 H. T. Vo and F. G. Shi, *Microelectronics J.*, 2002, **33**, 409–415.
- 142 I. M. Smallwood, *Handbook of organic solvent properties*, John Wiley & Sons Inc., London, 1996.
- 143 G. Wypych, *Handbook of Solvents*, ChemTec Publishing, Toronto, 2001.
- 144 N. Chong, L. James and M. L. Norton, *J. Electrochem. Soc.*, 1989, **136**, 1245–1246.
- 145 E. Fatas, D. Quimica, D. Ciencias, P. Herrasti and D. Madrid, *Electrochim. Acta*, 1988, **33**, 959–965.
- 146 J. Jorné and C. W. Tobias, *J. Appl. Electrochem.*, 1975, **5**, 279–290.





# Appendices

## Appendix to chapter 2.1.

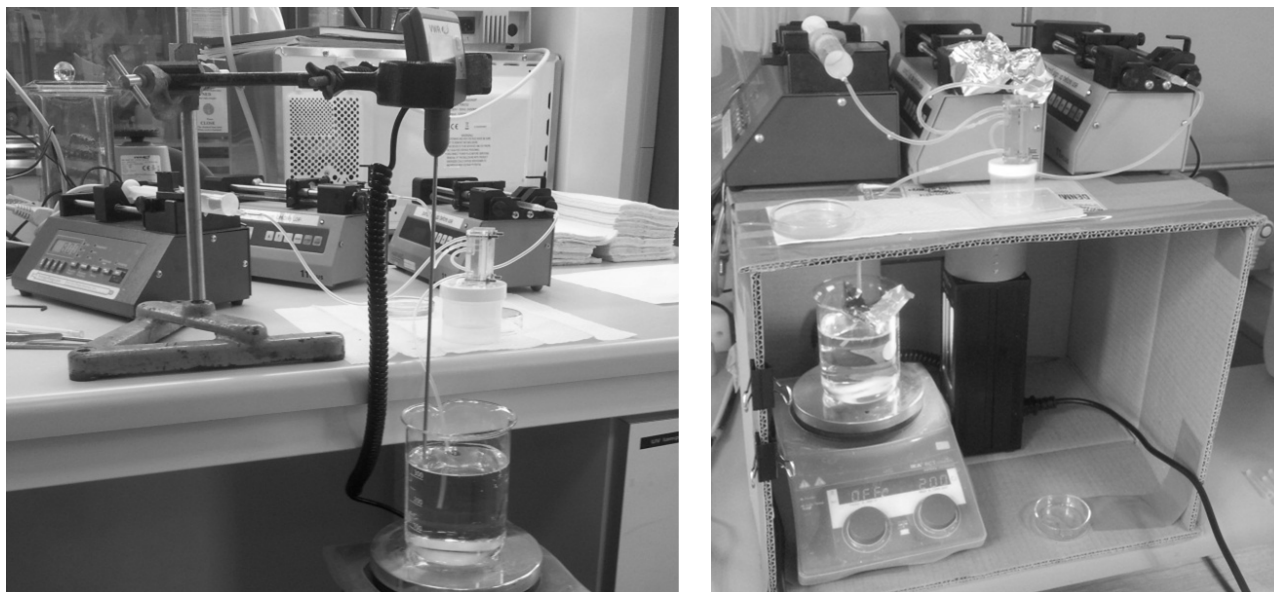


**Figure A-2.1.1.** Experimental setups for preparation of double emulsions. Left picture – S184 based shell; right picture – shell based on a custom made UV-curable thiol-ene PDMS formulation.

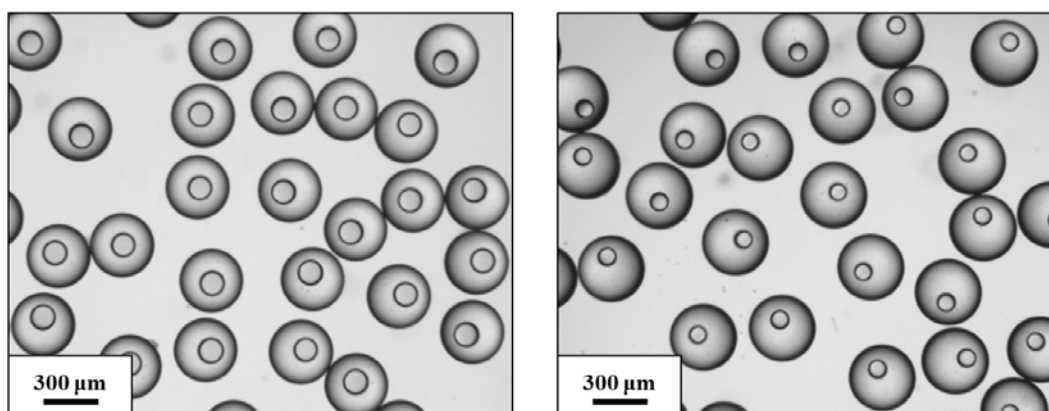


**Figure A-2.1.2.** Optical microscopy images of various water-in PDMS-in water double emulsions.

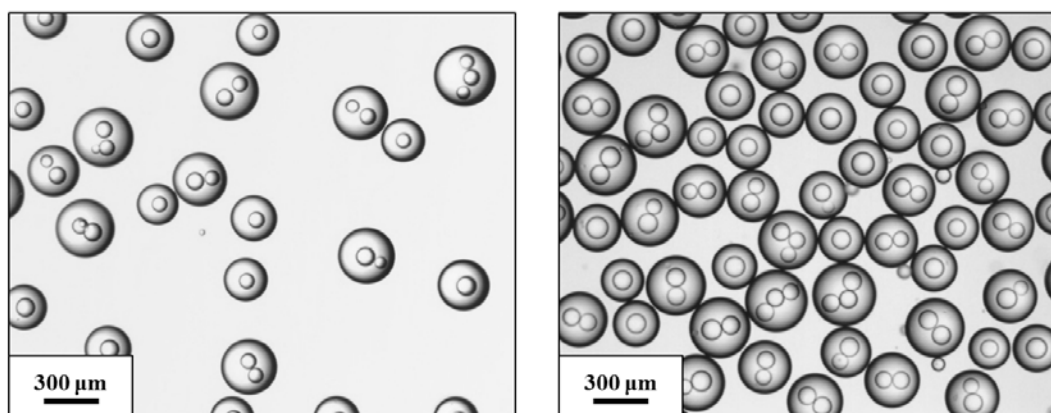


**Figure A-2.1.3.** Optical microscopy images of various IL-in PDMS-in water double emulsions.


 Cite this: *RSC Adv.*, 2015, 5, 15379

## Preparing mono-dispersed liquid core PDMS microcapsules from thiol–ene–epoxy-tailored flow-focusing microfluidic devices

 P. Mazurek,<sup>a</sup> A. E. Daugaard,<sup>a</sup> M. Skolimowski,<sup>b</sup> S. Hvilsted<sup>a</sup> and A. L. Skov<sup>\*a</sup>

An applied dual-cure system based on thiol–ene and thiol–epoxy “click chemistry” reactions was proved to be an extremely effective and easy to use tool for preparing microfluidic chips, thereby allowing for precise control over material properties and providing the possibility of covalently bonding chip wafers. Different thiol–ene–epoxy-based polymer compositions were tested with the help of DSC and ATR FTIR, in order to investigate their physical and chemical properties. Water contact angles were determined, thus verifying the high efficiency and selectivity of the chemical surface modification of compositions in relation to high hydrophilicity and hydrophobicity. An obtained microfluidic device was subsequently used in order to produce PDMS microcapsules of very narrow size distribution and which contained various common liquids, such as water and ethanol, as well as an ionic liquid 2-hydroxyethylammonium formate.

 Received 12th December 2014  
Accepted 26th January 2015

DOI: 10.1039/c4ra16255b

[www.rsc.org/advances](http://www.rsc.org/advances)

### Introduction

The importance of micro-encapsulation is undisputed, so significant effort is exerted nowadays to develop encapsulation techniques, although in many cases they are still far from optimal. Microcapsules, which by definition are solid or liquid spheres coated with a solid material separating the core from an outside medium, have great potential in the pharmaceutical, food, printing and coating industries, as well as in preparing engineering materials.<sup>1</sup> Many methods have been developed allowing for the rather effective formation of core–shell spheres. Additionally, distinguishing between solid and liquid core microcapsules is necessary, since preparation procedures may in many cases vary and require very different techniques. The production of a liquid core structure is considered more complex than producing a solid core, and several parameters have to be taken into account, depending strictly on the technique chosen. When preparing liquid-core microcapsules special attention should be given to mini emulsion techniques, for example the phase separation method. Here, shell formation is induced through polymer precipitation caused by either the evaporation of a volatile solvent from vesicles containing polymer, solvent and the initial core material or through polymerisation that takes place within vesicles and causes the growing polymer to precipitate on the droplet surface.<sup>2–4</sup> Shell

formation can also take place in systems where one monomer is dissolved in continuous phase and the second monomer is dissolved in core material forming vesicles in an emulsion. Reactions between the two monomers, taking place on the emulsion interface, are another effective way of encapsulating liquids.<sup>5</sup> These methods, although still in need of improvement, do not allow for full control over microcapsule dimensions and introduce many limitations concerning the choice of materials for use in these systems.

Modelling of the core–shell structure, which essentially means designing core material, and its size as well as shell thickness and physical and the chemical properties of the material allow for precise control over the release of core material as a result of, for example, shell degradation triggered by different factors such as UV-light, heat, pH, *etc.*<sup>1</sup> From this point of view, only one technique to date enables sufficient control over the encapsulation process and allows for preparing microcapsules extremely narrow in size distribution and tailored dimensions. This technique is based on flow-focusing microfluidic systems containing either a set of capillaries or a set of microchannel junctions of different wettability. Despite the fact that this method is still not used in mass production, we believe it is the most powerful tool for preparing core–shell microspheres on a laboratory scale. Many groups working on developing systems with improved efficiency and versatility have produced some fascinating results, all of which contribute to the increasing interest of material scientists in lab-on-chip techniques.<sup>6–9</sup>

In this paper we present a simple method for preparing a flow-focusing microfluidic device by applying thiol–ene click chemistry, which due to its great versatility and simple

<sup>a</sup>Danish Polymer Centre, Department of Chemical and Biochemical Engineering, Technical University of Denmark, Building 227, DK-2800 Kgs. Lyngby, Denmark. E-mail: [al@kt.dtu.dk](mailto:al@kt.dtu.dk)

<sup>b</sup>Fluidic Array Systems and Technology, Department of Micro and Nanotechnology, Technical University of Denmark, Denmark



chemistry is being increasingly used for fabricating lab-on-chip devices.<sup>10,11</sup> This fascinating chemistry exhibits a great number of advantages, for example very high reaction efficiency, rapid reactions triggered by exposing compositions to UV-light, low exothermic effects and no byproducts. One of the greatest advantages of these systems is good solvent resistivity, which allows for working with almost any type of material and thereby making thiol-ene systems excellent replacements for the currently most widely used PDMS microfluidic chips.<sup>7</sup> PDMS in some instances does not meet the requirements for lab-on-chip devices, for example poor shape consistency due to high flexibility of PDMS, very high gas permeability, rather poor solvent resistance against most organic solvents.

Thiol-ene chemistry is based on the reaction between vinyl-containing compounds and a mercapto-containing compound. In the first step, a thiyl radical is formed through hydrogen exchange between the thiol group and a radical source (Fig. 1). Subsequently the thiyl radical reacts rapidly with the vinyl group of the second compound, forming a thio-ether covalent bond and transferring the radical to the next thiol group. The reaction mechanism (Fig. 1) implies that only a minimal amount of photoinitiator is necessary for the reaction to progress and to reach maximum conversion. By applying different amounts of initiator and different UV-light intensities the reaction speed can be modified easily. Additionally, when 254 nm light is used, thiol-ene compositions with no photoinitiators can be cross-linked.<sup>12</sup> In this approach we make use of the off-stoichiometry thiol-ene (abbreviated OSTE) composition presented by Carlborg *et al.*,<sup>13</sup> in which a tetrafunctional thiol compound is crosslinked with a trifunctional allyl compound, thus forming a stable matrix which exhibits good solvent resistance and possesses tunable mechanical and chemical properties. Selective surface patterning, necessary for preparing double emulsions in flow-focusing microfluidic systems,<sup>14</sup> is achieved by again applying thiol-ene chemistry, which in turn allows for efficient grafting onto polymer surfaces.

One of the greatest challenges when using flow-focusing microfluidic systems is the prevention of leakages appearing in chips when high pressure is present in microfluidic channels. It is especially intractable when higher-viscosity liquids are introduced to the system, since in such cases higher flow rates are necessary for the dispersed phase stream break-up to occur. Research on bonding strength between wafers made of different OSTE compositions was conducted by Sikanen *et al.*<sup>16</sup> All combinations of OSTE wafers presented by this group were

tested, but none of them appeared to provide adhesion strong enough to eliminate leakages completely, and hence a better method for wafer bonding was required. Herein, we modify a two-step crosslinking method presented by Saharil *et al.*,<sup>17</sup> which is based on the covalent bonding of the two microfluidic chip wafers through the introduction of an epoxy-containing compound working as a bonding agent. With the help of this method we managed not only to avoid leakages but also preserved the possibility of surface modification.

The flow-focusing microfluidic device presented in this study was designed in order to enable the microcapsule formation of any type of material, provided that the surface tension between the inner/outer phase and the middle phase is sufficiently high.

## Experimental

### Materials and methods

Two component Sylgard 184 silicone kit, used for fabricating mirror image moulds and for preparing single and double emulsions, was purchased from Dow Corning. Pentaerythritol tetrakis(3-mercaptopropionate) (PETMP), triallyl-1,3,5-triazine-2,4,6(1*H*,3*H*,5*H*)-trione (TATATO) and (bisphenol A diglycidyl ether (BADGE)), forming a microfluidic chip matrix, as well as compounds used for grafting reactions (acrylic acid, allylmalonic acid (AMA), sodium hydroxide, 2,2,3,3,4,4,5,5,6,6,7,7-dodecafluoroheptyl acrylate (DFHA), allyl trifluoroacetate (ATFA), allylpentafluorobenzene (APFB), 1*H*,1*H*,2*H*-perfluoro-1-decene (PFD) and poly(ethylene glycol) methacrylate ( $M_n = 360 \text{ g mol}^{-1}$ ) (PEG), toluene, heptane) were purchased from Sigma Aldrich. Lucirin TPO-L and 2,2-dimethoxy-2-phenylacetophenone (DMPA) photoinitiators were obtained from BASF GmbH Germany and Sigma Aldrich, respectively. The thiol-epoxy reaction catalyst 1,5-diazabicyclo-[4,3,0]-non-5-ene (DBN) was purchased from Sigma Aldrich. Absolute ethyl alcohol, used for the grafting reaction, ionic liquid synthesis and the formation of a double emulsion, was supplied by Kemetyl A/S. Compounds used for forming single and double emulsions, namely sodium dodecyl sulfate (SDS) and isopropanol, were purchased from Sigma Aldrich, whereas polyvinyl alcohol (PVA) and glycerol were supplied by Fluka and Emmelev A/S, respectively. Formic acid and 2-hydroxyethylamine, used for synthesising ionic liquid, were purchased from J. T. Baker and Sigma Aldrich, respectively. Active carbon was provided by Sigma Aldrich. All chemicals were used as received.

A TA Instruments Differential Scanning Calorimeter Q1000 was used to determine the thermal behaviour of the samples. All tests were performed at a heating rate of  $10 \text{ }^\circ\text{C min}^{-1}$  across a temperature range of between  $-30 \text{ }^\circ\text{C}$  and  $120 \text{ }^\circ\text{C}$  in an  $\text{N}_2$  atmosphere. Reported glass transition temperatures of OSTE formulations were based on at least two independent measurements where deviations from individual tests were no higher than  $2 \text{ }^\circ\text{C}$ , whereas for OSTE+ formulations one measurement was conducted. Viscosities were measured with AR2000ex rheometer from TA Instruments. Nicolet iS50 FT-IR was used to obtain ATR FTIR spectra of neat and surface-modified polymer compositions as well as synthesised ionic liquid. Water wettability of polymers was investigated with the

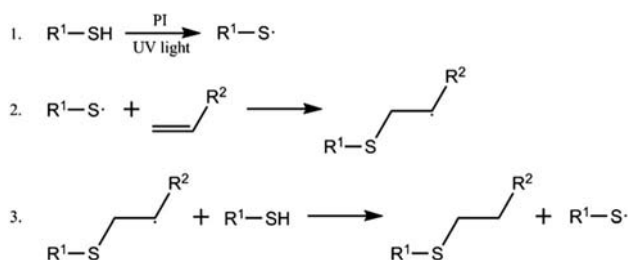


Fig. 1 Mechanism of a photoinitiated thiol-ene reaction.<sup>15</sup>



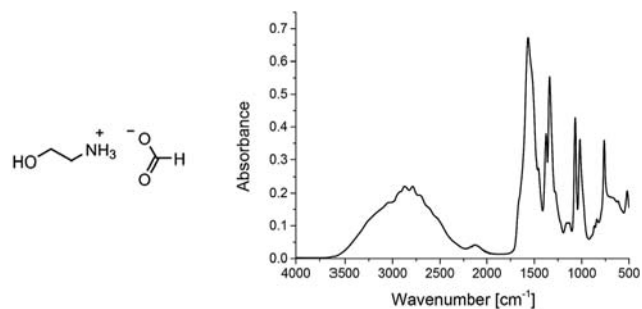


Fig. 2 Chemical formula (left) and ATR FTIR spectrum (right) of 2-hydroxyethylammonium formate, with a peak at a wavenumber of around  $1565\text{ cm}^{-1}$ , thereby indicating a  $\text{COO}^-$  stretch, and a peak at a wavenumber of around  $2125\text{ cm}^{-1}$ , corresponding to an  $\text{RNH}_3^+$  bend.

help of DataPhysics OCA20. Each surface was tested using the sessile drop method, and the average water contact angle was calculated from at least three measurements. A Leica DM LB optical microscope was applied, in order to determine the morphology and sizes of microspheres and microcapsules produced.

### Synthesis of 2-hydroxyethylammonium formate

An ionic liquid (IL) 2-hydroxyethylammonium formate (see chemical formula in Fig. 2) was synthesised following a procedure described by Yuan *et al.*<sup>18</sup> In total, 0.2 mole of 2-hydroxyethylamine and formic acid were dissolved in 40 mL of ethanol. Formic acid solution was added drop-wise to a round-bottomed flask equipped with a magnetic stirrer and reflux condenser and containing 2-hydroxyethylamine solution. The reaction was held for around 4 hours to ensure full conversion. Subsequently obtained ionic liquid was separated from the solvent *via* vacuum evaporation, dissolved again in ethanol, treated with carbon black and then filtered. The product was kept under low-pressure conditions in order to avoid water condensation. The ATR FTIR spectrum of the ionic liquid confirmed an exchange of protons between Brønsted acid and the base, as shown in Fig. 2.

## Results and discussion

### Preparing microfluidic device

The microfluidic device contained two main units, each consisting of two parts. The microfluidic chip entails a bottom part,

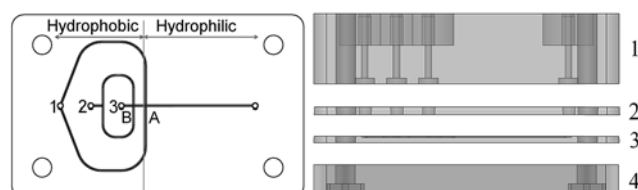


Fig. 3 Chip scheme (left) (channel width of  $280\text{ }\mu\text{m}$ ) and full microfluidic device (right). 1 – holder top, 2 – chip top, 3 – chip bottom, 4 – holder bottom.

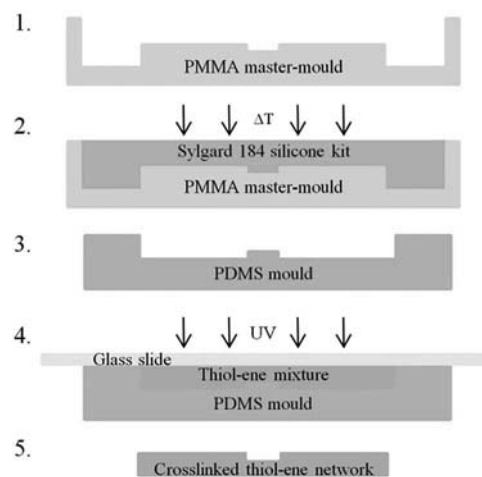


Fig. 4 Thiol-ene chip fabrication process scheme.

with all channels and junctions, and a top part, which seals the chip. The three inlets and one outlet placed in the top part enable liquid transfer throughout the chip. The two wafers of the chip are assembled and sandwiched between bottom and top parts of the holder (see Fig. 3).

The holder wafers were micromilled in polycarbonate. The microfluidic chip was then prepared in a two-step replica moulding process, where all geometries of a master mould were micromilled in a PMMA plate in the first step. Subsequently a Sylgard 184 silicone kit (mixing ratio 10 : 1) composition was prepared, degassed and cast onto the PMMA master mould, in order to obtain a mirror image PDMS mould. The composition was then crosslinked at  $80\text{ }^\circ\text{C}$  for 10 hours, after which the mirror image mould was ready to be used for preparing the microfluidic chip. A full scheme for the thiol-ene chip fabrication process is presented in Fig. 4.

For preparing the microfluidic chip we employed the composition of monomers reported by Carlborg *et al.*<sup>13</sup> The off-stoichiometry thiol-ene composition (OSTE) is based on a tetra-functional thiol compound and a tri-functional allyl compound (Fig. 5). The components form a stable network when mixed together with a photoinitiator and following subsequent exposure to UV-light. Depending on the stoichiometric amounts of both components, very different mechanical properties of the material can be obtained. Results for differential scanning calorimetry, presented in Fig. 6, show that when thiol and vinyl groups were used in stoichiometric balance, the glass transition temperature ( $T_g$ ) of the composition reached a maximum  $60\text{ }^\circ\text{C}$ , which can be attributed to the highest degree of crosslinking in

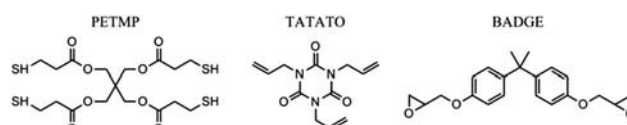


Fig. 5 Structural formulas of compounds used for preparing a flow-focusing microfluidic chip: tetrathiol (PETMP), triallyl (TATATO) and diepoxy (BADGE) working as a dual cure agent.



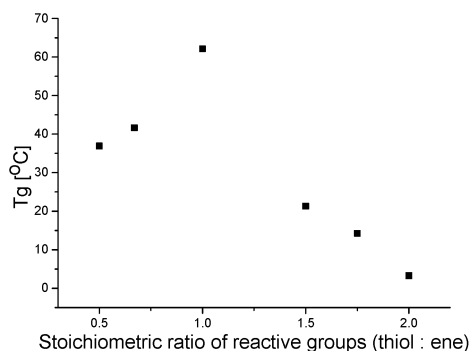


Fig. 6 Glass transition temperatures of different OSTE compositions.

this composition and the presumed absence of dangling chains. On the other hand, when stoichiometric imbalance is introduced, the glass transition temperatures decrease due to an increasing number of dangling chains with unreacted functional groups. It can also be hypothesised that excess triallyl monomer (TATATO) results in the formation of a stiffer structure than in the case of excess thiol monomer, which is finally attributed to the structure of monomers (shorter dangling chains and the cyclic nature of allyl monomer). The presence of both thiol and vinyl groups in different compositions was proven by FTIR tests, which for  $r = 2.0$  exhibited a peak at a wavenumber of around  $2550\text{ cm}^{-1}$ , attributed to the S–H stretch of the thiol groups, and no peaks in the range between  $3095$  and  $3010\text{ cm}^{-1}$ , attributed to the  $\text{sp}^2\text{C–H}$  stretch of the vinyl group and *vice versa* in the case of compositions with excess allyl monomer (see Fig. 7).

Due to the fact that the thiol–ene reaction is initiated at the mercapto groups, a composition with excess thiol groups was chosen for fabricating microfluidic chips. It is believed that grafting allyl containing compounds onto thiol-containing surfaces provides higher grafting selectivity, since active thiyl radicals, when fixed permanently to the polymer surface, cannot migrate, and hence the grafting reaction will take place on the UV-exposed area exclusively, which is an essential feature for preparing double emulsions in flow-focusing systems. Nevertheless the composition used for preparing the chip did not provide sufficient adhesion between the chip wafers, which in turn caused leakages when pumping liquids through the

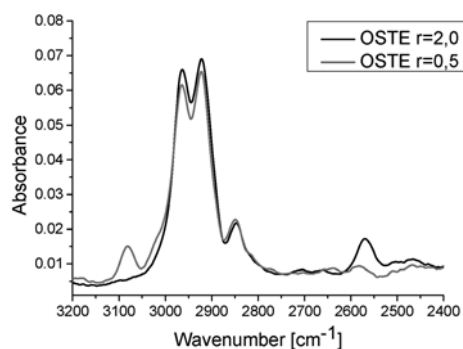


Fig. 7 FTIR spectra of OSTE compositions with  $r = 2.0$  and  $r = 0.5$ .

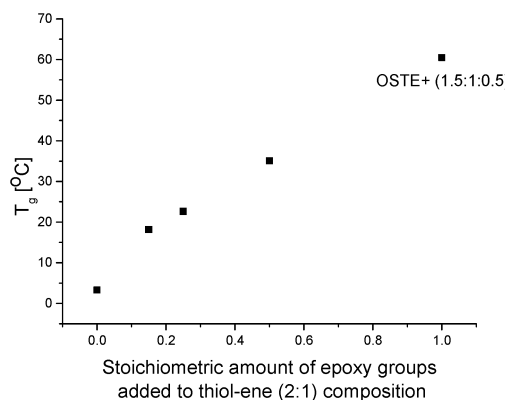


Fig. 8 Glass transition temperatures of different OSTE+ compositions (OSTE+ (1.5 : 1 : 0.5) as reference sample).

channels. Adhesion tests between different TATATO and PETMP compositions, as presented by Sikanen *et al.*,<sup>16</sup> reveal that the highest physical bond strength is achieved for formulations with excess allyl groups and for a combination of two different wafers (one wafer with excess allyl and one with thiol groups). For our application, none of the described systems showed sufficient adhesion, and therefore a third compound (BADGE) was introduced to the matrix, thereby making it a dual-cure polymer composition – as described by Saharil *et al.*<sup>17</sup> The new three-component formulation is abbreviated as OSTE+. In the dual-cure process a mixture of monomers was degassed, cast onto a PDMS mirror-image mould and UV-irradiated for a reaction between the thiol and allyl groups to take place. Afterwards, both chip wafers were demoulded and assembled together, thus avoiding the formation of air voids. No heating prior to demoulding was necessary due to the flexible nature of PDMS and the fact that the discussed OSTE+ composition after the UV-crosslinking step has  $T_g$  below room temperature. Therefore separation of chip wafers from the mould did not generate additional preparation steps as described by others.<sup>13</sup> The assembled wafers were then exposed to elevated temperatures ( $80\text{ °C}$  for 2 hours), where the reaction between the epoxy groups and the remaining thiol groups took place both in the bulk as well as at the wafer–wafer interface. The thiol–epoxy reaction was catalysed by DBN, which was added to the system in minor amounts. Different reactive group molar ratios between PETMP, TATATO and BADGE were investigated and analysed in terms of DSC. Bonding strength between the two assembled chip wafers was determined from organoleptic observations. Glass transition temperatures of the tested formulations showed increasing values in line with the increasing addition of BADGE into the initial thiol–ene composition, which was kept at a constant thiol/allyl ratio of  $r = 2.0$  (see Fig. 8). We observed that by adding a small amount of BADGE (stoichiometric ratio of thiol : allyl : epoxy groups 2 : 1 : 0.15), the glass transition temperature increased from around  $2\text{ °C}$  to almost  $20\text{ °C}$  and further to around  $25\text{ °C}$  and  $35\text{ °C}$  for samples with stoichiometric ratios of 2 : 1 : 0.25 and 2 : 1 : 0.5, respectively. As a reference point, a composition with molar ratio of 1.5 : 1 : 0.5, as reported by Saharil,<sup>17</sup> was prepared



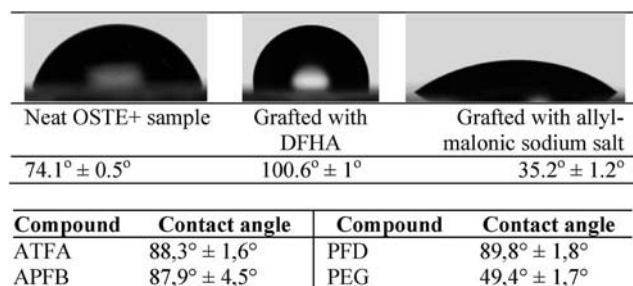


Fig. 9 Wetting properties of 2 : 1 : 0.15 OSTE+ samples grafted with different compounds in terms of static contact angle.

and also tested in terms of differential scanning calorimetry. As expected, the glass transition temperature of this formulation showed the highest value (around 60 °C), due to the fact that all functional groups reacted and left no dangling chains in bulk. Analogously, an increase in stiffness was observed in line with an increasing amount of BADGE in the system, followed by improved bonding strength between the wafers. For our purposes optimal properties were obtained for the 2 : 1 : 0.15 OSTE+ formulation, which showed improved adhesion between the wafers and additionally provided the highest amount of unreacted thiol groups on the surface – an important factor for further surface patterning.

As presented in Fig. 3, in order to prepare a water–oil–water emulsion it is desirable to create a microfluidic chip with one hydrophobic and one hydrophilic junction. To achieve this aim, thiol groups remaining on the surface of the OSTE+ composition react with different vinyl containing compounds, following which their influence on surface wettability is investigated. Surface patterning follows the same thiol–ene reaction mechanism, and therefore if more accurate surface modification is desirable, it is more effective to graft vinyl-containing compounds onto thiol-containing surfaces – and not *vice versa*. The grafting reactions were performed on the OSTE+ films by immersing them in 10 wt% solutions of different vinyl compounds in absolute ethanol along with the addition of DMPA as a photoinitiator. Reactions were carried out at a UV-light (365 nm) intensity of around 4 mW cm<sup>-2</sup> for 15–20 minutes, to ensure the full conversion of thiol groups. It has been reported, that the solvent-mediated thiol–ene grafting reaction can be accelerated significantly by applying UV-light of higher intensities.<sup>19</sup> A series of grafting reactions was performed in order to reveal the most suitable chemicals that would effectively and permanently change the wetting properties of the material to the highest possible levels of hydrophobicity and

hydrophilicity, respectively. Different grafting conditions were additionally tested in order to determine the most efficient grafting procedure. Experiments showed that increasing the amount of photoinitiator, from 0.5 to 3 wt%, did not improve grafting efficiency. Furthermore, Lucirin TPO-L proved to be an effective photoinitiator for grafting reactions when ethanol and isopropanol were used as reaction media. Different solvents (*e.g.* ethanol, isopropanol, toluene, heptane) used for surface modification reactions showed comparable contact angles albeit with one exception, where it was found that acrylic compounds tend to homopolymerise when toluene is used as a solvent. After just 3–4 minutes of UV-irradiation, a grafting solution changed colour from transparent to white, which indicates the progressing homopolymerisation of acrylic monomers. Increased concentrations of grafted compounds also did not improve grafting efficiency in the investigated range. We obtained same water contact angles for concentrations between 3 and 10 wt%. Results of the experiments, supported by static contact angle measurements, are presented in Fig. 9, and the structural formulas of the two grafted compounds that alter the surface properties most efficiently are shown in Fig. 10. The best results regarding obtaining the highest hydrophilicity were acquired through grafting AMA. The grafted surface was subsequently flushed with a 0.01 M NaOH solution, performed in order to replace the protons of AMA carboxyl groups with sodium cations, which resulted in a significant increase in hydrophilicity. The highest hydrophobicity was obtained for 2 : 1 : 0.15 OSTE+ grafted with DFHA, where the static contact angle increased from 74.1° for a neat sample to 100.6° for a modified sample. This value could be increased even further by grafting DFHA onto a 2 : 1 : 0.25 OSTE+ sample, which showed a static contact angle of 106.3 ± 0.4°.

Surface selectivity of the grafting reactions was finally proved by performing two-step surface patterning. The OSTE+ polymer film was first immersed in the DFHA ethanol solution with the addition of DMPA, while half of the film was covered with a stencil mask (black rubber film), thus preventing it from reacting when the sample was subsequently exposed to UV-light. After the first surface modification step was complete, the polymer film was thoroughly washed with a substantial amount of ethanol and blow-dried with N<sub>2</sub>. In the second step the sample was immersed in AMA solution but this time covering the already grafted half with the stencil mask and exposed to UV-light (a schematic illustration of the full process is in Fig. 11). Afterwards the polymer film was cleaned again, flushed with 0.01 M NaOH solution and then blow-dried. Static contact angle tests performed on both sides of the sample proved the validity of the two-step grafting process, by providing contact angle values comparable to results obtained from the simple surface modification process. The two-step surface patterning process was applied to the modification of the microfluidic chip channel surfaces, though the grafting reactions took place within chip channels exclusively after both wafers were covalently bonded.

The progress of the grafting reactions was monitored by ATR FTIR. It was shown that the grafting reaction of small molecules takes place not only on the surface of the material but also, to

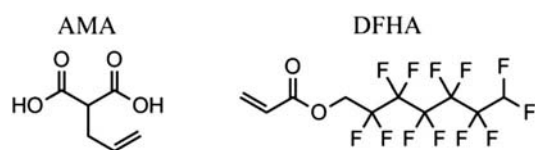


Fig. 10 Structural formulas of allylmalonic acid and 2,2,3,3,4,4,5,5,6,6,7,7-dodecafluoroheptyl acrylate.





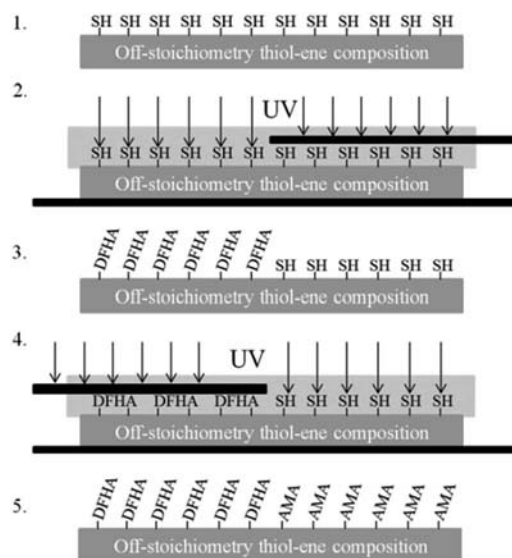


Fig. 11 Schematic illustration of the two-step surface patterning of the OSTE+ polymer film. SH represents unreacted thiol groups present on the polymer surface that subsequently react with DFHA and AMA in separate steps of the surface patterning process.

some extent, in bulk, which is attributed to the fact that the polymer network contains a substantial amount of dangling chains due to the relatively high off-stoichiometry ratio of the initial composition. The FTIR analyser beam usually penetrates through the first few microns of tested samples, so the spectra obtained should – in principle – show a small peak for the thiol group at the wavenumber of  $2550\text{ cm}^{-1}$ , as it is in the case of the initial network. Spectra obtained, for example, for OSTE+ grafted with sodium acrylate show no peaks in that region. Additionally, other strong peaks are to be observed at different wavenumbers, for example stretches typical for carboxylic salts at around  $1565\text{ cm}^{-1}$  and  $1425\text{ cm}^{-1}$  (Fig. 12), which was shown by Gonzalez *et al.*<sup>20,21</sup> In the case of grafting larger molecules, such as DFHA, there are no significant changes in FTIR spectra, although contact angle measurements show substantial divergence in wetting properties.

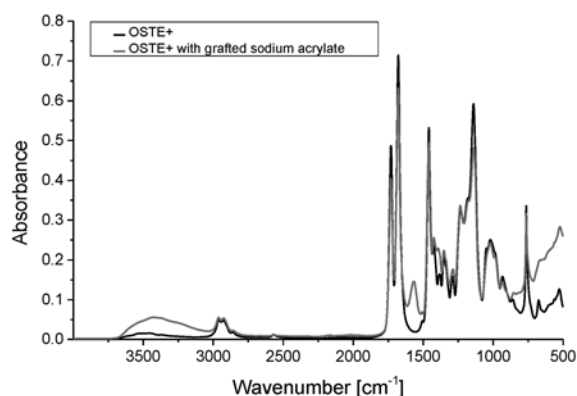


Fig. 12 ATR FTIR spectra of OSTE+ and OSTE+ grafted with sodium acrylate, presenting changes in absorbance at wavenumbers of  $2550\text{ cm}^{-1}$ ,  $1565\text{ cm}^{-1}$  and  $1425\text{ cm}^{-1}$ .

### Formation of a single emulsion

Separately controlled Harvard Apparatus 11 plus syringe pumps were used to introduce liquids to the microfluidic chip. Formation of a single emulsion was performed using inlets 1 and 2. Inlet 3 was plugged, which consequently blocked all liquid transfers through this connector (see Fig. 3). Two component Sylgard 184 silicone kit mixed to a ratio of 3 : 2 (base : crosslinker), was used as the dispersed phase ( $\eta = 1080\text{ mPa s}$  at shear rate of  $0.1\text{ s}^{-1}$ ) and injected into the system through inlet 2, while SDS/PVA aqueous solution (3 wt% and 1 wt%, respectively) was used as a carrier phase and was injected through inlet 1 ( $Q_1 > Q_2$ , where  $Q$  corresponds to the flow rates of liquids). Droplet formation took place at junction A. Initial flow rates for each experiment were  $10\text{ mL h}^{-1}$  and  $1\text{ mL h}^{-1}$  for  $Q_1$  and  $Q_2$ , respectively (initial droplet diameter was  $250\text{ }\mu\text{m}$ ). Depending on liquid flow rates single emulsions of different droplet sizes (between 100 and  $425\text{ }\mu\text{m}$ ) and very narrow size distributions were obtained (see Fig. 13). In order to obtain smallest droplet size, the outer phase was injected at a flow rate of  $50\text{ mL h}^{-1}$ . By increasing the flow rate even higher to  $100\text{--}200\text{ mL h}^{-1}$  the size distribution of spheres was significantly broadened. Nonetheless no leakages were observed. As an alternative method for altering droplet diameters, different carrier phase compositions were applied. Modifying the viscosity of the outer phase, which in this case could be done by increasing surfactant concentrations, works in favour of decreasing sphere sizes. As a result the range of sphere sizes can be shifted towards lower diameters. This effect can be achieved, for example, by increasing the amount of PVA, which substantially influences the viscosity of the solutions.

### Formation of a double emulsion

Three liquids have to be introduced to the microfluidic chip in order to obtain core-shell microspheres. In this study we present tests where deionised water, ionic liquid ((2-hydroxyethyl)ammonium formate), ethanol, isopropanol and different water-glycerol mixtures were used as the inner phase of double emulsions. In each experiment a Sylgard 184 silicone kit, mixed to a weight ratio of 3 : 2 (base : crosslinker), was used as the middle phase and water with various surfactants as the outer phase.

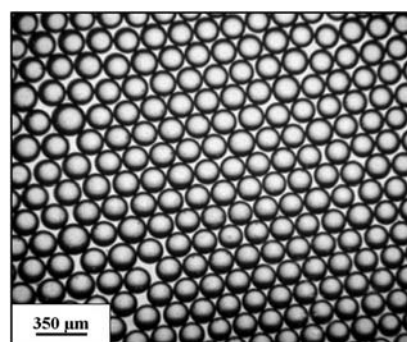


Fig. 13 Microscope image of silicone in water single emulsion obtained on junction A.



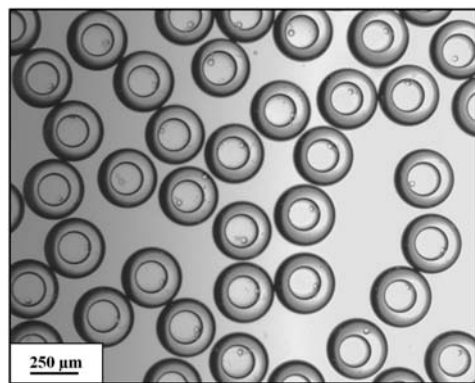


Fig. 14 Optical microscopy image of a water-in PDMS-in water double emulsion.

In the first experiment water was used as the inner phase of the double emulsion and SDS, PVA water solutions (3 wt% and 1 wt%, respectively) as the outer phase. In the first step the outer phase liquid is introduced to the chip *via* inlet 1 (see Fig. 3), followed by introducing the middle phase ( $Q_1 > Q_2$ ). Initial flow rates were  $Q_1 = 10 \text{ mL h}^{-1}$  and  $Q_2 = 1 \text{ mL h}^{-1}$ . As a result silicone droplet formation takes place at junction A and, as in the single emulsion case described paragraph above, droplets size is determined by the outer phase liquid flow rate. After a stable and mono-dispersed single emulsion is obtained, the inner phase is introduced to the chip *via* inlet 3 ( $Q_1 > Q_2 > Q_3$ ).  $Q_3$  is slowly increased until the desired core-shell morphology with designed core and shell dimensions is obtained. The resulting double emulsion is collected *via* the outlet of the microfluidic chip and then left for the crosslinking reaction of the PDMS shell to take place. We confirm that, as in case of low viscosity liquids,<sup>8,22</sup> the higher viscosity liquids investigated in this approach can also be used successfully in flow-focusing microfluidic chips. Additionally in these systems, core-shell microsphere dimensions can also be altered by varying the flow rates of injected liquids. Results of encapsulating water within a PDMS shell can be seen in Fig. 14.

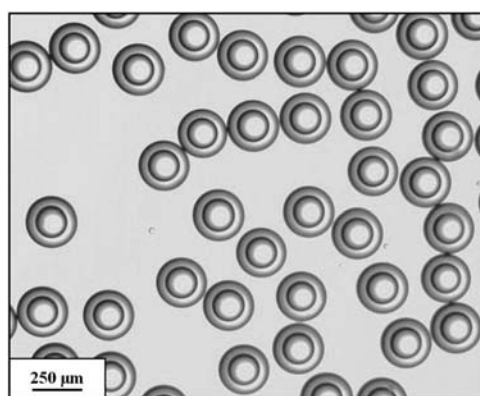


Fig. 15 Optical microscopy image of a 2-hydroxyethylammonium formate-in PDMS-in water double emulsion.

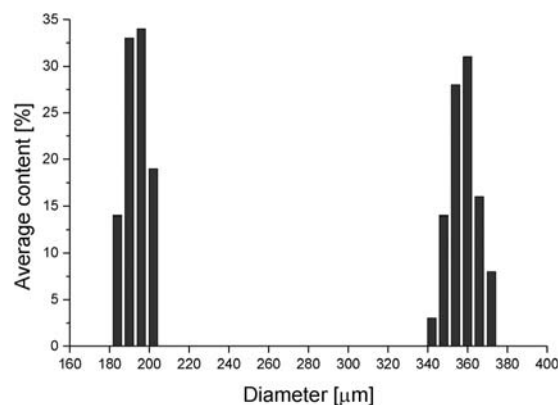


Fig. 16 An example of a size distribution of capsule cores (left columns) and capsules (right columns) obtained from the water-in PDMS-in water double emulsion.

The 2-hydroxyethylammonium formate was then used as a core material for the microcapsules, where PDMS was used as a shell material. The process for preparing the microcapsules followed the same scheme as in the water encapsulation case, whereby injection of the outer phase was followed by injection of the middle and then inner phases. An example of an acquired double emulsion can be seen in Fig. 15. Again, microcapsules of narrow size distribution were obtained, which proves that the flow-focusing microfluidic system we present in this study is a versatile method of encapsulation and can be applied to a broad range of materials. It was observed that by using IL (reported viscosity  $\eta = 118 \text{ mPa s}$  (ref. 18)), microcapsules of smaller diameters in comparison to water-core spheres were obtained. Attempts to encapsulate ethanol, isopropanol and different water and glycerol mixtures within a PDMS shell also resulted in the formation of microcapsules of very narrow size distribution, which again proves the versatility of the microfluidic system.

Size distribution of spheres in single and double emulsions was obtained by measuring diameters of at least 100 droplets. An average size and standard deviation were determined for each experiment. That allowed for calculations of coefficients of variation (CV), which were proved to be held at substantially low values ( $CV < 3\%$ ) for all experiments. An example of size distribution of water-in PDMS-in water emulsion is presented in Fig. 16.

The curing process for core-shell microspheres has been tested and optimised example water/PDMS/water double emulsion. The acquired double emulsion was collected into a beaker containing a water solution of SDS and PVA (3 wt% and 1 wt%, respectively) under constant stirring with a magnetic stirrer, which prevents the double emulsion from forming microcapsule aggregates. The collected capsules were left for 24 hours at room temperature for the PDMS composition to be crosslinked and then form a solid shell. Increasing the temperature at this stage effectively accelerates the curing process, although too high a temperature results in disruption to the double emulsion and causes a collapse in microcapsules. The solution containing solid-shell capsules was heated up to  $70 \text{ }^\circ\text{C}$  to ensure full crosslinking of the material.



After each use, the microfluidic chip was thoroughly flushed with soap water, ethanol and heptane, and then once again with ethanol in order to remove possible PDMS residues and other impurities from the chip channels. This allows for the multiple use of a single chip and maintains surface properties, even up to several months and potentially longer. Experiments show that flushing the channels with soap water and ethanol only significantly lowers the lifetime of the chip. This appears to be a big advantage of this system over microfluidic devices based on PDMS, where surface properties and wafer bonding are usually achieved through plasma treatment, thereby causing temporary effects only.

## Conclusions

A flow-focusing microfluidic device based on thiol-ene “click” chemistry was designed and fabricated. Due to the applied chemistry, physical and chemical properties of the chip could be adjusted to the intended application of producing elastomeric microcapsules. As a result it was possible to modify chemically the microfluidic chip channel surfaces in a controlled way and additionally to prevent any leakages while pumping liquids through the channels at very high flow rates. The developed system is an efficient tool for preparing core-shell microspheres of extremely narrow size distribution with tunable core diameters and shell thicknesses. We have demonstrated that very different liquids can be encapsulated within a PDMS shell where the only limitations are surface tension between liquids and their viscosities. The developed microfluidic device additionally has a very long lifespan, which efficiently saves time when conducting experiments on double emulsions. The versatility of the design creates a robust basis for fabricating new flow-focusing microfluidic devices for forming any type of core-shell microspheres for various applications. We believe that encapsulating liquid substances within soft PDMS shells is a great step towards self-healing elastomeric materials.

## Acknowledgements

The authors acknowledge funding from Innovationsfonden Denmark.

## Notes and references

- 1 A. Latnikova, D. O. Grigoriev, H. Möhwald and D. G. Shchukin, *J. Phys. Chem. C*, 2012, **116**, 8181–8187.
- 2 L. Gonzalez, M. Kostrzewska, M. Baoguang, L. Li, J. H. Hansen, S. Hvilsted and A. L. Skov, *Macromol. Mater. Eng.*, 2014, **299**, 1259–1267.
- 3 E. B. Murphy and F. Wudl, *Prog. Polym. Sci.*, 2010, **35**, 223–251.
- 4 B. J. Blaiszik, N. R. Sottos and S. R. White, *Compos. Sci. Technol.*, 2008, **68**, 978–986.
- 5 V. Mittal, *Encapsulation Nanotechnologies*, John Wiley & Sons, Inc., Hoboken, 2013.
- 6 T. Nisisako, S. Okushima and T. Torii, *Soft Matter*, 2005, **1**, 23–27.
- 7 G. T. Vladislavjević, I. Kobayashi and M. Nakajima, *Microfluid. Nanofluid.*, 2012, **13**, 151–178.
- 8 N. N. Deng, Z. J. Meng, R. Xie, X. J. Ju, C. L. Mou, W. Wang and L. Y. Chu, *Lab Chip*, 2011, **11**, 3963–3969.
- 9 W. A. C. Bauer, M. Fischlechner, C. Abell and W. T. S. Huck, *Lab Chip*, 2010, **10**, 1814–1819.
- 10 A. B. Lowe, *Polym. Chem.*, 2010, **1**, 17–36.
- 11 C. E. Hoyle and C. N. Bowman, *Angew. Chem., Int. Ed.*, 2010, **49**, 1540–1573.
- 12 N. B. Cramer, S. K. Reddy, M. Cole, C. Hoyle and C. N. Bowman, *J. Polym. Sci., Part A: Polym. Chem.*, 2004, **42**, 5817–5826.
- 13 C. F. Carlborg, T. Haraldsson, K. Öberg, M. Malkoch and W. Wijngaart, *Lab Chip*, 2011, **11**, 3136–3147.
- 14 W. C. Joeng, M. Choi, C. H. Lim and S. M. Yang, *Lab Chip*, 2012, **12**, 5262–5271.
- 15 J. A. Carioscia, J. W. Stansbury and C. N. Bowman, *Polymer*, 2007, **48**, 1526–1532.
- 16 T. M. Sikanen, J. P. Lafleur, M. E. Moilanen, G. Zhuang, T. G. Jensen and J. P. Kutter, *J. Micromech. Microeng.*, 2013, **23**, 037002.
- 17 F. Saharil, F. Forsberg, Y. Liu, P. Bettotti, N. Kumar, F. Niklaus, T. Haraldsson, W. Wijngaart and K. B. Gylfason, *J. Micromech. Microeng.*, 2013, **23**, 025021.
- 18 X. L. Yuan, S. J. Zhang and X. M. Lu, *J. Chem. Eng. Data*, 2007, **52**, 595–599.
- 19 G. Pardon, F. Saharil, J. M. Karlsson, O. Supekar, C. F. Carlborg, W. Wijngaart and T. Haraldsson, *Microfluid. Nanofluid.*, 2014, **17**, 773–779.
- 20 L. Gonzalez, A. L. Skov and S. Hvilsted, *J. Polym. Sci., Part A: Polym. Chem.*, 2013, **51**, 1359–1371.
- 21 L. Gonzalez, A. L. Skov and S. Hvilsted, *Macromol. Symp.*, 2014, **342**, 8–20.
- 22 F. Chang and Y. Su, *J. Micromech. Microeng.*, 2008, **18**, 065018.



## Appendix to chapter 2.2.

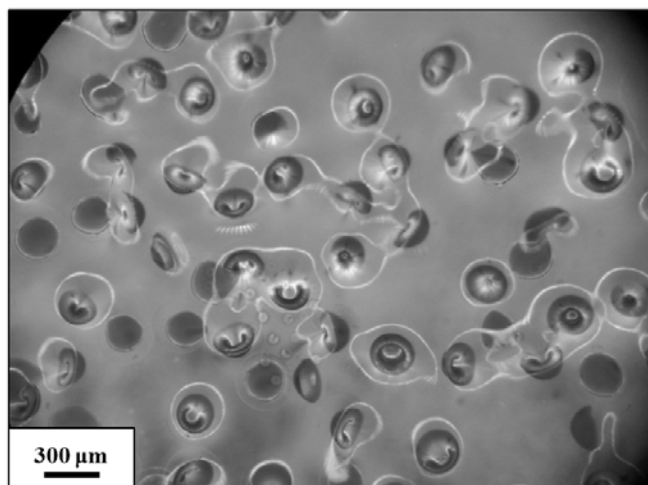


**Figure A-2.2.1.** Optical microscopy image of a PDMS film with incorporated PDMS-shell capsules with a dyed water as a core material. The composition was exposed to vacuum prior to crosslinking in order to investigate a behaviour of the pre-elastomer at low-pressure conditions.

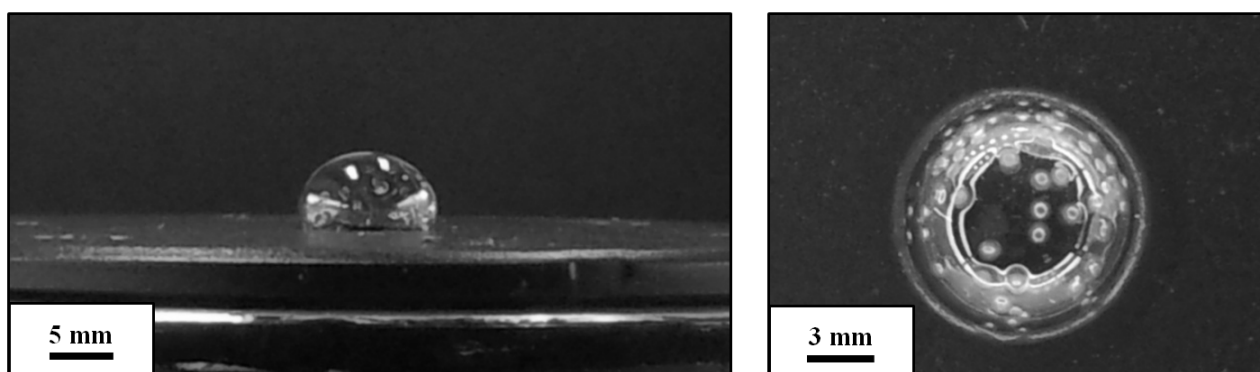


**Figure A-2.2.2.** Images representing membrane-inflation experiments (left – side view, right – top view). The PDMS film was filled with a minor amount of water-containing microcapsules.

# Novel encapsulation technique for incorporation of high permittivity fillers into silicone elastomers

Piotr Mazurek, Søren Hvilsted, Anne Ladegaard Skov\*

Technical University of Denmark, Department of Chemical and Biochemical Engineering

## ABSTRACT

The research on soft elastomers with high dielectric permittivity for the use as dielectric electroactive polymers (DEAP) has grown substantially within the last decade. The approaches to enhance the dielectric permittivity can be categorized into three main classes: 1) Mixing or blending in high permittivity fillers, 2) Grafting of high permittivity molecules onto the polymer backbone in the elastomer, and 3) Encapsulation of high permittivity fillers. The approach investigated here is a new type of encapsulation which does not interfere with the mechanical properties to the same content as for the traditionally applied thermoplastic encapsulation. The properties of the elastomers are investigated as function of the filler content and type. The dielectric permittivity, dielectric loss, conductivity, storage modulus as well as viscous loss are compared to elastomers with the same amounts of high permittivity fillers blended into the elastomer, and it is found that the encapsulation provides a technique to enhance some of these properties.

Keywords: DEAP, PDMS, encapsulation, filler, relative permittivity, microfluidic device

## 1. INTRODUCTION

There is no unequivocal answer to the question of what increases actuation performance of dielectric electroactive polymers most efficiently. Scientists all over the globe discuss this issue presenting new ways of handling these materials but none of them seems to outdistance other methods. The actuation performance of DEAP, which in another words can be defined as strain produced on elastomer when applying electric field and can be defined as:

$$S = \frac{\epsilon_0 \epsilon_r}{Y} \left( \frac{V}{d} \right)^2 \quad [1]$$

where  $\epsilon_0$  and  $\epsilon_r$  are vacuum permittivity and relative permittivity, respectively.  $Y$  is the Young's modulus of material,  $V$  is applied voltage and  $d$  thickness of investigated elastomer. According to Equation 1 there are four parameters that can be altered in order to increase the actuation performance. These are  $\epsilon_r$ ,  $Y$ ,  $d$  and the maximal value of quotient  $V/d$  which is defined by breakdown strength of polymer composition. Goswami *et al.* discussed merit of varying these parameters and concluded that modification of relative permittivity of material gives most prominent results and leaves most room for improvements [1]. The relative permittivity ( $\epsilon_r$ ) is a parameter that together with vacuum permittivity ( $\epsilon_0 = 8.85 \times 10^{-12}$  F/m) defines the permittivity of the material ( $\epsilon$ , Equation 2). Relative permittivity is directly related to electric susceptibility ( $\chi$ ) which is a measure of degree of polarization (polarization density  $P$ , Equation 3) of a dielectric which finally is a property that describes actuation capability of dielectric materials when exposed to electric field  $E$ .

$$\epsilon = \epsilon_0 \epsilon_r = \epsilon_0 (1 + \chi) \quad [2]$$

$$P = \epsilon_0 \chi E \quad [3]$$

Different approaches have been performed in order to increase relative permittivity of dielectric elastomers. One of the most frequently reported methods is based on mixing elastomers with high permittivity fillers like carbon nanotubes, carbon black, titanium dioxide etc. [2,3]. Composites containing different amounts of fillers can potentially improve not only the actuation performance but also mechanical properties of final material. Increasing attention is also attracted towards grafting of polar molecules onto the silicone polymer backbone which significantly improves the dielectric permittivity without compromising its high inherent breakdown strength and increasing dielectric loss [4]. It was also reported that grafting of less than 0.5 wt.% of push-pull dipoles onto a crosslinker of the silicones can enhance the dielectric constant by 19% [5,6].

As alternative to methods described above, Opris *et al.* [7] presented a novel way of incorporation of conductive fillers encapsulated within an insulating shell into elastomer networks. In their approach poly(aniline) (PANI) was encapsulated in poly(divinyl benzene) (PDVB) forming capsules of less than 1  $\mu\text{m}$  diameter, which were later dispersed in poly(dimethylsiloxane) (PDMS) films. In this way the filler particles were efficiently separated from each other by non-conductive layers preventing formation of conductive paths throughout the material, which may lead to significant and uncontrolled increase of dielectric loss as well as decrease of breakdown strength of materials. By applying this technique they successfully improved the relative permittivity of PDMS based composites keeping breakdown strength at an acceptable level.

In this paper we focus on preparation of liquid-core microcapsules of extremely narrow size distribution and incorporating them into PDMS matrix. We show how different amounts of encapsulated filler influence mechanical and electrical properties of the formed composites. We present an efficient method of encapsulation of high permittivity polar liquids into PDMS shells. The shells allow for further reaction since they are prepared from an elastomer with excess of silicone hydrides. These will allow for further crosslinking by covalent grafting into the matrix of silicone elastomer possessing excess of vinyl groups. The excess of vinyl groups in PDMS compositions still allows for formation of strong and elastic networks [8].

The core-shell microspheres (water surrounded by crosslinked PDMS) were prepared with the help of a flow-focusing microfluidic device, which has previously been reported as a successful tool for preparation of microcapsules of extremely narrow size distribution [9]. The composition used for preparation of a microfluidic chip presented in this report is based on thiol and allyl terminated compounds mixed in stoichiometric imbalance and then crosslinked under UV-irradiation. The preparation procedure of this rapidly curable and solvent resistant composition was presented and described by Haraldsson *et al.* [10]. Thiol-ene “click chemistry” was also used for surface modification of channels in the microfluidic chip.

## 2. EXPERIMENTAL DETAILS

### 2.1 Materials

Sylgard 184 silicone kit used for preparation of mirror-image mold was purchased from Dow Corning. All three monomers used for preparation of the microfluidic chip polymer matrix (pentaerythritol tetrakis(3-mercaptopropionate) (PETMP), triallyl-1,3,5-triazine-2,4,6(1H,3H,5H)-trione (TATATO) and bisphenol A diglycidyl ether (BADGE)) as well as monomers used for grafting reactions (allylmalonic acid and 2,2,3,3,4,4,5,5,6,6,7,7-dodecafluoroheptyl acrylate (DFHA)) were purchased from Sigma Aldrich. Thiol-ene reaction photoinitiator Lucirin TPO-L was obtained from BASF GmbH Germany. Grafting reaction photoinitiator 2,2-dimethoxy-2-phenylacetophenone (DMPA), thiol-epoxy reaction catalyst 1,5-diazabicyclo(4.3.0)non-5-ene (DBN), sodium hydroxide, sodium dodecyl sulfate (SDS), poly(vinyl alcohol) (PVA) as well as all solvents used in this study were obtained from Sigma Aldrich. Structural formulas of the three compounds forming the microfluidic chip matrix can be seen in Figure 1.

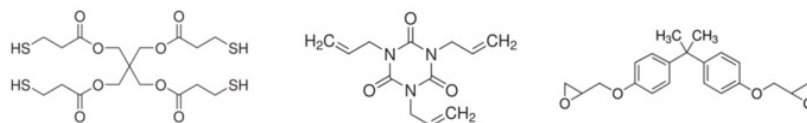


Figure 1: Structural formulas of compounds used for preparation of flow-focusing microfluidic chip (tetrathiol (left), triallyl (middle), diepoxy (right)).

## 2.2 Microfluidic chip preparation

**Mold preparation.** After the master-mold was designed, all channels and geometries were micro-milled in a poly(methyl methacrylate) (PMMA) plate. Sylgard 184 silicone kit was used for producing the mirror-image mold. Base and crosslinker were mixed together in 10 : 1 weight ratio respectively, degassed and casted on the PMMA master-mold. The PDMS curing reaction was allowed to proceed for two hours at 120 °C.

**Crosslinking reaction step.** The off-stoichiometric mixture of monomers used for preparation of microfluidic chip consisted of pentaerythritol tetrakis(3-mercaptopropionate), triallyl-1,3,5-triazine-2,4,6(1H,3H,5H)-trione and bisphenol A diglycidyl ether (BADGE) (molar ratio of reactive groups was 2 : 1 : 0.15, respectively). Lucirin TPO-L was used as a photoinitiator for the thiol-ene crosslinking reaction and DBN was introduced to accelerate the thiol-epoxy reaction. Schematic thiol-ene and thiol-epoxy reactions are presented in Figure 2.

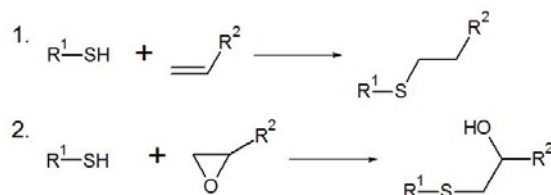


Figure 2: 1) The thiol-ene photoinitiated reaction; and 2) the DBN catalyzed thiol-epoxy reaction.

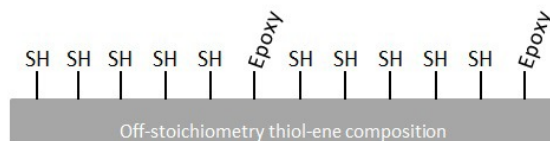


Figure 3: Schematic illustration of UV-cured network resulting from off-stoichiometric mixture of tetrathiol, triallyl and diepoxy compounds (2 : 1 : 0.15, respectively).

The composition of all five compounds was thoroughly mixed, degassed and transferred onto the PDMS mirror-image mold and exposed to UV-irradiation for a few minutes at light intensity of  $\sim 4\text{mW/cm}^2$  in order to initiate the crosslinking reaction between thiol and allyl components exclusively. Schematic illustration of the obtained network is presented in Figure 3. After two wafers of microfluidic chip were cured, they were assembled together (avoiding formation of air voids) and placed in the oven for 2 hours at 80 °C. In this step the thiol and epoxy groups present on the surfaces of both wafers react with each other assuring not only covalent bonding of the two wafers but also increase of degree of crosslinking resulting in increased glass transition temperature and stiffness of the material. The amount of BADGE used in this system was kept at the lowest possible level leaving as many thiol groups on the surfaces of the channels as possible. The remaining thiol groups made it possible to modify the surface of the channels later, which is a crucial step in the preparation of flow-focusing microfluidic chips.

Surface modification of microfluidic chip channels. The surface grafting reaction follows the same thiol-ene chemistry mechanism as presented above for the crosslinking reaction of the main matrix. In this system we take advantage of the thiol groups remaining on the surface of the material and induce the grafting reaction by injecting different grafting solutions into the chip channels. Structural formulas of the grafted compounds can be seen in Figure 4. In the first step of the process the 10 wt.% solution of DFHA in ethanol with additional 1 wt.% DMPA as photoinitiator was prepared. After the channels were filled with the solution, a part of the chip that was intended to remain hydrophilic was covered with a stencil mask in order to block the grafting reaction in that area. Subsequently the chip was exposed to UV-irradiation at light intensity of  $\sim 4\text{mW/cm}^2$ . In the following step the channels were thoroughly washed with substantial amounts of ethanol to dispose of the grafting solution. Afterwards a 10 wt.% solution of allylmalonic acid in ethanol with 1 wt.% DMPA was prepared and injected into the channels of the chip. The area of the chip that was designed to be hydrophobic was masked with stencil mask to avoid grafting reaction of allylmalonic acid in that area. The chip was again exposed to UV-irradiation and after the reaction was complete, it was flushed with ethanol. Subsequently a 0,01M NaOH aqueous solution was injected into the channels in order to replace protons of the carboxylic groups with sodium cations. This process was proved to significantly increase the hydrophilicity of the material.

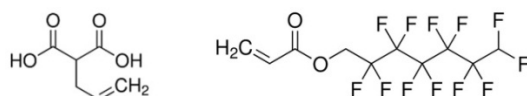


Figure 4: Structural formulas of allylmalonic acid and 2,2,3,3,4,4,5,5,6,6,7,7-dodecafluoroheptyl acrylate.

### 2.3 Formation of double emulsion in microfluidic chip cross-junctions

After microfluidic chip fabrication (see scheme of the chip in Figure 5) it was sandwiched between custom made polycarbonate holder plate equipped with three inlet holes and one outlet hole. All liquids were introduced to the chip with the help of separately controlled Harvard Apparatus 11 plus syringe pumps capable of precise adjusting flow rates.

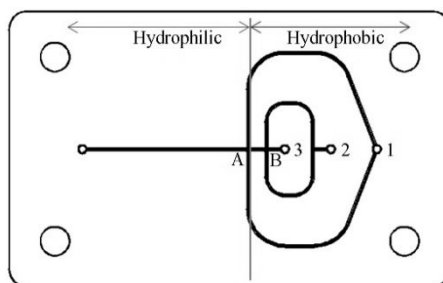


Figure 5: Schematic visualization of wetting properties of the channel surfaces in microfluidic chip used for preparation of o/w and w/o/w emulsion where o=oil and w=water. Chip dimensions are 47 x 29 mm with 280  $\mu\text{m}$  broad channels.

SDS/PVA (3 wt.% and 1 wt.%) aqueous solution was used as outer phase and pure water was used as inner phase. Both liquids were introduced to the chip via inlets 1 and 3 respectively (see Figure 5). Two component Sylgard 184 silicone kit mixed in ratio 3:2 was used as middle phase and was injected via inlet 2. In the first step of the process the outer phase was introduced to the system followed by injection of middle phase. After the silicone droplet formation (at junction A) was balanced, the inner phase liquid was slowly injected ( $Q_1 > Q_2 > Q_3$ , where Q refers to liquid flow rate) increasing the flow rate until the intended size of the microcapsule core was obtained. The resulting double emulsion was collected and was left for 24 hours at room temperature for the shell of the core-shell microspheres to be crosslinked and form a solid layer. Subsequently the double emulsion was heated up to 50  $^{\circ}\text{C}$  for 1 hour to ensure full crosslinking of PDMS. Subsequently, the collected core shell microspheres were transferred onto large petri dish and left for drying for 5 hours at room temperature.



## 2.4 Preparation of PDMS films with incorporated liquid core microspheres.

Various amounts of dried liquid core microcapsules were mixed with different commercial PDMS compositions and carefully transferred onto a metal mold with 1 mm thick spacers. The material was finally cured at 40 °C for 5 hours and additionally left overnight at room temperature for possible postcuring to take place. The PDMS crosslinking process was kept at lowest possible temperatures in order to avoid evaporation of encapsulated water that due to relatively high vapor pressure tends to migrate through the thin silicone shell. The microcapsules were mixed in various weight ratios (10, 20, 30) with Sylgard 184 silicone kit mixed in ratio 13:1 (base : crosslinker) (all formulations are listed in Table 1). Significant excess of vinyl groups in the PDMS composition allows covalent bonding between PDMS network and PDMS shell of microcapsules possessing excess of silicone hydrides.

Table 1: Sample names with different amounts of incorporated core-shell microspheres with corresponding amounts of encapsulated filler.

Sample name	Amount of microcapsules incorporated into PDMS film [wt. %]	Amount of filler (water) incorporated into PDMS film [wt. %]
S-13:1	0	0
S-13:1_10	10	1.5
S-13:1_20	20	3
S-13:1_30	30	4.5

## 2.5 Characterization methods

Leica DM LB optical microscope was used to determine diameter and morphology of single and double emulsions as well as PDMS films containing various amounts of microcapsules. All PDMS composites were studied in terms of mechanical and electrical properties. Frequency sweep tests performed on Ares G2 TA Instruments rheometer were conducted in order to determine both storage and loss moduli of investigated compositions. 25 mm of diameter and 1 mm thick disc samples were tested in the frequency range between 100 Hz and 0.001 Hz and under controlled strain mode (2% strain) at room temperature. Novocontrol broadband dielectric spectrometer was used to investigate dielectric permittivity, dielectric losses and conductivity of samples. 20 mm of diameter and 1 mm thick disc specimens were tested in the frequency range between  $10^6$  Hz and  $10^{-1}$  Hz.

# 3. RESULTS AND DISCUSSION

## 3.1 Preparation of PDMS-microcapsules composites

The produced core-shell microspheres used for preparation of composites had average diameter and core diameter of 350  $\mu\text{m}$  and 200  $\mu\text{m}$  respectively (Figure 7). These relatively large dimensions of microcapsules comparing to the designed film thickness result from technical limitations of microfluidic chip and viscosity of middle phase in double emulsion which in this case was off-stoichiometric mixture of Sylgard 184 silicone kit. It is believed that by decreasing dimensions of microfluidic chip channels and introducing liquids of lower viscosities smaller microcapsules could be obtained.

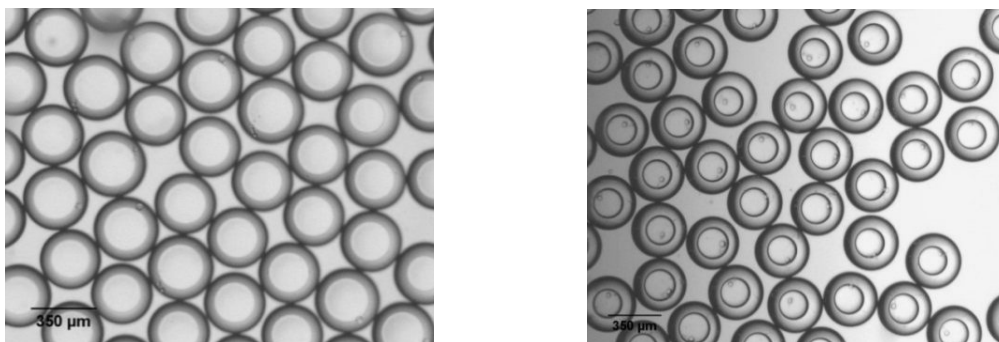


Figure 7: Microscope images of the microcapsules obtained from water in silicone in water double emulsions.

The liquid-core microcapsules were successfully incorporated within PDMS network forming stable films. Optical microscope images confirm that the microcapsules were well distributed and that water was still present in the capsules although the samples were exposed to elevated temperatures during PDMS crosslinking process. Black spots that can be seen in Figure 8 correspond to air bubbles which indicate that, to some extent, water evaporated from the core of the spheres. Nevertheless the fraction of empty capsules is acceptable and in case of samples with smaller amounts of filler becomes negligible. Specimens with higher microcapsules content are more influenced by emerging air voids since the percentage amount of filler in the polymer film becomes larger. Relatively high vapor pressure of water and its polar nature are the two main factors that are responsible for complications in handling of PDMS-water core microcapsules composites.

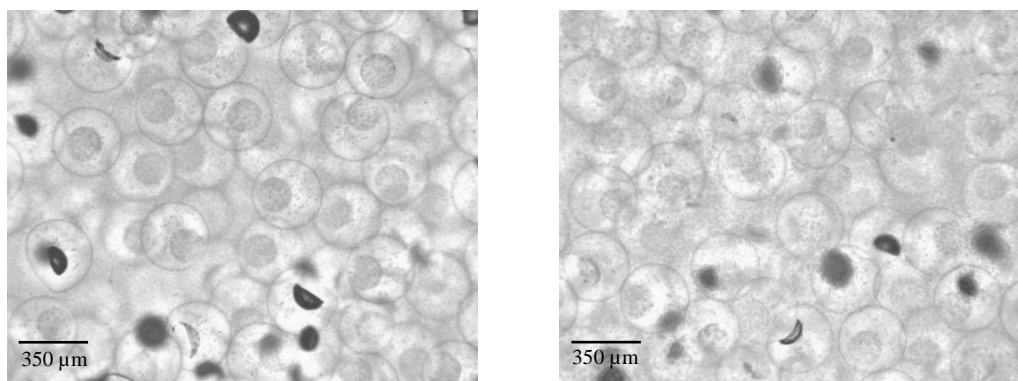


Figure 8: Microscope images of crosslinked PDMS films with incorporated core-shell microspheres. Dark spots present in the matrix are most likely air voids.

### 3.2 Mechanical properties

The prepared films are stable and free-standing at the current film thicknesses and have considerable strength when handling them. This implies that there is a significant crosslinking of the microcapsules into the elastomer as was also concluded from Gonzalez et al. [11]. Frequency sweep tests were conducted in order to determine viscoelastic properties of prepared composites and characterize how increasing amounts of core-shell microspheres influence mechanical properties. Rheology measurements were carried out on four different specimens and results summarizing changes of storage modulus and tan delta as function of frequency were plotted in Figure 9.

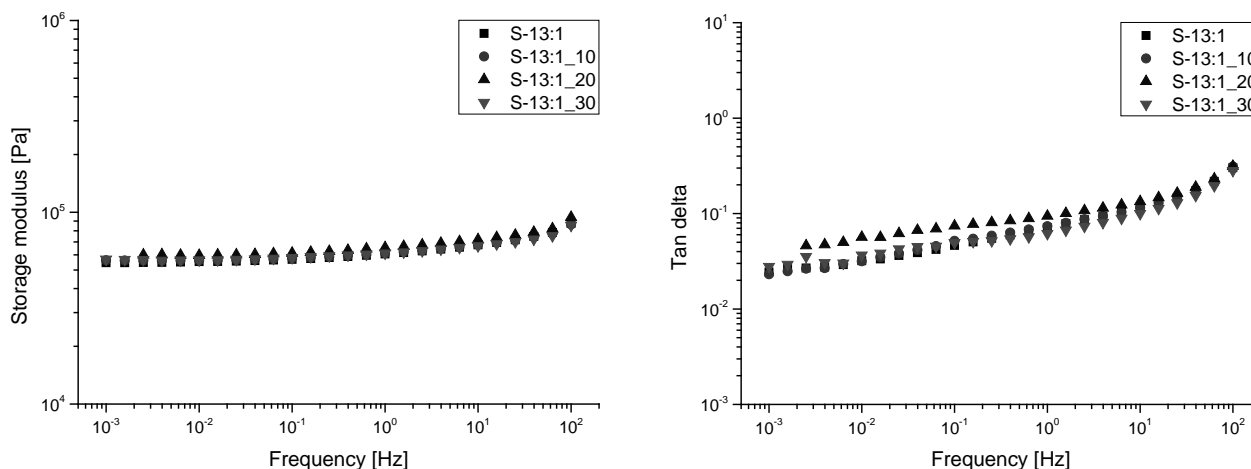


Figure 9: Storage modulus (left) and tan delta (right) of unfilled elastomer and different PDMS-microcapsules composites obtained from frequency sweep tests performed at controlled strain mode at 2% strain. The S-13:1 is the pure off-stoichiometric mixture of Sylgard 184.

It can be seen clearly that curves representing storage moduli of all tested compositions indicate nearly identical elastic behavior when applying stress. In all cases the elastic modulus at plateau region (from  $10^{-1}$  –  $10^{-3}$  Hz) varies from 55 kPa to 60 kPa. These small differences are within the range of measurement error so it can be assumed that incorporation of core-shell microspheres of the structure described in our study does not influence significantly the viscoelastic behavior of tested PDMS composition. This observation is confirmed by tan delta of tested samples plotted as function of frequency, which, as can be seen in Figure 9, remains also nearly unchanged with increasing amounts of incorporated microcapsules.

When interpreting this phenomenon it has to be mentioned that there are few factors influencing viscoelastic properties of the discussed formulations. On one hand a substance of dominant viscous behavior and negligible elastic behavior is incorporated into PDMS network which in this case is water (and also to some extent air), and on the other hand we deal with more rigid structure of microcapsules shell which locally enhances elasticity of composites. These two coexisting and competitive factors determine the resulting overall viscoelastic behavior of tested composites.

### 3.3 Dielectric spectroscopy measurements

As described previously, the main reason for introducing microcapsules into PDMS films is to enhance the relative permittivity of the final product without compromising its other dielectric and mechanical properties. Results of investigating of this parameter are summarized in Figure 10. The dielectric constant of Sylgard 184 mixed in ratio 13:1 was successfully increased by incorporation of water-core microcapsules. The values measured at frequency of  $10^3$  Hz indicate an increase from 2.8 for unfilled network to 3.6 for composite containing 30 wt.% of microcapsules (4.5 wt.% of water). These are very promising values in context of possible decrease of dielectric constant caused by the presence of air voids in the structure – higher amount of air bubbles for higher loading of microcapsules in the sample. By eliminating empty microcapsules the dielectric permittivity is expected to increase even more making PDMS-water composites competitive for other high permittivity materials. Dielectric spectroscopy measurements proved also that the dielectric loss of each specimen is at the same level in the function of frequency.

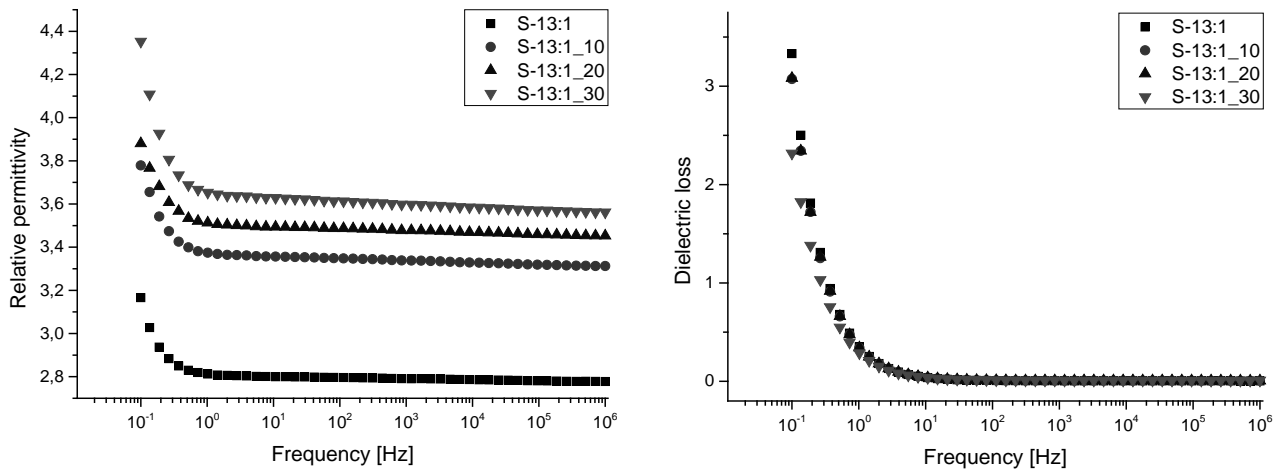


Figure 10: Relative permittivity and dielectric loss of elastomer reference and different PDMS-microcapsules composites as a function of frequency measured at room temperature.

Conductivity was proved to remain at nearly same level for all tested compositions (Figure 11). Although all samples exhibit similar conductivity, small deviations in the high frequency region can be observed. As expected the lower the filler loading the lower the conductivity. This phenomenon is in perfect agreement with presumptions which implied that water, as a high conductivity filler potentially decreasing resistivity of materials, does not influence significantly the conductivity which is explained by the fact that each portion of water in the investigated systems was hermetically encapsulated within PDMS insulating shell and therefore conductive pathways throughout the material were unlikely to appear and wherefore the overall conductivity remained almost unaffected.

At this step we decided to resign on investigating PDMS-microcapsules composites in terms of breakdown strength and their ultimate mechanical properties like tear strength and maximum elongation. It is believed that attempts of determination of these parameters would give unreliable outcome due to relatively high thickness of prepared samples.

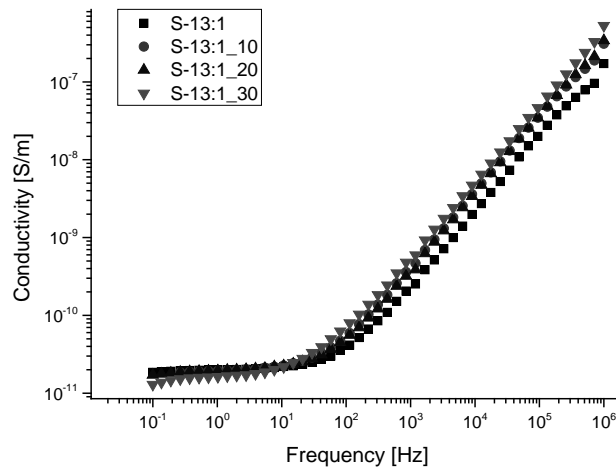


Figure 11: Conductivity of different PDMS-microcapsules composites as a function of frequency measured at room temperature.

## 4. CONCLUSIONS

In this study we present an easy and efficient way of preparation of liquid-core microcapsules with PDMS forming solid insulating shell encapsulating high permittivity polar liquids. The thiol-ene flow-focusing microfluidic system was proved to be a powerful tool capable of producing microspheres of extremely narrow size distribution and various sizes of individual layers. Encapsulated water was successfully incorporated into the PDMS matrix increasing its relative permittivity without compromising dielectric losses and resistivity. Mechanical properties remained also unaffected by different microcapsule loadings in the investigated composites.

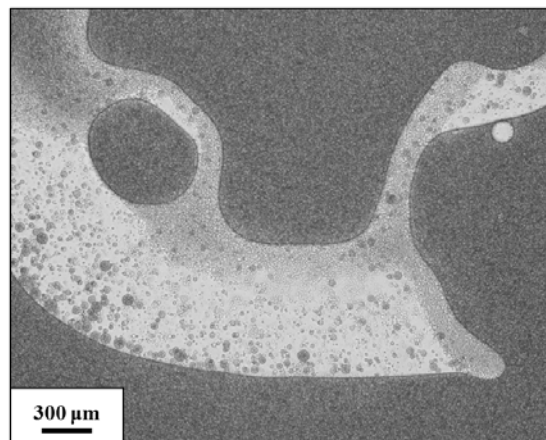
Although these pioneering attempts of incorporation of polar liquids into silicone networks gave very promising results there are many parameters and steps in the preparation procedure that require further optimization. We believe that through incorporation of smaller microcapsules with thinner shells and by eliminating of hollow spheres the overall performance of this type of composites can be further enhanced.

## ACKNOWLEDGEMENTS

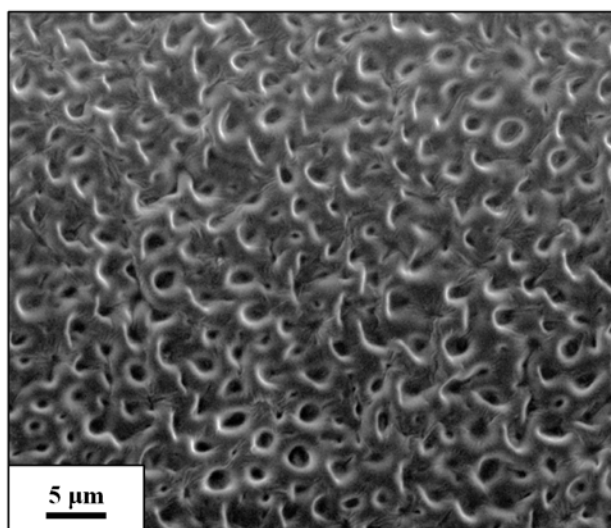
We acknowledge financial support from DTU Proof of Concept as well as from the Danish Advanced Technology Foundation.

## REFERENCES

- [1] Goswami, K., Galantini, F., Mazurek, P., Daugaard, A. E., Gallone, G., Skov, A. L., "Reinforced poly(propylene oxide): a very soft and extensible dielectric electroactive polymer", *Smart Mater. Struct.* 22, 115011 (2013)
- [2] Skov, A. L., Vuduagiri, S., Benslimane, M. Y., "Novel silicone elastomer formulations for DEAPs", *Proc. of SPIE*, 8687, 86871I-1 (2013)
- [3] Galantini, F., Bianchi, S., Castelvetro, V., et al., "Functionalized carbon nanotubes as a filler for dielectric elastomer composites with improved actuation performance", *Smart Mater. and Struct.*, 22, 5, 055025 (2013)
- [4] Racles, C., Cazacu, M., Fischer, B., Opris, D. M., "Synthesis and characterization of silicones containing cyanopropyl groups and their use in dielectric elastomer actuators", *Smart Mater. Struct.* 22, 104004 (2013)
- [5] Madsen, F. B., Daugaard, A. E., Hvilsted, S., Skov, A. L., "Dipolar cross-linkers for PDMS networks with enhanced dielectric permittivity and low dielectric loss", *Smart Mater. Struct.* 22 104002 (2013)
- [6] Madsen, F. B., Dimitrov, I., Daugaard, A. E., Hvilsted, S., Skov, A. L., "Novel cross-linkers for PDMS networks for controlled and well distributed grafting of functionalities by click chemistry", *Polymer Chem.*, 4 (5), 1700 – 1707 (2013)
- [7] Molberg, M., Crespy, D., Rupper, P., Nüesch, F., Månson, J. A. E., Löwe, C., Opris, D. M., "High Breakdown Field Dielectric Elastomer Actuators Using Encapsulated Polyaniline as High Dielectric Constant Filler", *Adv. Funct. Mater.*, 3280–3291 (2010)
- [8] Larsen, A. L., Hansen, K., Sommer-Larsen, P., Hassager, O., Bach, A., Ndoni, S., Jørgensen, M., "Elastic Properties of Nonstoichiometric Reacted PDMS Networks", *Macromolecules*, 36, 10063 (2003)
- [9] Abate, A. R., Weitz, D. A., "Faster multiple emulsification with drop splitting", *Lab Chip*, 11, 1911 (2011)
- [10] Carlborg, C. F., Haraldsson, T., Öberg, K., Malkoch, M., van der Wijngaart, W., "Beyond PDMS: off-stoichiometry thiol-ene (OSTE) based soft lithography for rapid prototyping of microfluidic devices", *Lab Chip*, 11, 3136 (2011)
- [11] Gonzalez, L., Kostrzevska, M., Ma, B., Hansen, H., Li, L., Hvilsted, S., Skov, A. L., "Preparation and Characterization of Thermoplastic Encapsulated PDMS Microspheres with Reactive Handles", *Macromol. Mater. and Engin.* (2013)

**Appendix to chapter 3.1.**

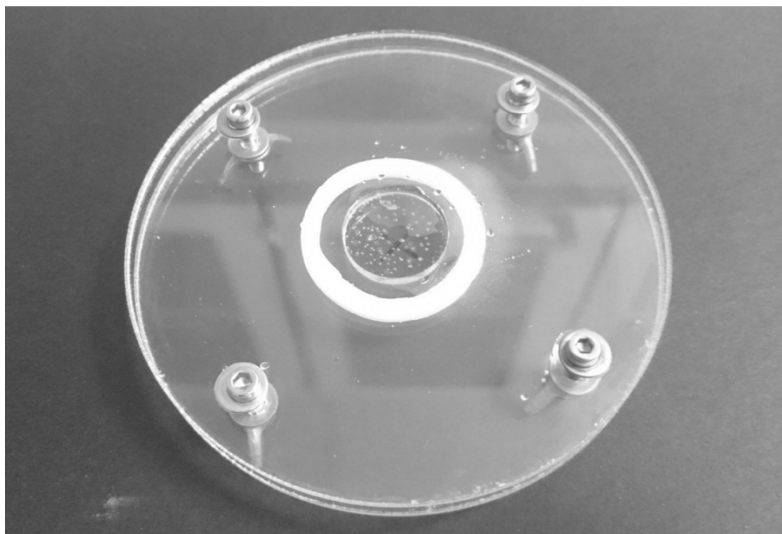
**Figure A-3.1.1.** Emulsion based on G170\_S184 formulation. Occurrence of a phase inversion is represented, which is followed by a phase split.



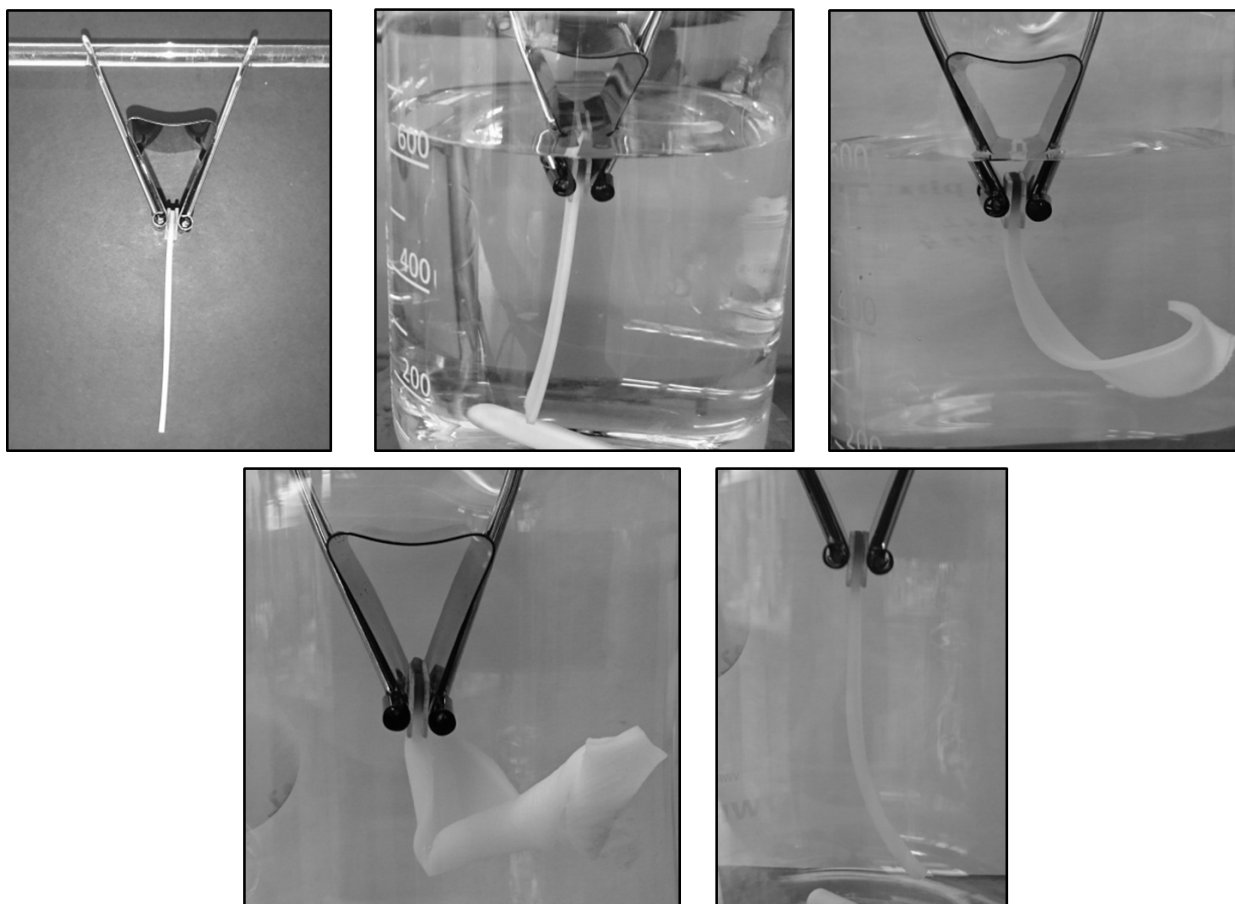
**Figure A-3.1.2.** Upper surface of the cross-linked G100\_S184 formulation.



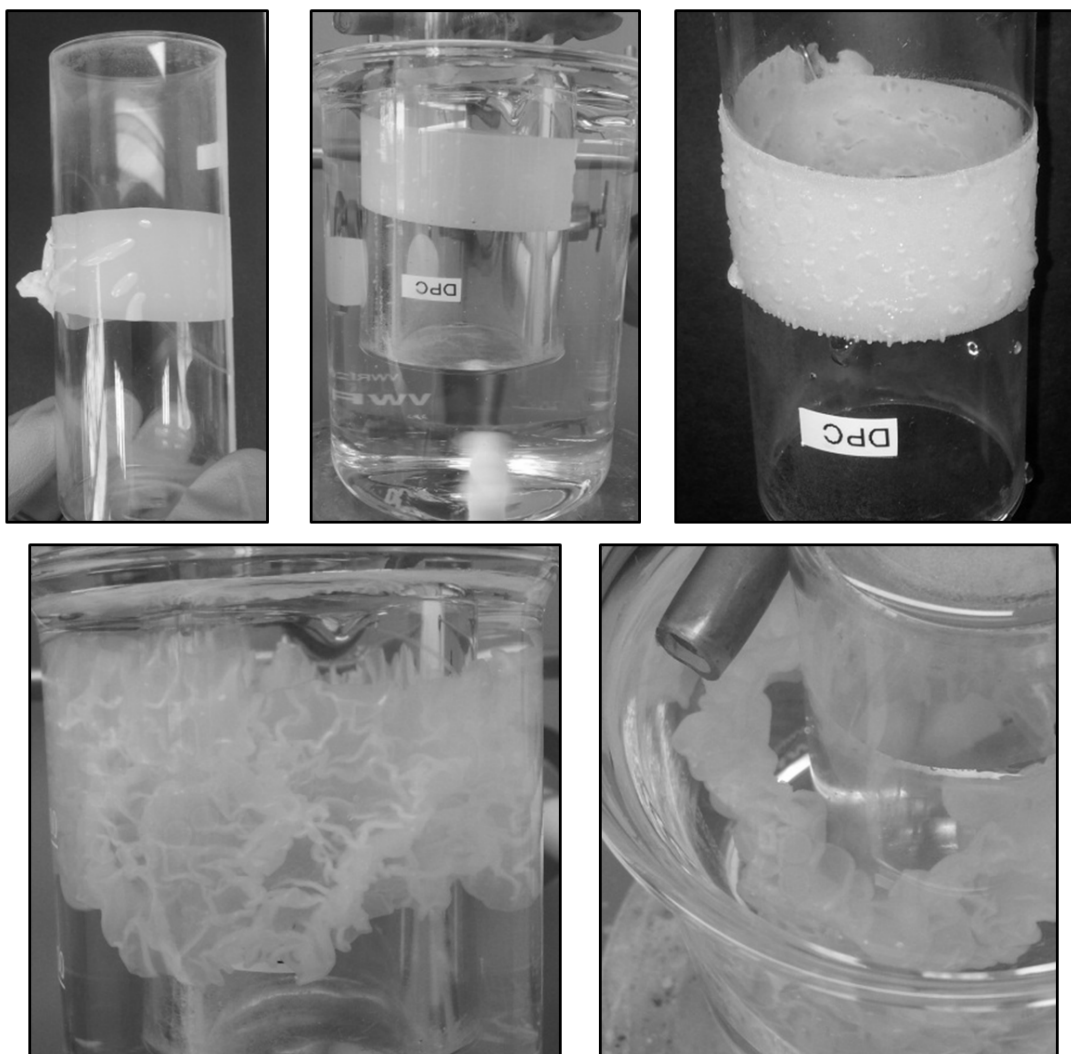
**Figure A-3.1.3.** Water droplet on top of a crosslinked 25 mm in diameter G80\_S184 disc sample after approximately 1 hour.



**Figure A-3.1.4.** An O-ring prepared from a 1 mm-thick film of G100\_S184 sample (inner diameter = 20 mm; outer diameter = 25 mm). Diameter of the PMMA disc from the middle of the sample has a diameter of 20 mm. Sample was kept in water for 24 hours.

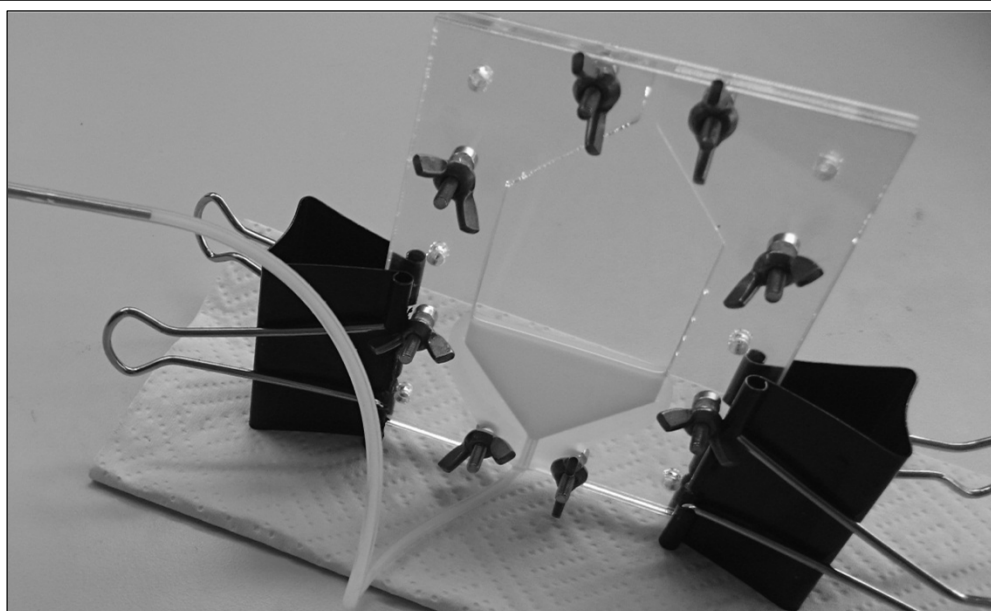
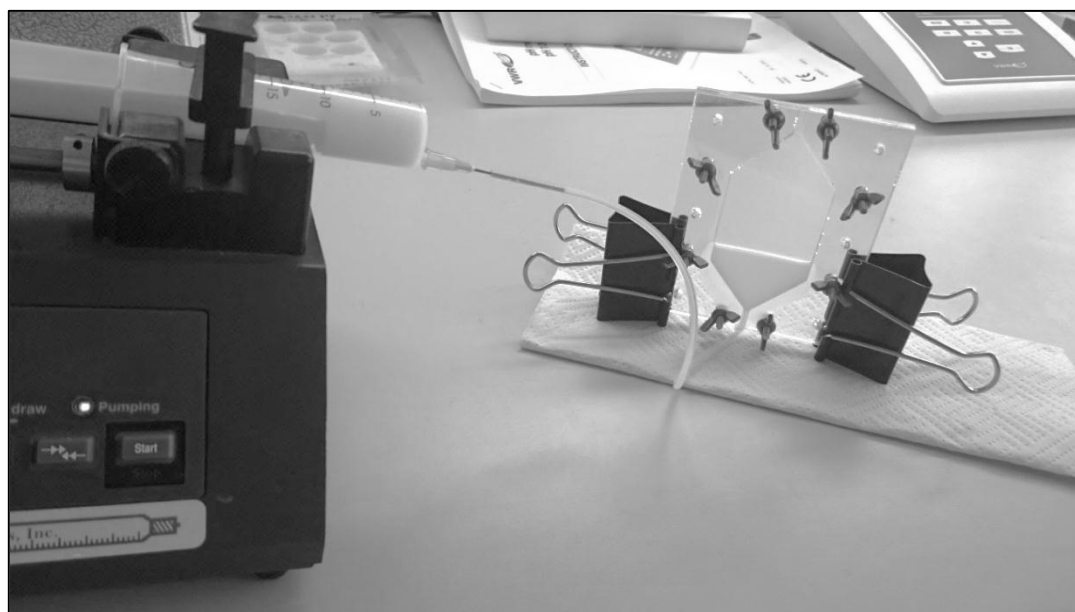


**Figure A-3.1.5.** 1 mm thick G100\_S184 strip at different stages of water absorption/evaporation experiment.



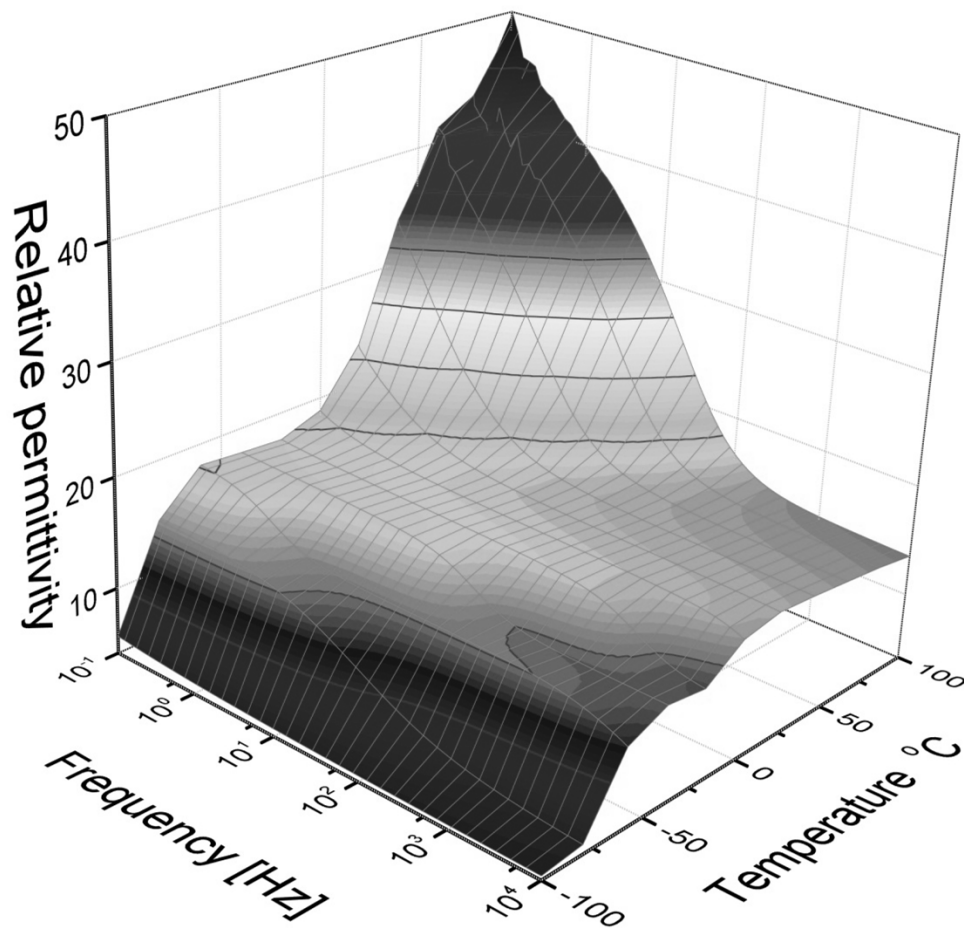
**Figure A-3.1.6.** 200  $\mu\text{m}$  thick G100\_S184 film at different stages of water absorption experiment.





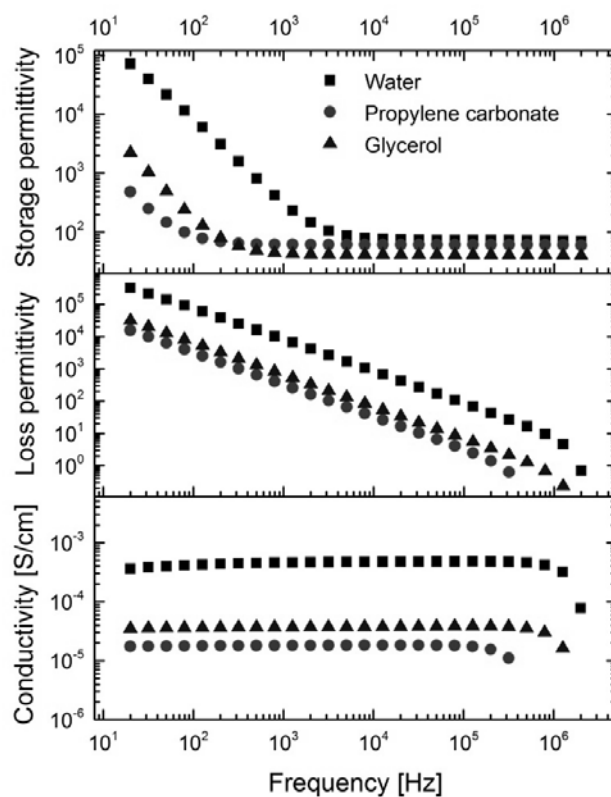
**Figure A-3.1.7.** A setup mimicking the injection moulding of a G40\_S184 formulation. After a cross-linking step a uniform film was obtained, proving the stability of glycerol-silicone emulsions.

## Appendix to chapter 3.2.

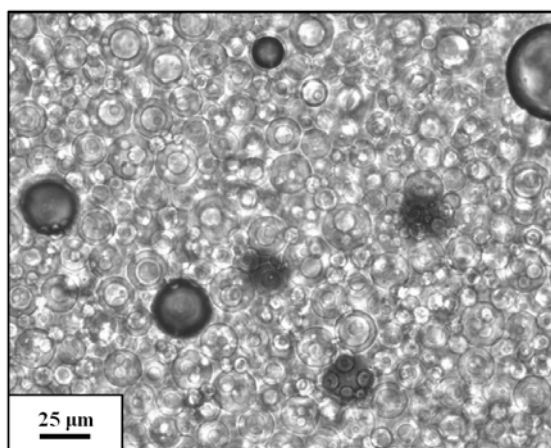


**Figure A-3.3.2.** Relative permittivity of the sample G100\_S184 measured at 350 V (AC) and temperatures between -100 °C and 100 °C. The results indicate the deterioration of properties at very low temperatures (due to exceeding the glass transition temperature of glycerol) and high temperatures (very high charge mobility, leading to increased conductivity).

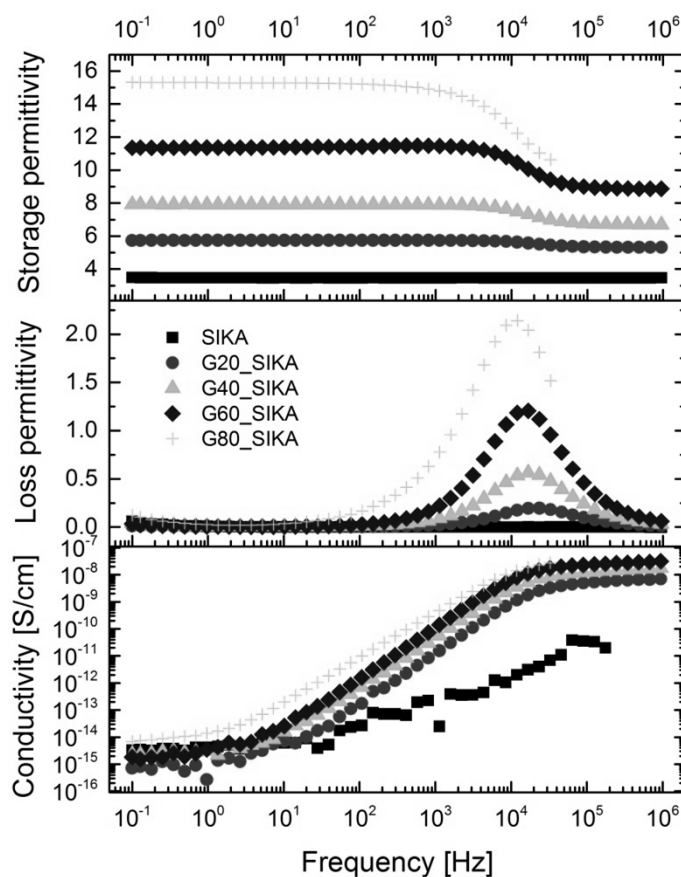
## Appendix to chapter 3.3.



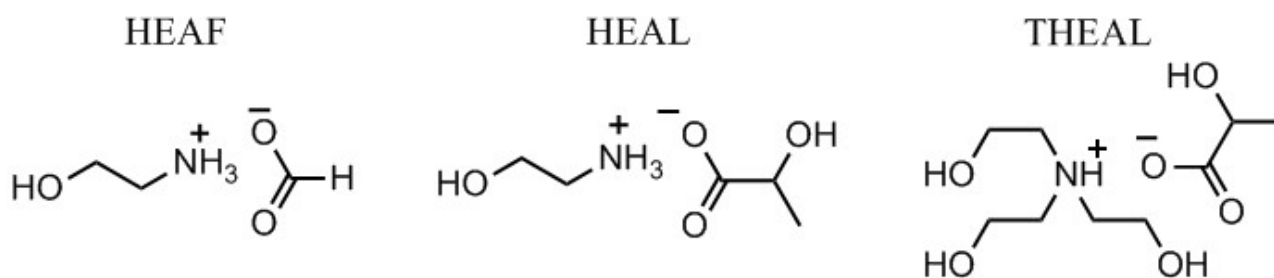
**Figure A-3.3.1.** Storage permittivity, loss permittivity and conductivity of various polar liquids.



**Figure A-3.3.2.** An emulsion produced from 100 phr of glycerol, a custom-made condensation cure PDMS formulation. A maximum of 80 phr of glycerol could be incorporated into this PDMS composition. After this value, double, triple and quadruple emulsions were produced (glycerol as a continuous phase). The emulsion might create a basis for producing PDMS-shell glycerol-core microcapsules.



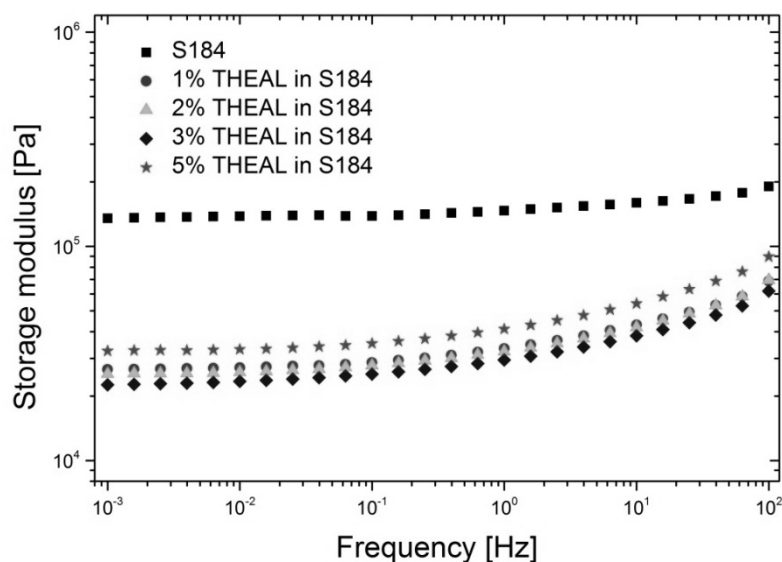
**Figure A-3.3.3.** Storage permittivity, loss permittivity and conductivity of various glycerol-PDMS composites at room temperature. The PDMS system is a custom-made condensation type of formulation based on substrates provided by Sika Corp.

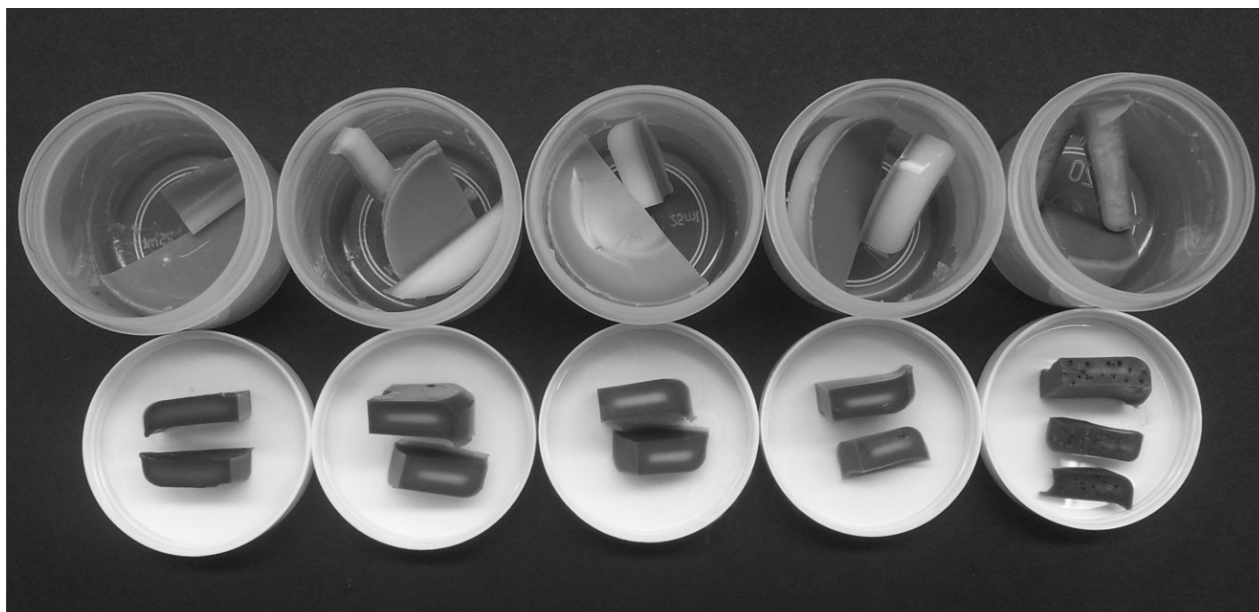


**Figure A-3.3.4.** Structural formulas of three synthesised ionic liquids: 2-hydroxyethylammonium formate (HEAF), 2-hydroxyethylammonium lactate (HEAL) and tris-(2-hydroxyethyl)ammonium lactate (THEAL). Preparation procedure followed the same steps as described in Chapter 2.1.

**Table A-3.3.1.** Organoleptic observations of blending of polar ionic liquids into various PDMS compositions.

	THEAL $\epsilon=60$	HEAF $\epsilon=61$	HEAL $\epsilon=86$
Sylgard 184	<ul style="list-style-type: none"> <li>• Cross-linked at low IL loadings (up to 5 phr), significantly weaker structure than pure S184</li> <li>• Free-standing of 100 <math>\mu\text{m}</math> and 1mm</li> <li>• Change in color after several hours at 115 <math>^{\circ}\text{C}</math></li> <li>• Very poor structure at higher IL loadings (improved by adding additional Pt-catalyst)</li> </ul>	<ul style="list-style-type: none"> <li>• No curing even at 115 <math>^{\circ}\text{C}</math></li> </ul>	<ul style="list-style-type: none"> <li>• Gelled after 1 hour at 115 <math>^{\circ}\text{C}</math></li> <li>• After additional 24 hours at 115 <math>^{\circ}\text{C}</math> no changes were observed</li> <li>• Far too weak to form free-standing films</li> </ul>
Elastosil LR 3040/30 A/B	<ul style="list-style-type: none"> <li>• No curing, even at 115 <math>^{\circ}\text{C}</math></li> </ul>		
Powersil XLR 630 A/B	<ul style="list-style-type: none"> <li>• No curing, even at 115 <math>^{\circ}\text{C}</math></li> </ul>		
Custom-made hydrosilylation type PDMS	<ul style="list-style-type: none"> <li>• No curing, even at 115 <math>^{\circ}\text{C}</math></li> </ul>		
Custom-made UV-curable thiol-ene PDMS	<ul style="list-style-type: none"> <li>• Cross-linking at low IL loadings (up to 5 phr)</li> <li>• Poor cross-linking at increasing loadings due to poor UV-light transmission</li> </ul>		
UV-curable UV LSR Shin-Etsu X-34-4208 A/B	<ul style="list-style-type: none"> <li>• No curing even after 24 hours of exposure to UV (light intensity of around 4 <math>\text{mW}/\text{cm}^2</math>)</li> </ul>		
Custom-made condensation type PDMS	<ul style="list-style-type: none"> <li>• Compositions with up to 80 phr of ionic liquids were prepared</li> <li>• All compositions cross-linked at room temperature after around 3 months (extremely slow curing)</li> <li>• Very poor mechanical properties of the samples</li> </ul>		

**Figure A-3.3.5.** Frequency sweep tests performed on Sylgard 184 blended with various amounts of THEAL.



**FigureA-3.3.6.** Images of five samples based on THEAL20\_S184 with different amounts of additional Pt-catalyst (from left 0 ppm, 10 ppm, 20 ppm, 30 ppm, 100 ppm). After 24 hours of exposure at 115°C, all samples were cured to a different extent. Color change was observed from white to light-brown. After an additional few days of high-temperature curing the colour changed to dark-brown. The colour change propagated from elastomer-air interphase and propagated towards further layers. HEAL\_S184 with an addition of 30 ppm of Pt-catalyst did not cross-link (colour change similar to the sample THEAL20\_S184).

**Table A-3.3.2.** Organoleptic observations from the experiment presented in Figure A-3.3.6.

	<b>Stickiness</b>	<b>Other observations</b>
<b>0 ppm</b>	Very high	Very poor cross-linking
<b>10 ppm</b>	Medium	-
<b>20 ppm</b>	Low	-
<b>30 ppm</b>	Very low	Single air-voids in the structure of cured samples
<b>100 ppm</b>	Not sticky	Many air-voids in the structure of cured samples

